BRNO UNIVERSITY OF TECHNOLOGY

VYSOKÉ UČENÍ TECHNICKÉ V BRNĚ

FAKULTA CHEMICKÁ

FACULTY OF CHEMISTRY

ÚSTAV CHEMIE MATERIÁLŮ

INSTITUTE OF MATERIALS SCIENCE

EFFECT OF BODY FLUIDS ON SETTING, STRUCTURE AND MECHANICAL PROPERTIES OF PHOSPHATE BONE CEMENTS

VLIV TĚLNÍCH TEKUTIN NA TUHNUTÍ, STRUKTURU A MECHANICKÉ VLASTNOSTI FOSFÁTOVÝCH KOSTNÍCH CEMENTŮ

MASTER'S THESIS
DIPLOMOVÁ PRÁCE

AUTHOR — **Bc. Vendula Bednaříková**
AUTOR PRÁCE

SUPERVISOR — **Doc. Ing. Lucy Vojtová, Ph.D.**
ŠKOLITEL

BRNO 2017/2018

BRNO UNIVERSITY OF TECHNOLOGY
FACULTY OF CHEMISTRY

Master's Thesis Assignment

Number of thesis:	FCH-DIP1162/2017	Academic year: 2017/18
Institute:	Institute of Materials Science	
Student:	**Bc. Vendula Bednaříková**	
Study programme:	Chemistry, Technology and Properties of Materials	
Study field:	Chemistry, Technology and Properties of Materials	
Head of thesis:	**doc. Ing. Lucy Vojtová, Ph.D.**	

Title of Master's Thesis:

Effect of body fluids on setting, structure and mechanical properties of phosphate bone cements

Master's Thesis assignment:

1. Lit. searching on phosphate cements and their interaction with biological fluids
2. Preparation of cements and monitoring of self-setting in body fluids
3. Biomechanical sample testing and morphology assessment
4. Evaluation and disscussion
5. Conclusion

Deadline for Master's Thesis delivery: 7.5.2018

Master's Thesis is necessary to deliver to a secretary of institute in the number of copies defined by the dean. This assignment is part of Master's Thesis.

Bc. Vendula Bednaříková
Student

doc. Ing. Lucy Vojtová, Ph.D.
Head of thesis

prof. RNDr. Josef Jančář, CSc.
Head of institute

prof. Ing. Martin Weiter, Ph.D.
Dean

In Brno, 31. 1. 2018

ABSTRACT

Presented diploma thesis describes the preparation and characterization of composite calcium-phosphate bone cements (CPCs). In the literature review properties and structure of tricalcium phosphates (TCPs) are described, including their interaction with body environment. In the experimental work, first of all, sample preparation technique was determined by experiments with setting reactions provided in ultrapure water environment. Optimal technique of setting CPC samples included memory foam setting mold, ending setting reactions by absolute cold ethanol and vacuum drying procedures. Consequently, the work describes the sample preparation and process of TCP bone cement setting in both natural (pig blood) and simulated body fluids (physiological, Hank´s and Ringer´s solutions). Morphology study by Scanning Electron Microscopy (SEM) was performed for samples set for 1 day, 1 week, 2 weeks and 1 month, due to the significant change in crystalline structure proving as well by X-ray diffraction (XRD) analysis by determining α-TCP conversion to calcium-deficient hydroxyapatite (CDHA). Porosity investigated by X-ray computed microtomography (μ-CT) was slightly higher at sample set in natural blood. Mechanical properties of CPC samples measured by mechanical compression tests showed stable cement strength set in physiological solution already after 1 day while cements set in blood has shown still increasing strength even at 1 month. On contrary, strength of cement samples rapidly decreased after 2 weeks of setting in both Hank´s and Ringer´s solutions probably due to its slightly acidic pH accelerating CPC disintegration. As a result, setting environment has significant effect on resulting CPC properties and natural blood in comparison to simulated plasma had shown better CPC properties while more closely imitating the *in vivo* conditions.

KEYWORDS

calcium phosphate bone cement, self-setting reactions, simulated body fluids, heparinized blood, morphology

ABSTRAKT

Předložená diplomová práce se zabývá přípravou a charakterizací vzorků z kompozitního kostního cementu na bázi fosforečnanu vápenatého (CPC). V teoretické části jsou popsány vlastnosti a struktura fosforečnanů vápenatých, včetně jejich interakce s tělním prostředím. Experimentální část nejdříve popisuje stanovení optimální techniky přípravy vzorků pomocí experimentů prováděných v ultračisté vodě. Optimální technika pro vytvrzování zahrnuje použití formy z paměťové pěny, ukončení vytvrzovacích reakcí pomocí absolutního chladného etanolu a sušení vzorků ve vakuové sušárně. Následně je v práci popsána příprava vzorků a proces vytvrzování CPC jak v přirozeném (prasečí krev), tak v prostředí simulovaných tělních tekutin (fyziologický roztok, Hankův a Ringerův roztok). Byla provedena morfologická studie pomocí skenovací elektronové mikroskopie (SEM) pro vzorky vytvrzené 1 den, 1 týden, 2 týdny a 1 měsíc kvůli očekávané významné změně v jejich krystalické struktuře, která byla taktéž zkoumána pomocí rentgenové difrakce (XRD), stanovující přeměnu α-fosforečnanu vápenatého na kalcium deficitní hydroxyapatit (CDHA). Porozita vzorků byla zkoumána rentgenovou mikrotomografií (μ-CT) a vzorky vytvrzené v krvi vykazovaly mírně vyšší porozitu. Mechanické vlastnosti CPC vzorků byly zkoumány pomocí mechanických kompresních testů. Výsledky testů ukázaly stabilní pevnost cementových vzorků vytvrzených ve fyziologickém roztoku už po jednom dni vytvrzování, zatímco vzorky vytvrzené v krvi vykazovaly nárůst pevností dokonce i po jednom měsíci vytvrzování. Naopak pevnost vzorků vytvrzených jak v Hankově, tak v Ringerově roztoku rychle klesla po 2 týdnech vytvrzování pravděpodobně důsledkem mírně kyselého pH vytvrzovacích roztoků, které urychluje rozpad CPC vzorků. Výsledky práce ukazují významný vliv vytvrzovacích prostředí na vlastnosti CPC kostních cementů. Vzorky vytvrzené v krvi oproti vzorkům vytvrzených v umělé tělní plazmě vykázaly lepší vlastnosti, protože krev imituje *in vivo* podmínky.

KLÍČOVÁ SLOVA

kostní cement, samo-vytvrzovací reakce, simulované tělní tekutiny, heparinizovaná krev, morfologie

BEDNAŘÍKOVÁ, V. *EFFECT OF BODY FLUIDS ON SETTING, STRUCTURE AND MECHANICAL PROPERTIES OF PHOSPHATE BONE CEMENTS*: master's thesis. Brno: Brno University of Technology, Faculty of Chemistry, Institute of Materials Science, 2017/2018. 117 p. Supervisor Doc. Ing. Lucy Vojtová, Ph.D.

I declare that the diploma thesis has been worked out by myself and that all the quotations from the used literary sources are accurate and complete. The content of the diploma thesis is the property of the Faculty of Chemistry of Brno University of Technology and all commercial uses are allowed only if approved by both the supervisor and the dean of the Faculty of Chemistry, BUT.

Brno, 2018 Bc. Vendula Bednaříková

ACKNOWLEDGEMENT

I would like to thank my supervisor Doc. Ing. Lucy Vojtová, Ph.D. for her professional approach, willingness and tolerance during our cooperation. I would also like to thank Ing. Lenka Michlovská, Ph.D. for her support and kindly cooperation during this research, Ing. Petr Poláček, Ph.D. for his help with measurement and evaluation of mechanics, Doc. Ing. Klára Částková, Ph.D. for the providing and evaluation of particle size measurement, Ing. Radka Bálková, Ph.D. for her help with XRD analysis, Ing. Jaroslav Kaštyl, Ph.D. for his time devoted to machine milling, Martin Kareš for μ-CT providing, Mgr. Jan Žídek, Ph.D. for μ-CT evaluation, Bc. Simona Debnárová for polymer synthesis, Ing. Pavel Janál for his support with distribution of biological material, MVDR. Eduard Göpfert, Ph.D. for pig blood donation, RNDr. Otakar Humpa from Masaryk University for NMR measurement of copolymer, Edgar Benjamin Montufar Jimenez, Ph.D. for his help with XRD evaluation. I express my thanks to my partner Ing. Radek Řihák and to rest of my family for their great support throughout the study period. This work was supported by the CEITEC 2020 (LQ1601) with financial support from the Ministry of Education, Youth and Sports of the Czech Republic under the National Sustainability Programme II.

Brno ....

(author's signature)

CONTENTS

INTRODUCTION

Calcium phosphate cements (CPCs) are a class of bioactive materials that have been widely used in bone tissue engineering, especially for bone tissue repair and augmentation with successful applications in cranio-maxillofacial, dental, and orthopedic surgery fields.

CPCs possess surface properties that support osteoblast adhesion/proliferation and stimulate new bone formation, both related to the specific interactions of their surface with the extracellular fluids and cells. Probably the first CPC composed of calcium oxide powder and orthophosphoric acid was prepared by Ostermann in 1832 and applied in dentistry. [1] However, the first CPC properly known is that prepared by Brown and Chow in 1986. They prepared mixtures of dicalcium phosphate dihydrate or dicalcium phosphate with tetracalcium phosphate and water or diluted aqueous solution of orthophosphoric acid. [2]

On the other hand, α-TCP based bioceramics are biocompatible materials used in bone tissue engineering most often in the form of injectable cement paste. Injectability is the important property of α-TCP bone cements, provided by using an appropriate liquid phase added to powders. Therefore, polymer water solutions as liquid phase can be used to reduce CPC brittles and increase ductility, improve rheological properties for better injectability and enable biological active species bonding. Another special function of polymeric liquid phase components is their biodegradability, which causes the formation of pores after polymer degradations.

The main aim of this work was to study the effects of body fluids (synthetic and native) on the structure and mechanical properties of biodegradable polymer/α-TCP composite bone cement samples. Generally, *in vitro* experimental works are performed only under humid conditions or in either physiological solution or buffers. However, there is no information about the effect of native environment like blood on the self-setting process going along with physicochemical properties of resulted CPC. Here, simulated blood plasma represented by Hank´s and Ringer´s solutions and native heparinized pig blood have been used as a setting environments for comparison resulting CPC properties.

1 LITERATURE REVIEW

In literature review, structure and properties of tricalcium phosphates (TCPs) are described. This chapter describes structural characteristics and polymorphs of TCPs with focus on α-tricalcium phosphate, its properties such as solubility, biodegradability and interaction with body fluids. This chapter goes on with description of CPCs biomedical applications.

1.1 Tricalcium phosphates

Calcium phosphate-based bioceramics have revolutionized orthopedic and dental repair of damaged parts of the bone system. As a class of materials, bioceramics are generally defined as inorganic nonmetallic solids. Two main classes of bioceramics used as biomaterials are structural (or technical) and resorbable (or soluble). Structural ceramics such as alumina (Al_2O_3)and zirconia (ZrO_2) dispose, among other properties, their low chemical reactivity and essential insolubility in water. The most common types of soluble bioceramics resemble calcium-based minerals that naturally occur in mammalian bodies, such as hydroxyapatite (HAp) with a molecular formula of $Ca_{10}(PO_4)_6(OH)_2$, tricalcium phosphate (α-TCP, α-$Ca_3(PO_4)_2$), octacalcium phosphate ($Ca_8H(PO_4)_6 \cdot 5H_2O$). HAp is the main component of mineralized tissue, such as bones, dentine and cementum. Later, studies were conducted to form calcium-deficient hydroxyapatite (CDHA) with formula $Ca_9(HPO_4)(PO_4)_5(OH)$ since CDHA is considered to be compositionally closer to bone mineral than is stoichiometric HAp. [4, 5, 62]

Surgical treatment in traumatology, oncology, and orthopedics often leads to the formation of extensive bone defects. Defects are treated using calcium phosphate cements (CPCs) that offer a series of advantages such as: [6]

- The graft does not require a shaping.
- Minimum filler cavity.
- CPC is prepared during surgery.
- Excellent contact and connection between bone and graft.
- Biocompatibility and bioactivity of the material.

Calcium phosphate bioactive bone cements based on α-TCP have attracted increasing attention since the 1980s. The term "calcium phosphate cement" was introduced by Gruninger et al. [3] According to them, this type of cement can be prepared by mixing a calcium phosphate salt with water or with an aqueous solution to form a paste that reacts at room or body temperature, giving rise to a precipitate containing one or more calcium phosphates, which sets by the intercrossing of crystals of this precipitate. This cement consists of two components, one basic and one acid, which react when mixed with water, producing one or more products with an intermediary acidity. Among various biomaterials, calcium phosphate based materials including HAp, α-TCP and β-TCP are widely used as scaffold materials in bone tissue engineering. Nowadays, α-TCP is receiving growing attention as a raw material and major constituent of powder component for several injectable bone cements with *in situ* hydraulic setting, biodegradable bioceramics and composites for bone repair. [6–9]

1.1.1 Structural characteristics and its polymorphs

The chemistry of calcium phosphates is generally complex, and the phases with stoichiometry $Ca_3(PO_4)_2$ provide no exception. In the phase equilibrium diagram of the CaO-P_2O_5 system depicted in Fig. 1.1, three polymorphs corresponding to the composition of $Ca_3(PO_4)_2$ are recognized: the low-temperature β-TCP and the high-temperature forms, α- and $\bar{\alpha}$-TCP. The valid diagram for the CaO-P_2O_5-H_2O system in wet conditions is depicted in Fig. 1.2. [7, 10]

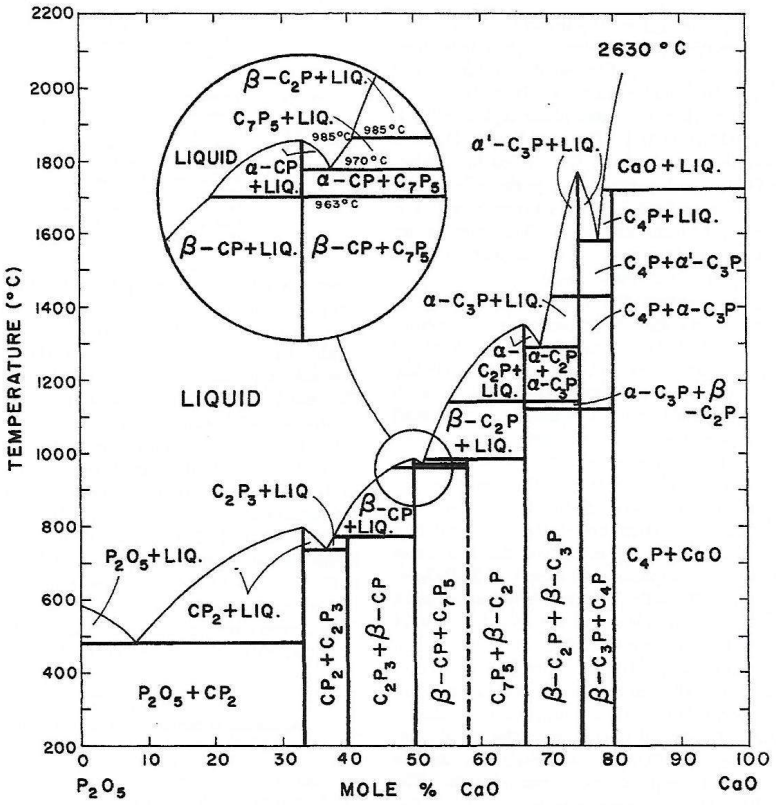

Fig. 1.1 – Equilibrium diagram for system CaO-P_2O_5, $C = CaO$; $P = P_2O_5$. *[10]*

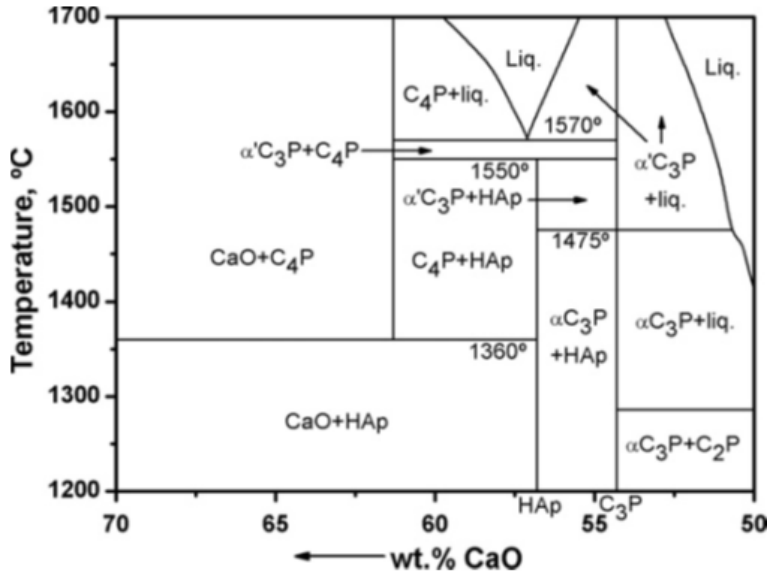

Fig. 1.2 – Equilibrium diagram for system $CaO\text{-}P_2O_5\text{-}H_2O$ *at a fixed* $p_{H_2O} = 500$ *mg Hg. [10]*

α-TCP is formed by heating the low-temperature polymorph β-TCP or by the thermal crystallization of amorphous precursors with proper composition above the transformation temperature. α-TCP phase may exist at room temperature in a metastable state, and its range of stability is strongly influenced by ionic substitution. [7]

α-TCP crystalline structure was related to that of the mineral glasserite ($K_3Na(SO_4)_2$) and studied by Dickens and Brown in 1972 and later studied in detail by Mathew et al. in 1977 and more recently by Yashima and Sakai [11], [12]. A brief general description of these phases was provided on the crystal structure of pure β-TCP by Dickens, Schroeder and Brown in 1974 [11]. The α-phase of $Ca_3(PO_4)_2$ is thermodynamically stable in temperature range between 1120-1470 °C in the absence of impurities. Below 1120 °C the β form is stable and α form is metastable. Above the temperature of 1470 °C the $\bar{\alpha}$ form is stable. [11]

α-TCP crystallizes in the monoclinic crystal system and belongs to the space group of $P2_1/a$ while β-TCP crystallizes in the rhombohedral crystal system belongs and belongs to the space group of R3C. On the other hand $\bar{\alpha}$-TCP crystallizes in hexagonal crystal system belonging to the space group of $P6_3/mmc$. Structural data and polymorphs of $Ca_3(PO_4)_2$ shows Tab. 1.1. There are a cell parameters (a, b, c, α, β, γ), cell volume (V), number of formula units per cell (Z), volume per formula unit (V_0), theoretical density (D_{th}) and the projections of the unit cells along the [0 0 1] direction.

Ca^{2+} and PO_4^{3-} ions constitute the unit cells of α-TCP. Polymorphs of Ca^{2+} and PO_4^{3-} ions are packed in columns along the [0 0 1] direction. Two types of columns exist in α-TCP structure: C-C and C-A. These types of columns are shown in Fig. 1.3 and in Fig. 1.4. C-C column contains only Ca^{2+} cations, and C-A column contains Ca^{2+} cations and PO_4^{3-} anions. Each C-C column is surrounded by six C-A columns, and in turn, alternating C-C and C-A columns to the total number of six surround each C-A column. The thin solid-line rhombus inscribed within the unit cell of α-TCP in Fig. 1.3 outlines a cell related to that of hydroxyapatite, in which the OH columns could replace the C-C columns at the cell corners. By analogy, the Ca-PO_4 columns in hydroxyapatite may be considered as high distorted C-A "columns"and each column is surrounded by three

C-A columns as in α-TCP, and by two C-C and one OH column. A significant structural difference between α-TCP and β-TCP is that there are no C-C columns in the β-TCP structure. Instead, there are two types of C-A columns in β-TCP: A columns with the sequence ...-P-Ca-Ca-P-..., and B columns with the order ...-P-Ca-Ca-Ca-P-P-.... Each A column is surrounded by two A and four B columns. In contrast, $\bar{\alpha}$-TCP consists of C-C and C-A columns alternating like in α-TCP. [7]

Property	β-$Ca_3(PO_4)_2$	α-$Ca_3(PO_4)_2$	$\bar{\alpha}$-$Ca_3(PO_4)_2$
Symmetry	Rhombohedral	Monoclinic	Hexagonal
Space group	R3C	$P2_1/a$	$P6_3/mmc$
a (nm)	1,04352(2)	1,2859(2)	0,53507(8)
b (nm)	1,04352(2)	2,7354(2)	0,53507(8)
c (nm)	3,74029(5)	1,5222(3)	0,7684(1)
α (°)	90	90	90
β (°)	90	126,35(1)	90
γ (°)	120	90	120
Z	21	24	1
V (nm^3)	3,5272(2)	4,31(6)	0,19052(8)
V_0 (nm^3)	0,1680(2)	0,180(6)	0,19052(8)
D_{th} ($g\,cm^3$)	3,066	2,866	2,702

Tab. 1.1 – Structural data and polymorphs of $Ca_3(PO_4)_2$. *[7]*

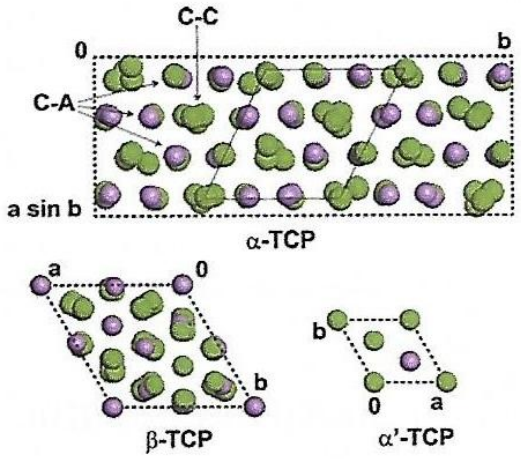

Fig. 1.3 – Schematic representation of the conformations of α-TCP, β-TCP and $\bar{\alpha}$-TCP unit cells along the [0 1 1] direction. Colors are: green – Ca^{2+}, purple – P^{5+}, O^{2-} ions has not been represented for the sake of clarity, C-C means cation-cation column; C-A means cation-anion column. The thin-line rhombus inscribed within the unit cell of α-TCP outlines a cell related to that of hydroxyapatite. [7]

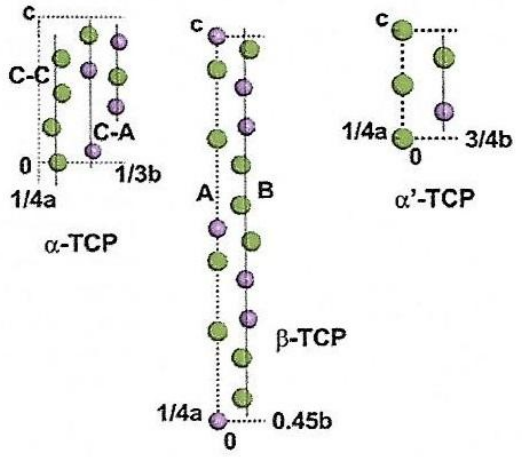

Fig. 1.4 – Fractional projections of α-TCP, β-TCP and ᾱ-TCP unit cells on the bc plane illustrate the disposition of constituent atoms in columns oriented along direction [0 0 1]. Colors are: green – Ca^{2+}, purple – P^{5+}, O^{2-} ions has not been represented for the sake of clarity, C-C means cation-cation column; C-A means cation-anion column. A means A column, B means B column. [7]

1.1.2 TCP – solubility and biodegradability

The structural differences between β- and α-TCP are responsible for their different chemical and biological properties, among them, solubility and biodegradability. The structure of α-TCP is less densely packed than β-TCP and more densely than $\bar{\alpha}$-TCP, as shown by their properties in Tab. 1.1. The difference in packing densities of the three polymorphs is consistent with thermodynamic consideration and with their stability temperature ranges. The difference between crystal structures of two polymorphs (α, β) of TCP shows the Fig. 1.5.

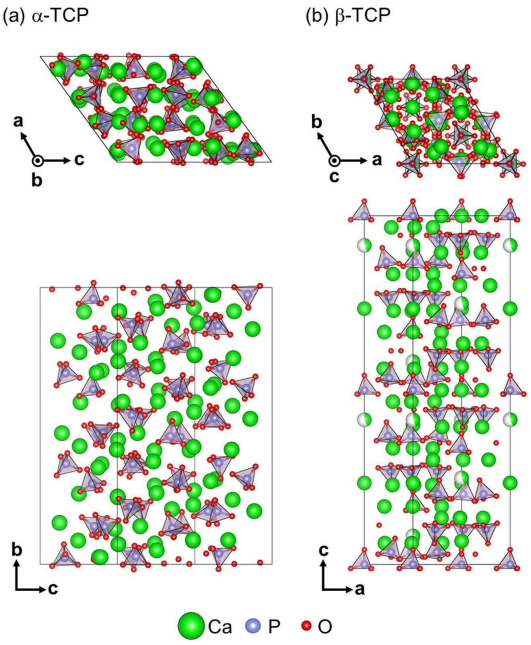

Fig. 1.5 – Crystal structures of α-TCP (a) and β-TCP (b). PO_4^{3-} *groups are represented by tetrahedrons for clarity. [20]*

Solubility

With structure correlation, it should be expected that the dissolution and degradation of the α-TCP structure proceeds faster than β-, as has been observed experimentally. The most important property of α-TCP is probably its solubility in water because the *in vivo* behavior of α-TCP can be predicted to a large extent by its solubility. α-TCP reacting with water leads to entangled network of CDHA crystals, which imparts high biocompatibility to the cement. This conversion is responsible for the setting and progressive hardening properties of the cement paste.

Classification of CPCs is depicted in Fig. 1.6. From top to bottom there are CPCs classified by the type of end-product (apatite or brushite), number of components in the solid phase (single or multiple), type of setting reaction (hydrolysis or acid-base reaction, setting mechanism and microstructure evolution during the setting). [52]

Hardening of apatitic calcium phosphate cements, in contrast to brushite cements, does not require use of acidic pH values. End products of hydrolysis of apatitic CPCs are HAp and CDHA. HAp can be formed by an acid-base reaction of tetra-calcium phosphate (TTCP) and slightly acidic dicalcium phosphate anhydrous (DCPA). CDHA is product of hydrolysis of metastable calcium phosphates, e.g. α-TCP. End product of hydrolysis of brushite CPCs is slightly acidic brushite ($4CaHPO_4 \cdot 2H_2O$). It can be obtained for instance by reaction between almost neutral β-TCP and acidic monocalcium phosphate monohydrate (MCPM, $Ca(H_2PO_4) \cdot H_2O$). Therefore it was considered that apatitic CPCs would be more biocompatible. [13–17]

The analysis reveals that at physiological pH (7.2-7.4) the concentration of Ca^{2+} and P^{5+} ions dissolved from calcium orthophosphates decreases in the order of TTCP > α-TCP > dicalcium phosphate dihydrate (DCPD) > DCPA > octacalcium phosphate (OCP) > β-TCP > HAp. Thought, in those conditions (37 °C), HAp is the most stable of all calcium orthophosphates, and in this way it should precipitate as α-TCP dissolution proceeds. [7]

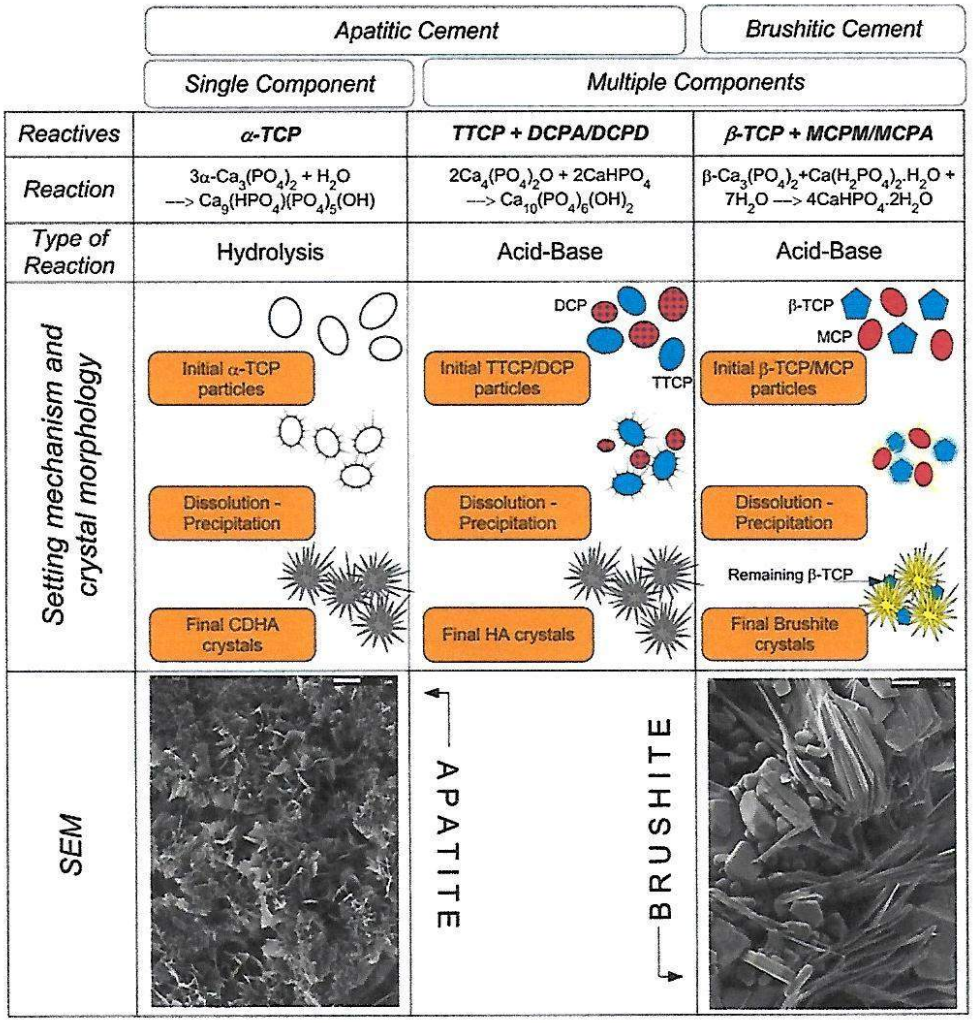

Fig. 1.6 – Classification of CPCs. From the top to bottom CPCs are classified by the type of end product. [52]

Porosity

The HAp-forming ability of porous α-TCP ceramics increases with surface area per unit pore volume of the samples when they have similar pore structure. A large surface area per unit pore volume leads to an increased local concentration of Ca^{2+} ions in the simulated body fluids impregnated into the porous body, increasing the degree of saturation with respect to HAp. Thus, the porosity and specific surface area are significant parameters for determining not only absorbability but also the ability to form HAp. [18]

The setting time of CPCs can be modified: [19]

(a) With a change of the powder size – smaller size ⇒ shorter setting time.
(b) With a change of the amount of mixing liquid – smaller amount ⇒ shorter setting time.
(c) By adding rapidly available calcium and/or phosphate ions (either pre-dissolved in the mixing liquid or as a freely soluble salt) – higher salt concentration ⇒ shorter setting time.
(d) By adding crystal nuclei, e.g. apatite nanocrystals for apatite cements, more nuclei ⇒ shorter setting time.
(e) By adding crystal growth inhibitors – more inhibitor ⇒ longer setting time.

It is important to control the dissolution behavior of α-TCP, because α-TCP is unstable in aqueous solutions systems and is eventually converted into HAp. For this purpose, addition of foreign cations was observed. Divalent cations such as magnesium (Mg^{2+}), strontium (Sr^{2+}) and zinc (Zn^{2+}) are often used as dopants in TCP. These foreign cations are known such as biologically active particles stimulated bone formation. Their role is not only in controlling the dissolution rate of TCP but also in promoting the bone formation. [7, 20]

In general, mechanical strength of CPCs is influenced by particle size of powders, liquid to powder ratio (L/P) and type of solvent used [48, 49]. Porosity is a main factor influences the mechanical properties of CPCs and porosity is related with L/P ratio as a main factor controlling the workability and injectability. A lower L/P ratio decreases the porosity, which results in an increase in mechanical strength. [16, 21]

Mechanical properties

Though, decreased porosity may result in decreased osteoconductivity. However, high compressive strength does not mean the capability of withstanding shear forces *in vivo*. Tensile strength is an important property in developing a formulation for *in vivo* applications. The compressive- and tensile-strength of most CPCs are diverse, ranging from 10-100 MPa for compressive strength and 1-10 MPa for tensile strength. Compressive- and tensile-strength depends on the formulation. Apatite cements usually fall in the higher end of this scale [16]. For comparison, compressive strength of human femur cortical bone ranging from 119-142 MPa depends on sex as shows Tab. 1.2. [59]

Accordingly, an increase of the L/P ratio improves fluidity, making the cement injectable through minimally invasive surgery techniques. However, the surgeon should not increase the L/P ratio on its own during a procedure if necessary because the porosity of the cement is affected and mechanical properties are drastically diminished. For this reason, the development of injectable bone cements is of real interest. In particular, the effect of citric acid is of real interest because citrate ions are present in bone mineral and play an important role in the formation and/or dissolution of bone apatite. A study showed

	Male	Female
Tensile strength (MPa)	39.74 ± 4.80	30.08 ± 7.96
Compressive strength (MPa)	146.6 ± 15.91	118.91 ± 18.99
Young´s modulus (MPa)	338.3 ± 179.74	404.7 ± 314

Tab. 1.2 – Mechanical properties of human cortical femur bone for female and male. [59]

that citric acid appeared to increase the fluidity of the cement pastes during the first stages of cement mixing. The dissolution-precipitation reactions of the α-TCP are retarded with the addition of citric acid and the compressive strength at saturation increased. In conclusion, citric acid can behave as a water-reducing additive. [22]

1.1.3 TCP – interaction with body fluids

It is known that the initial cellular response to the bone cement is partly dependent on the proteins absorbed onto the material surfaces. Because of dissolution of calcium phosphate (CaP) from the surface of the implant in the human body contributes to the bioactivity of the CaP surface, the dissolution property of CPC may be critical to implant success.

Dissolution study was performed by Schmitz, J.P. et al. They studied effects of biofluids environment on the dissolution and flexural strength of CPCs. They prepared CPC by mixing a Norian SRS (Norian Corp., Cupertino, CA) CaP powder with a buffered sodium phosphate liquid by hand and allowing the cement to set in a 27.4×2.4×2.6 mm mold in pH of 7.4 at 37 °C . Prepared cement bars were allowed to set for three days, removed from the molds, and sterilized overnight under ultraviolet light. Results of this study showed that there was a continual increase in Ca^{2+} and P^{5+} dissolution detected in all test media: Group I: 1.0 mol L^{-1} Tris buffer with 80 μmol L^{-1} NaCl; group II: 5% fetal bovine serum in Tris buffer with 80 μmol L^{-1} NaCl; group III: tissue fluid substitute containing 93.9 mmol L^{-1} NaCl, 1.24 mmol L^{-1} K_2HPO_4, 0.66 mmol L^{-1} K_2HPO_4, 0.94 mmol L^{-1} $MgCl_2$, 1.48 mmol L^{-1} of $CaCl_2$, and 18 mmol L^{-1} of $KHCO_3$) throughout the 21 days in pH 7.4 at 37 °C. No statistical difference in overal Ca^{2+} release in different media was observed. However, the P^{5+} release from Tris solution and fetal bovine serum solution was significantly higher than the P^{5+} release from tissue fluid substitute. Next measurement showed no significant difference in transverse strength for samples immersed in these solutions during the 21-day period. However, the transverse strength for immersed samples at 37 °C was statistically greater than the transverse strength for non-immersed bars. Thus, it was concluded from this study that the dissolution of Ca^{2+} from CPCs was independent of the dissolution media, whereas P^{5+} release was dependent on the constituents of the dissolution media. It was also concluded that the transverse strength of the CPCs was not significantly affected by the dissolution process but by the temperature at which the bone cement was exposed. [23]

Animal studies have been used to examine the bioresorption of CPCs, which can be defined as a removal of material by cellular activity and/or dissolution of the material in a biological environment. Bioresorption of CPCs generally occurs layer-by-layer, because the pores are typically considered too small to facilitate tissue ingrowth. Several animal studies focused on bioresorption are summarized in the Tab. 1.3 [24]. Apelt et al. implanted set cement samples in cylindrical bone defects with diameter 8 mm and 13 mm deep. They used sheep animal models [53]. Ooms et al. injected CPC paste into cortical bone defects of goats (diameter 5 mm) [54]. Knaack et al. implanted autologous bone implants of CPC

into femoral slot (0.5 mm×4-6 mm) defects in dogs [55]. Miño-Fariña et al. injected CPC into bone defects (diameter 0.6 mm, 8 mm deep) of rabbits. [56]

Author	Maximum duration	CPC type	Resorbed volume
Apelt et al.	26 weeks	ChronOS Inject (brushite)	60
		Experimental cement (brushite)	90
		Norian SRS (apatitic)	Bulk remained
Ooms et al.	24 weeks	Norian SRS (apatitic)	Bulk remained
Knaack et al.	26 weeks	Alpha-BSM (apatitic)	99
Mino-Farina et al.	12 weeks	Macroporous cement (apatitic)	65

Tab. 1.3 – A selection of animal studies investigating in the bioresorption of different CPCs. [24]

The variation of bioresorption may be attributed to inherent variation in animal studies, duration of the study, and also the type, size and porosity of CPC sample. Brushite CPCs generally resorb faster than apatitic-based CPCs. Faster resorption is due to metastability of brushite in body environment. Brushite CPCs is not only resorbed by natural remodeling process but also by physiochemical dissolution. Resorption rate was influenced by size of samples and their porosity which dictate a quantity of CPC. It was observed that smaller (Knaak et al.) and more porous (Miño-Fariña et al.) samples had faster rate of resorption than larger less porous samples (Norian SRS tested by Apelt et al. and Ooms et al.). Norian SRS had a lower porosity ($\sim 50\%$) than the macroporous apatitic cement tested by Miño-Fariña et al. ($\sim 75\%$). However, bioresorption process of CPCs and its influence is more complex that simply dictating the quantity of cement. [24]

The biological behavior of α-TCP-based biomaterials has been studied both *in vitro* [25–28] and *in vivo* [29, 31–36].

Mayr-Wohlfart et al. studied effects of four bone substitute on the growth behavior on the human-osteoblast-like cell line culture *in vitro*: three-dimensional porous scaffolds of pure α-TCP(α-TCP = BIOBASE®), a bioactive glass, a neutralized-glass ceramic, and solvent dehydrated bone. Their results showed that cells proliferate and differentiate into osteoproductive osteoblasts better on the α-TCP scaffolds than on the other materials tested. [25]

Effects on α-TCP and TTCP on the proliferation, differentiation a mineralization of cultures of newborn mouse were also *in vitro* studied. Results showed that the presence of α-TCP and TTCP promote osteogenesis by increasing collagen synthesis and calcification of the extracellular matrix. [26]

Similarly, surface- and non-surface-related cell viability of several commercial bone substitute materials, specifically α-TCP (BioBase, Germany) and β-TCP (Cerasorb, Germany), among them, was investigated towards cultures of human primary osteoblasts, bone marrow mesenchymal cells and non-adherent myelomonocytic cells. Results showed that α-TCP and β-TCP support surface- and non-surface-related cell viability. [27]

However, it was reported that α-TCP is more cytotoxic than HAp towards cultured Chinese hamster V79 lung fibroblasts. The cytotoxic study revealed that cytotoxicity of α-TCP resulted from a decrease in pH of the medium by the phosphoric acid, which produced by hydrolysis of the α-TCP. [28]

Kojic et al. presented the study of the irritant properties of calcium phosphate ceramics based on α-TCP after single application to intact skin of the rabbit. Results showed that the pure α-TCP solid material led to no skin irritation after 24, 48 and 72 hours of contact. Cement paste consists of pure α-TCP powder and phosphate solution (2.5 wt.% solution of Na_2HPO_4) at a liquid to powder ratio of 0.32 ml g^{-1} was investigated too. Results showed that skin contact with this paste led to no skin irritation after 24, 48 and 72 hours. [29]

Wiltfang et al. observed a degradation of α- and β-TCP in minipigs. In seven Goettingen minipigs 3.5–4.7 ml of cancellous bone defects were created in the area of tibial head on both sides. The defects were filled with either α- or β-TCP. After 86 weeks 95-97% of both (α- and β-TCP) were absorbed. Ceramic residual stayed within the newly formed trabeculae thus resisted degradation until remodeling occurred. The bone regeneration started from the borders of the defect and carried on centripetally. Both α- and β-TCP showed a comparable degradation process. After 86 weeks only small residuals of the ceramics can be found. These residuals stayed within the newly formed trabeculae, which showed a functional orientation. The α- and β-TCP material shows an accelerated degradation activity and has an optimal reactivity with the surrounding tissues. According to the results of this *in vivo* experiment both materials can be classified as bone-rebuilding materials. [30]

Biodegradation process of pure α-TCP particles was observed by Kihara et al. The purpose of this study was to determine the efficacy of α-TCP particles diameter 300 μm as a space maintainer in a bone defect. In this short-term work 14 rabbits were observed with prepared two cranial bone defects in each rabbit. One defect was left empty as a control and the other was filled with α-TCP particles. Particles worked well as space maintainers, preventing the invasion of the soft tissue into the wound, and demonstrated osteoconductive properties, with new bone growing on the surface of the particles and in the reticulate structures. [31]

The effects of blood to the CPC were observed. Biopex® (BPR) powders were mixed with the malaxation liquid. Chemical composition of powder and liquid is depicted in the Tab. 1.4. One minute later, fresh human blood was added to the mixture samples. Each sample was placed in a cylindrical plastic container to induce setting and was immersed into the simulated body fluid (SBF) immediately after setting and left standing at 37 °C. Results of Musha´s et al. experiments showed, that crystals on the cross section of blood-mixed CPC tended to be rather round, and the spaces between particle became larger as the blood content increased. The results indicate that the blood contamination can affect the microstructure of CPC crystals (BPR). The increase in the spaces between particles results to the increase of porosity, which implies that blood stimulates the hardened BPR to become more porous: accordingly the BPR becames more absorbable *in vivo*. Results of their following experiment showed the decrease in strength as the volume fraction of blood increased (different volume fractions of blood were used). Realized *in vivo* experiment showed that the absorption and the bone-replacement were the most advanced in highly blood-contaminated samples. [32]

BPR Powder	chemical formula	percentage volume
α-TCP	α-$Ca_3(PO_4)_2$	74.9
Tetracalcium phosphate	$Ca_3(PO_4)_2O$	18
Dicalcium phosphate dihydrate	$CaH(PO_4) \cdot 2H_2O$	5
Hydroxyapatite	$Ca_{10}(PO_4)_6(OH)_2$	2
Magnesium phosphate	$Mg_3(PO_4)_2$	0.1
Liquid phase	chemical formula	percentage volume
Sodium chondroitin sulfate		5
Disodium succinate	$(CH_2COONa)_2$	12
Sodium hydrogensulfate	$(NaHSO)_3$	0.3
Water	H_2O	82.7

Tab. 1.4 – Chemical composition of BPR powder and liquid. [32]

Turner et al. investigated CPCs in field of vertebroplasty. They used a canine model and showed that CPCs are biocompatible alternatives to poly(methyl methacrylate) (PMMA) cements in the treatment of large vertebral defects [33]. Osteoconductivity of α-TCP-based CPCs was tested in comparison with titanium-alloy rods (Ti-6Al-4V) and poly(methyl methacrylate) bone cement. CPCs were implanted into drilled holes in the left and right sides of the femoral condyles of adult New Zealand rabbits. Osteoconduction was evaluated by measuring the affinity index, bone density and X-ray diffraction at the implants after 1, 3 and 9 weeks as observation periods. X-ray diffraction patterns of HAp formed by hydrolysis of α-TCP-based bone filler powder showed higher and higher intensity in HAp peak with increase of time period. There was more bone density increase containing α-TCP-based bone filler powder around implant site than in the groups without α-TCP powder. It is suggested that HAp formed by hydrolysis of α-TCP-based bone filler powder will play some parts in enhancing osteconducting ability in clinical settings. [34]

Histological and histomorphometrical comparison study of α-TCP and β-TCP as a bone graft material for augmenting alveolar ridges of white Japanese rabbit was conducted. Porous blocks of α-TCP and β-TCP were inserted in titanium cylindrical cages, and the set was implanted in 0.5-mm-deep circular slits. Animals were sacrificed after 2, 4 and 8 weeks. Significant differences between both materials were observed after 4 and 8 weeks. The block of α-TCP started degrading after 4 weeks, while degradation of β-TCP blocks had just began at that time and scarcely progressed after 8 weeks. However, α-TCP block were degraded after 8 weeks and residual α-TCP particles surrounded by newly formed bone deceased over time. Both particles and newly formed bone were simultaneously absorbed by osteoclast-like cells. The results suggested that α-TCP particles surrounded by newly formed bone may disappear progressively and could be incorporated into the new bone formation cycle in combination with newly formed bone. [35]

α-TCP particles have also been investigated as drug carriers of simvastin, which is a drug able to stimulate bone morphogenetic protein (BMP-2) and vascular endothelial growth factor (VEGF) mRNA expression is osteoblasts and promote bone growth. Calvarial defects were created in adult Wistar rats and filled with α-TCP particles containing different doses of simvastin. Observation periods were 2, 4 and 8 weeks. Results showed that simvastin doses > 0.1 mg caused inflammation of surrounding tissue, but the microtomography analysis revealed that the α-TCP with 0.1 mg simvastin yielded significantly

higher volumes of bone than control group at all periods of time. The percentage of defect closure, bone mineral content and bone mineral density were higher in the group of α-TCP particles filler contained 0.1 mg of simvastin that in the others. α-TCP is a good carrier for simvastin and probably for other osteogenic drugs. [36]

Another study focused on drug-delivery property of α-TCP was provided by Colpo, J. C. et al. Their study is focused on antibiotic and anesthetic drug release from double-setting α-TCP. They prepared α-TCPand double-setting α-TCP(α-TCP DS) composed of acrylamide samples containing gentamicin sulfate, lidocaine hydrochloride, bupivacaine hydrochloride and levobupivacaine hydrochloride. α-TCP DS has better mechanical properties than traditional α-TCP cement. The α-TCP DS cement was able to store and transport the drugs tested, so it functioned as an *in vitro* controlled drug-release system. [37]

1.1.4 Biomedical applications of CPCs

Cements with a precipitation process occur at around neutral pH is the most suitable for biomedical applications [61]. CPCs are easy to use in case of surgical intervention, are capable of supporting bone tissue cell ingrowth into a material. CPCs are produced by mixing a reactive CaP powders with a liquid solvent to produce a rapidly setting paste [19]. An advantage of CPCs is that their setting is not accompanied by any heat release. Heat release might cause a necrosis of surrounding tissue, like in case of polyacrylate-based (e.g. poly(methyl methacrylate)) polymer cements. [38]

Polymer-based CPCs

A mixture of α-TCP and β-TCP as a powder phase and aqueous solution of 2 wt % Na_2HPO_4 as the liquid phase have been used to produce a CPC. Results showed that α-TCP was fully hydrolysed to CDHA, whereas β-TCP remained unreacted and embedded in the CDHA matrix. Increasing percentage representation of β-TCP phase resulted in an increased setting time and a reduction in the compressive strength of the set cement. In point of fact pastes produced with only β-TCP and water are generally regarded to be non-setting and are used as a model paste system to represent unset CPC. [24]

A major issue inhibiting successful delivery of CPC is the occurrence of phase separation during injection process. A phase separation mechanism observed during extrusion of pastes is depicted in Fig. 1.7. There are illustrated main 3 mechanisms of phase separation: [24]

(i) *Filtration* in the barrel, where the pressure exerted by the plunger on the paste causes drainage of the liquid phase. It leads to consolidation of solid phase.

(ii) *Suction*, driven by the dilation of the powder phase network as it flows into the matrix.

(iii) *Filtration* in the needle exacerbated with the formation of solid mats.

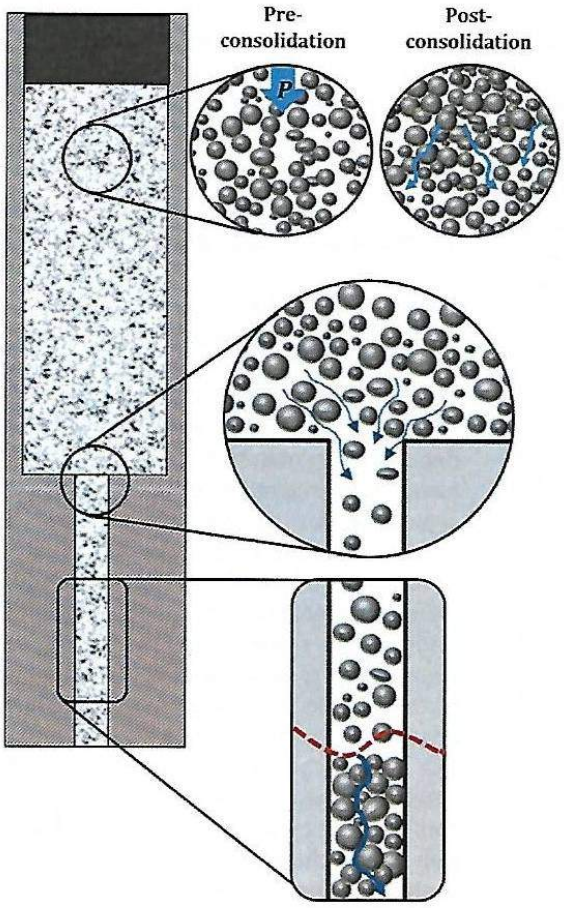

Mechanism (i): Filtration. When the pressure, *P*, exerted on a paste is high relative to the permeability of the paste system, consolidation of the powder phase and drainage of the liquid phase occurs.

Mechanism (ii): Suction. If the solid volume fraction of a paste is sufficiently high, particles must move apart to enable flow, i.e. the powder must dilate. Liquid is then drawn through the powder network to fill voids created by the dilating powder.

Mechanism (iii): Filtration in the needle. Above the red dotted line represents normal flow in die, below the same line shows the formation of a solid mat or powder blockage. As the powder is static or slow moving in the die, but the plunger is still moving, the liquid must flow through the mat, until the mat is broken

Fig. 1.7 – Phase separation mechanism observed during extrusion of CPCs. Schematic diagram is not on scale. [24]

Injectable CPCs are formed by a reactive CaP powders with a polymeric matrix as a liquid phase of system. One of the main advantages of injectable systems as tissue engineering devices is their ability to allow for the use of minimally invasive surgical procedures. These procedures minimize the damaging effects of large muscle retraction, reduce the size of scars and reduce postoperative pain, allowing the patients to achieve rapid recovery. The polymeric system also offer the possibility of incorporation of particles of various sizes (microspheres, nanospheres, etc.) which might encapsulate cells, growth factors or drugs and deliver them to the target location. Some common polymers used in CPCs are for example chitosan, poly(lactide), poly(ethylene glycol), poly(lactic-co-glycolic acid), i.e. PLA-PEG-PLA (PLGA) and poly(ortho esters). [17, 24]

Amphiphilic copolymers in bone regeneration

Properties of an amphiphilic degradable polymer/HAp composite were investigated by Kutikov A. B. and Song J [57]. They modified hydrophobic poly(lactic acid) (PLA) by hydrophilic poly(ethylene glycol) (PEG). The triblock copolymer PLGA was synthetized by melt ring-opening polymerization. HAp-PLGA composite better promoted osteochondral lineage commitment of bone marrow stomach cells in unstimulated culture.
HAp-PLGA also supported far more potent osteogenic gene expression upon induction than HAp-PLA. They demonstrated that the chemical incorporation of PEG is an effective strategy to improve the performance of degradable polymer/HAp composites for bone tissue engineering applications. [57]

Study of CPC scaffolds with PLGA fibers provided Vasconcellos, L. A. and Dos Santos, L. A [40]. Preparation of their scaffolds was provided by following steps. First of all, the lyophilized fibers were selected, separated (to maintain mixture homogeneity) and mixed with α-TCP powder (in levels of 0, 1, 2, 3, 4 % in volume) and added to the paraffin spheres followed by the liquid phase at the rate of 1 ml per 1 g of cement. Paraffin spheres as porogen were added in 57, 63 and 66 % (percentage per volume). The paste was placed in various types of molds: stainless steel molds and two types of silicone molds. Than samples were put in the container at 100% humidity and placed in a furnace at 37 °C for 48 h. After 48 h they were removed from their molds and put into heating and chemical treatment to extract the paraffin. Samples were placed on adsorbent paper and extracting the paraffin in an oven at 100 °C for 24 h and then the samples with PLGA were submerged in hydrogen peroxide for 48 h at room temperature and returned to the oven at the temperature of 100 °C. Results of resistance compression tests showed that composite PLGA fiber decreased compressive strength in relation to pure α-TCP sample. Cytotoxicity assays α-TCP-based CPC with 3 % PLGA had the degree index zone equal to two, which means slight cytotoxicity. [40]

Barbieri, D. et al. studied influence of polymer molecular weight in osteoinductive composites for bone tissue regeneration. They prepared two composites by extruding two different molecular weights of L/D,L-lactide copolymers with calcium phosphate apatite. Weight average molecular weight (M_w), number average molecular weight (M_n) and polydispersity of the two polymers as determined with gel permeation chromatography (GPC) are listed in the Tab.1.5. Results of this study showed that lower molecular weight copolymer allowed larger fluid uptake in the composite thereof, which was correlated with a higher capacity to adsorb proteins *in vitro*. They provides following study of intramuscular implantation in sheep. Results of *in vivo* study showed that only the composite with the lower molecular weight polymer could induce heterotopic bone formation. [41]

	Polymer as supplied	polymer extuded alone
	M_w (kDa)	M_w (kDa)
	M_n (kDa)	M_n (kDa)
	polydispersity	polydispersity
sample M38	758.5	555
	513	400.5
	1.46	1.38
sample M60	1096.5	776
	652.5	489.5
	1.68	1.59

Tab. 1.5 – Molecular weights and polydispersity of polymers. [41]

α-TCP-based materials have limited bone cement application and are typically used in dentistry, orthopedics, craniofacial and maxillofacial surgery, vertebroplasty and kyphoplasty procedures, and as a drug carriers [51]. CPC has showed as suitable material for watertight closure in transtemporal surgery. [42] α-TCP-based CPCs are very hard materials that can be used for filling bone defects as well as for joining another (e.g. metallic) biomaterial with bone tissue [13]. List of commercial α-TCP-based apatite ending CPCs with their brand names and compositions shows Tab. 1.6.

Manufacturer	Brand name	Components
Teknimed SA, France	Cementek®	*Powder:* α-TCP, TTCP, Na glycerophosphate *Solution:* H_2O, $Ca(OH)_2$, H_3PO_4
Teknimed SA, France	Cementek LV®	*Powder:* α-TCP, TTCP, Na glycerophosphate, dimethylsiloxane *Solution:* H_2O, $Ca(OH)_2$, H_3PO_4
Biomet, Europe	Calcibon®	*Powder:* α-TCP (61%), DCP (26%)[1], $CaCO_3$ (10%), PHA (3%)[2] *Solution:* H_2O, Na_2HPO_4
Biomet, USA	Mimix®	*Powder:* TTCP, α-TCP, $(C_6H_5O_7Na_3) \cdot 2H_2O$ *Solution:* H_2O, $C_6H_8O_7$
Mitsubishi materials Co., Japan	Biopex®	*Powder:* α-TCP (75%), TTCP (18-20%), DCPD (5%)[3], HAp (0-2%) *Solution:* H_2O, sodium succinate (12-13%), sodium chondroitin sulphate (5-5.4%)
Mitsubishi materials Co., Japan	Biopex-R®	*Powder:* α-TCP, TTCP, DCPD, HAp, $Mg_3(PO_4)_2$, $NaHSO_3$ *Solution:* H_2O, sodium succinate, sodium chondroitin sulphate
Kyphon	KyphOs™	*Powder:* $MgHPO_4$ (4.8%), $Mg_3(PO_4)_2$ (14%), α-TCP (77%), $SrCO_3$ (14%) *Solution:* H_2O, $(NH_4)_2HPO_4$ (3.5 M)
Synthes-Norian, USA	Norian SRS® Norian CRS®	*Powder:* $CaCO_3$ (12%), MCPM (3%)[4] α-TCP(85%) *Solution:* H_2O, Na_2HPO_4
Biomatlante, France	MCPC™	*Powder:* α-TCP, ACP[5], BCP[6]
Skeletal Kinetics, USA	Callos™	*Powder:* α-TCP, $CaCO_3$, MCPM

Tab. 1.6 – List of commercial α-TCP-based CPCs with their compositions. [7, 19]

Hydraulic cements based on α-TCP are usually composed of many others components. For example, hydraulic cements based on α-TCP-sulfate dehydrate mixtures (CSD) were invented in 2004. The addition of CSD powder to α-TCP-water cement mixtures strongly decreased their setting time, particularly when the phosphate concentration was high. TCP/chitosan in combination with autologous platelet-rich plasma turned out to be an injectable material for the treatment of bone defects. The introduction of platelet-rich plasma into TCP/chitosan can improve the biocompatibility and osteoinductivity of TCP/chitosan without compromising its mechanical strength or injectability. [43, 44]

Post-implanted infections are severe problem in orthopedic surgery. In the Siek´s, D. et al. study α-TCP-based silver doped hydroxyapatite CPCs were examined. Their materials showed mild antibacterial activity which depended on the kind of bacterial strain and the

[1]Dicalcium phosphate
[2]Precipitated hydroxyapatite
[3]Dicalcium phosphate dihydrate
[4]Monocalcium phosphate monohydrate
[5]Amorphous calcium phosphate
[6]Biphasic calcium phosphate

type of test. Presence of silver in the tested materials increased the antibacterial activity in the extracts only for E. coli strain. They also observed reduction of osteoblast viability *in vitro* resulted from the synergic effect: decrease in concentrations of Ca^{2+}, Mg^{2+}, and PO_4^{3-} ions in the culture medium and the presence of silver ions. [45]

Interconnecting macroporosity enhances bone regeneration allowing stabilization of the defects and improves the healing process. Methods used to enhance macroporosity of CPCs include the addition of porogenic agents.

Used porogenic agents can be divided into following groups: [24, 46]

- Gas generating compounds – e.g. sodium bicarbonate
- Water-soluble agents – e.g. albumen, gelatin, soybean gelatin combinations
- Low molecular weight surfactants – e.g. Polysorbate 80, Poloxamer 407
- Other used – e.g. mannitol, sucrose.

Douglas, T. E. L. et al. observed self-gelling injectable mineralized hydrogel/α-TCP composites for bone regeneration. The Ca^{2+} ions released during α-TCP hydrolysis can be exploited to crosslink anionic, calcium-binding polymers such as polysaccharide gellan gum (GG) to induce hydrogel formation. In their study, three different amounts of α-TCP particles were added to GG polymer solution to generate novel, injectable hydrogel-inorganic composites. Their results demonstrated the potential of composites as alternatives to traditional α-TCP-based bone cement. Potential advantage of combining α-TCP with the GG hydrogel phase is the incorporation of biologically active, water-soluble molecules in the hydrogel phase. [47]

2 MAIN AIMS OF MASTER´S THESIS

The main goal of presented master´s thesis was observing structure and mechanical properties of CPCs samples based on thermosensitive copolymer and α-TCP set in simulated and native body fluids. The individual steps of proposed master´s thesis can be summarized as follows:

1. Determination of optimal weights and ratios of chemicals for preparing samples.
2. Optimization of the setting mold to enable the highest interaction with the liquid environment, surface treatment to the required dimensions and way of ending the setting reactions performed in liquid environment.
3. Performance setting reactions in body fluids environments:
   (a) synthetic (simulated plasma) - physiological solution, Ringer´s and Hank´s solutions
   (b) native - heparinized pig blood.
4. Chemical, morphological and biomechanical evaluation.
5. Comparing and discussing effects of the setting liquids on the CPCs structures and properties.

3 EXPERIMENTAL WORK

In the experimental work, chemicals, sample preparation process and used methods are described.

3.1 Chemicals

Following chemicals were used in the experimental work:

(a) Chemicals for CPC sample preparation:
α-TCP - was purchased from Premier Biomaterials Co. Tipperary, Ireland.
Monocalcium phosphate (MCP) – was purchased from Sigma-Aldrich Co., St. Loius, USA.
Polymer – triblock copolymer of PLGA-PEG-PLGA, synthetized at BUT according to Michlovská et al. [58]
Ethanol - absolute p.a. was purchased from Penta, s. r. o., Praha, Czech Republic.

(b) Chemicals for setting environments:
Physiological solution – NaCl 0.9% - was purchased from Braun, Melsungen, Germany.
Hank´s balanced salt solution - was purchased from Sigma-Aldrich Co., St. Louis, USA.
Ringer´s tablets for the preparation of Ringer´s solution – was purchased from Merck Co., Praha, Czech Republic. Ringer´s solution was prepared by autoclaving (121 °C, 20 min) at Veterinary Research Institute, Brno, Czech Republic.

(c) Other chemicals:
Hydroxyapatite - calcined at 1000 °C/1 h, with chemical formula $Ca_{10}(PO_4)_6(OH)_2$, mean particle size 130 nm, specific surface area 4.7 $m^2\ g^{-1}$, was manufactured by Riedel-de Haen, Germany.

3.2 Sample preparation

3.2.1 Preparation I.

First of all, samples were prepared and their setting was performed in ultrapure water. The reason was to test new preparation technique including the use of porous polyurethane foam as a mold. Construction of polyurethane mold and used equipment shows the Fig. 3.1(b). There is depicted older rubber mold too (Fig. 3.1(a)).

Sample preparation was consisted of several separate phases:

- Drying phase of powders (α-TCP, MCP) - at 110 °C for 24 hours.
- Cooling phase of 20% copolymer solution mixture with potassium buffer - at 5 °C.
- Mixing phase of powders - addition of α-TCP (98 wt %) to the MCP (2 wt %) and homogenized for 1 minute.
- Mixing phase of mixture of powders with polymer-buffer solution - homogenized properly for 30 seconds with L/P = 0.5. Homogenous mass was sticky and had consistency similar to toothpaste.

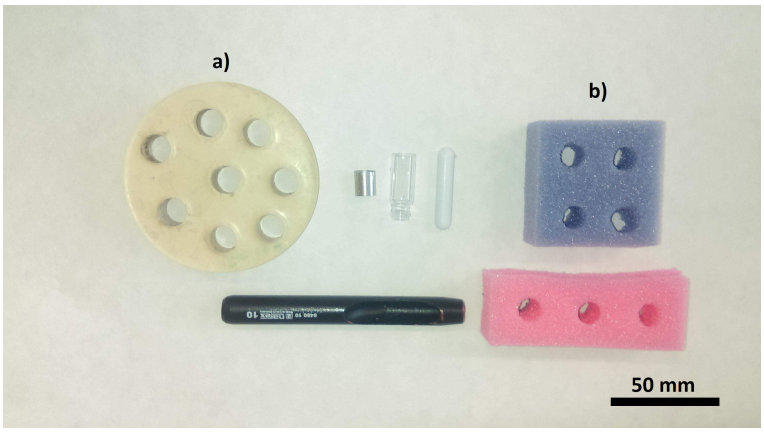

Fig. 3.1 – Constructions of used setting molds: a) rubber mold, b) polyurethane molds.

- Homogenous mass was dosed into polyurethane mold.
- Setting phase - in ultrapure water environment at 37 °C for 3 days.
- Ending of setting phase - set samples were covered with liquid nitrogen and then were freeze-dried cause to stop setting reactions.

3.2.2 Preparation II.

Preparation was consisted of the same steps as in sample preparation I., but weights of chemicals and ending of setting were different. L/P ratio was not changed (L/P = 0.5). A new type of mold was used. The new mold was made from memory foam material. Constructions of used setting molds with bone-cement are depicted in Fig. 3.2. Preparation was performed analogously by two operators. Prepared bone cement was set in ultrapure water at 37 °C for 3 days. Ending of setting reactions prepared bone cement was provided with cold absolute ethanol (100%, 5 °C , 2 hours). Samples were dried on air after taking out from ethanol. Then samples were vacuum dried after 3 days for 4 hours. Surface of samples was modified by hand sharpening to cylindrical shape with proportions ratio 1.5 -2 : 1 equal depth to diameter.

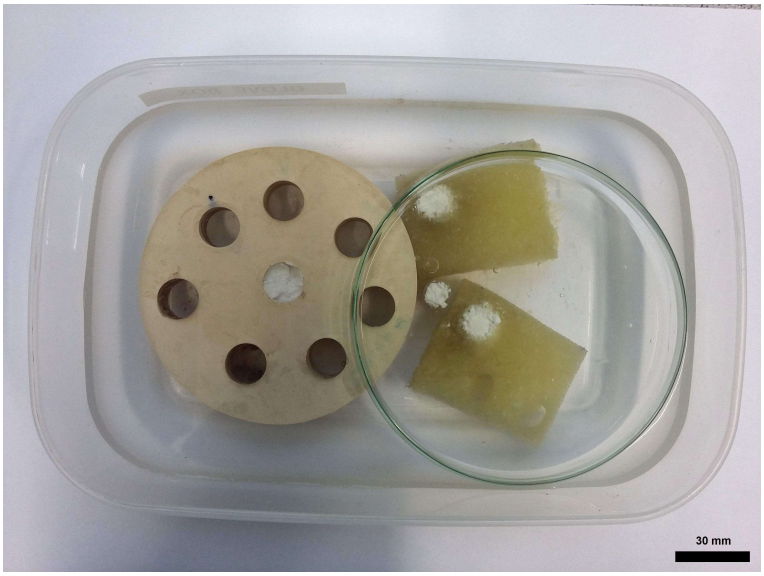

Fig. 3.2 – Used molds with bone cement inside.

3.2.3 Preparation III.

Preparation was consisted of the same steps as in sample preparation I. and II. but the weights of chemicals were different and L/P ratio was not changed (L/P = 0.5). Prepared bone cement was set in ultrapure water at 37 °C for 3 days. Memory foam was used as material of setting mold. Ending of setting reaction was performed by using a cold ethanol (5 °C, 2 hours), than samples were vacuum dried according to time-table depicted in the Tab. 3.1. Samples were left in an evacuated chamber without tempering overnight after first and second period of drying. Surface of samples was modified by machine milling to cylindrical shape with proportions ratio 1.5 -2 : 1 equal depth to diameter.

Period	Temperature (°C)	time (hours)
1.	26	2
2.	37	8
3.	37	5

Tab. 3.1 – Time-table of vacuum-drying phase.

3.2.4 Preparation IV.

Based on previous results, this preparation was consisted of the same steps as in previous experiments but the weights of chemicals were different and L/P ratio was not changed (L/P = 0.5). Dry setting mold was situated into plastic boxes and heated at 37 °C before dosing a cement paste to the mold. The paste was immediately after mixing transferred to a 2 ml syringe with an 2.38 mm outlet diameter and piston area equal to 65.76 mm^2. The extrusion of cement paste to the setting memory foam mold was provided immediately after mixing liquid with powders. The volume of each sample is approximately 1.3 ml. Setting mold with prepared samples was put into incubator at 37 °C for half an hour. Than setting mold with prepared samples was taken out and memory foam mold was moistened as much as possible with setting liquid. Prepared bone cement was setting in four setting environments at 37 °C. Physiological solution, Hank´s solution, Ringer´s solution and heparinized whole pig blood were used as a liquid setting environments. Physiological solution represent an isotonic solution with human blood plasma. Hank´s and Ringer´s solutions represents SBF as a protein-free solutions with ion concentration similar to those of human blood plasma. Chemical compositions of used Hank´s and Ringer´s solutions are depicted in the Tab. 3.2. [63, 64] Setting liquids were refreshed every 3 days.

These setting times were determined as follows: 12 hours, 1 day, 3 days, 1 week, 2 weeks and 1 month. After 3 days of setting, each sample was taken out from setting mold and continued setting in plastic dose. In a quantity of 3 samples were prepared for each setting period and for each setting environment. Ending of setting reactions was performed by using a cold ethanol (5 °C, 2 hours), than samples were vacuum dried to constant weight (for 10 hours). Surface of samples was modified by machine milling to cylindrical shape with proportions ratio 1.5 -2 : 1 equal depth to diameter.

	Ingredients	concetration ($mg\ L^{-1}$)
Hank´s solution	Inorganic salts	
	Sodium chloride	8000.000
	Potassium chloride	400.000
	Calcium chloride dihydrate	185.400
	Sodium bicarbonate	350.000
	Magnesium sulfate heptahydrate	200.000
	Potassium phosphate monobasic anhydrous	60.000
	Sodium phosphate dibasic heptahydrate	90.000
	Other	
	Dextrose anhydrous	1000.000
Ringer´s solution	Inorganic salts	
	Sodium chloride	2250.400
	Potassium chloride	105.000
	Calcium chloride	120.000
	Sodium bicarbonate	50.000

Tab. 3.2 – Chemical compositions of Hank´s and Ringer´s solutions. [63, 64]

3.3 Methods

3.3.1 Chemicals characterization techniques

Morphology by Scanning Electron Microscopy (SEM)

Morphology of CaP powders was studied using scanning electron microscopy MIRA3 Tescan, Czech Republic. Samples were applied to carbon straps then Au/Pd sputtered (Leica EM ACE600) in ratio of Au/Pd equal to 80 : 20 and observed with using secondary electron (SE) detector with work distance 15 mm, beam intensity 10 and HW 10 kV. Used scan mode was depth.

Particle size measurement

Distribution of particle size was measured at the LA-950 Horiba, Japan. α-TCP powder was dispersed in water, MCP powder was dispersed in ethanol. Both samples were ultrasonicated for 30 minutes before the measurement.

Nuclear Magnetic Resonance (NMR)

Polymer characterization were confirmed using proton nuclear magnetic resonance spectroscopy on 700 MHz Bruker AVANCE III HD instrument using 128 scans in deuterated chloroform solvent at 25 °C. Chemical shifts were reported in ppm relative to tetramethylsilane. ^{1}H NMR spectra were evaluated using ACD/1D NMR Processor.

3.3.2 Sample preparation techniques

Milling

Sample machine milling was performed by using AZK, Troll HWT E-442 CNC, Czech Republic. Samples were situated on highly-adhesive tape. Cylinders of 6 ± 1.1 mm in diameter and 12 ± 3.4 mm in length were milled from bone cement samples. CNC codes were created using by Autodesk Inventor Professional 2018 (sample modeling) with Autodesk HSM Ultimate 2018 module (parametres setting and modeling of milling trajectories). Generated code was uploaded to Comets control system.

3.3.3 Sample characterization techniques

pH measurement

Solution pH were measured at the pocket pH meter H138 Minilab Hach, USA at laboratory temperature of 23 °C.

Mechanical test in compression

Samples after machine milling were compression tested using by Zwick/Roell Z010, USA using a cross speed of 1%/min, load equal 1 kN and preload equal 10 g at room temperature of 23.5 °C. The average compressive strength of 3 cylinders with standard deviation (SD) was calculated. Measured data were collected and evaluated by testXpert software version 3.61.

X-ray diffraction analysis (XRD)

The kinetic study of transformation of α-TCP to CDHA by X-ray diffractometer Rigaku MiniFlex 600, Japan was performed. Broken samples after mechanical testing and fracture analysis by SEM were crushed in ceramic mortar and pestle by hand to obtain a fine powder to be characterized by XRD. Powder was placed into glass holder with Bragg-Brentano geometry, accelerating tube voltage 40 kV and a tube current 15 mA, having 1D detector IHS 10.0 mm (divergence slit: 1.250 deg, scattering slit: 8.0 mm, receiving slit: 13.0 mm) with K-beta(x1) filter in scan range 5-50 deg. at room temperature of 24 °C. Diffraction data of analyzed samples were collected and evaluated by PDXL2 software. Calculation of w_t represents an average percentage amount of α-TCP in CPC sample was provided. Results of w_t calculation were used to construction of graph shows a conversion of α-TCP to CDHA with calculated SD from values of integrated intensities for 5 selected peaks.

Attenuated Total Reflectance Fourier Transformed Infrared Spectroscopy (ATR-FTIR)

Chemical analysis of CaP powders and CPC samples were investigated using by attenuated total reflectance Fourier transformed infrared spectrometer (ATR-FTIR) Bruker Vertex 70v with diamond ATR crystal in a range between 4500-500 cm^{-1}. The measurements were provided in vacuum (100-200 Pa). Chemical analysis of copolymer was investigated by ATR-FTIR Bruker Tensor 27 with diamond ATR crystal in the same

conditions. CaP powders and copolymer were measured after direct application on the ATR-crystal. All spectra (128 scans at 4 cm^{-1} resolution) were recorded at laboratory temperature and evaluated by Opus 7.5 software.

X-ray computed microtomography

The processed data have been acquired using a GE Phoenix v|tome|L240 computed tomography system equipped with a 70 kV/120 μA high-power nanofocus X-ray tube and a flat panel GE DXR detector array (voxel size equal 8 μm). The scan was carried out in an air-conditioned X-ray cabinet at 21 °C. Tomographic data for histogram constructions to evaluated porosity were collected and evaluated by VGSTUDIO MAX 3.1.1 software. 3D-visualisation were provided by MyVGL software.

4 RESULTS AND DISCUSSION

In this chapter, results of master´s thesis are presented. First of all, powder and polymer characterization are resulted with view to morphology provided by Scanning Electron Microscopy (SEM), particle size measurement and copolymer chemical composition analysis provided by Nuclear Magnetic Resonance (NMR). Results of preparations are presented and discussed.

4.1 Powder and polymer characterization

Morphology

Micrographs of used CaP powders are depicted in Fig. 4.1 (α-TCP) and in Fig. 4.2 (MCP).

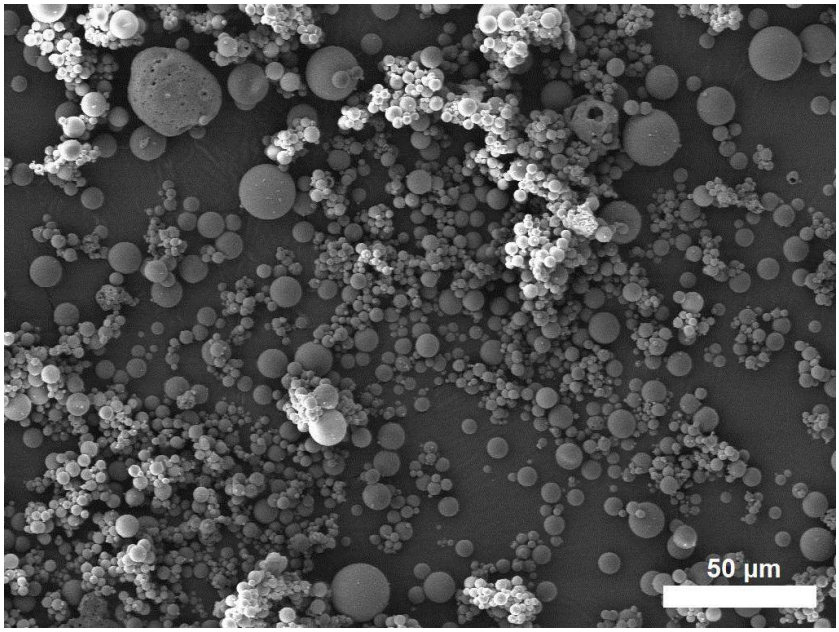

Fig. 4.1 – Scanning electron micrograph of used α-TCP.

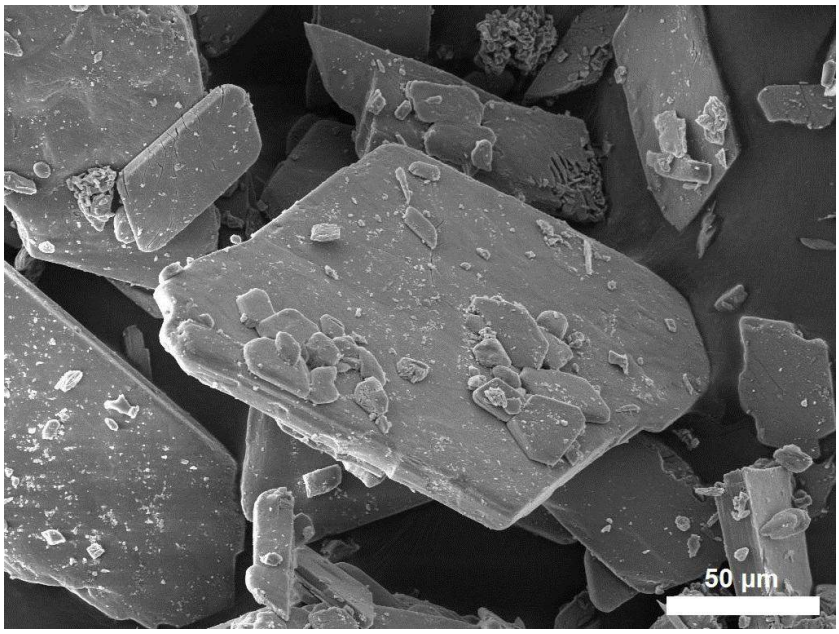

Fig. 4.2 – Scanning electron micrograph of used MCP.

Particle size measurement

Diameter distribution of α-TCP particles shows graph in Fig. 4.3. Mean particle size distribution was equal to 6.3 μm. α-TCP is formed largely by spherical particles.

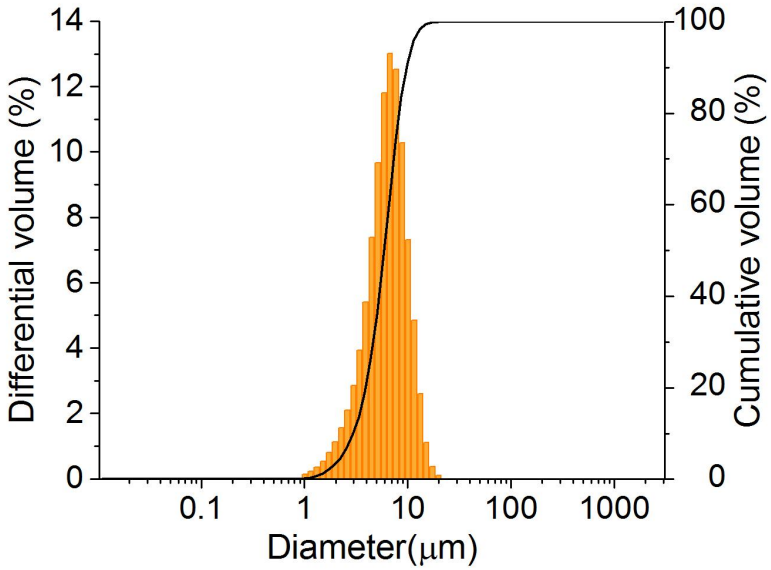

Fig. 4.3 – Graph of the diameter distribution of α-TCP particles.

Diameter distribution of MCP particles (used for setting acceleration) shows graph in Fig. 4.4. Mean particle size distribution was found of 51.5 μm. Graph shows bimodal distribution of particle diameters due to presence of agglomerates or non-isometric character of particles. However, this powder dissolves very fast and already after 12 hours there is no detectable amount of MCP (see XRD technique).

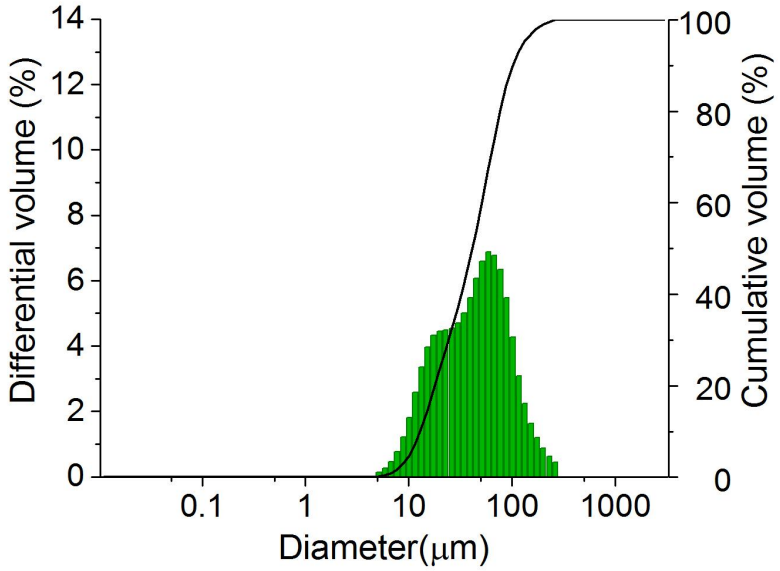

Fig. 4.4 – Graph of the diameter distribution of MCP particles.

Copolymer chemical composition

PLGA-PEG-PLGA triblock copolymer with PLGA/PEG weight ratio equal to 2.47 and PLA/PGA molar ratio equal to 2.96 was synthesized via ring opening polymerization. Molecular weight M_n and molar composition of sample was determined by ^{1}H NMR spectroscopy and calculated by comparing lactic acid (LA) methylene (1.55 and 5.17 ppm), glycolic acid (GA) methylene (4.80 ppm) and PEG methylene (3.65 ppm) integrations as we reported previously [58]. Molecular weight determined by ^{1}H NMR (5210 g mol^{-1}) was in very good agreement with theoretical value (5250 g mol^{-1}).

Nuclear magnetic resonance (NMR)

Spectrum of the triblock copolymer of PLGA-PEG-PLGA is depicted in Fig. 4.5.

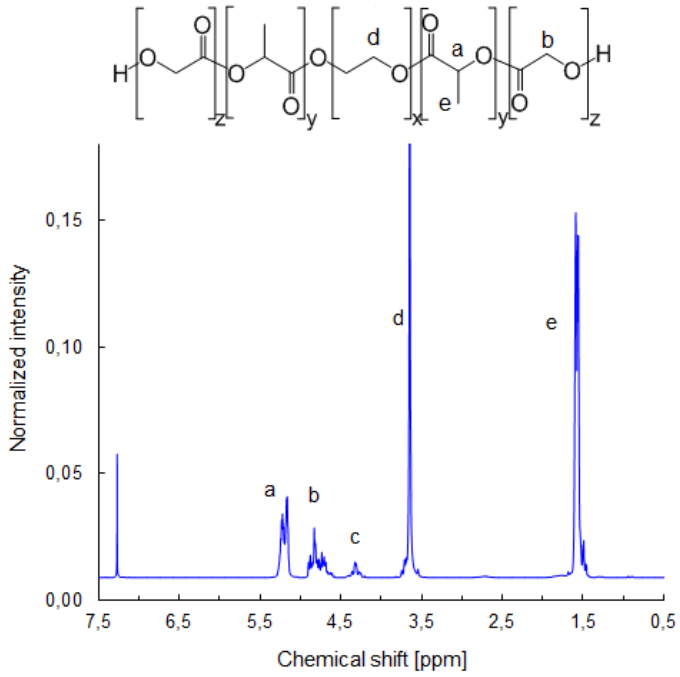

Fig. 4.5 – NMR spectrum of triblock copolymer of PLGA-PEG-PLGA. Peak "a" belongs to the hydrogen in CH group of lactide; peak "b" belongs to the hydrogen in CH_2 group of glycolide; peak "c" belongs to hydrogen in end group between PLGA and PEG; peak "d" belongs to CH_2 hydrogens in PEG; peak "e" represents hydrogens in CH_3 group in lactide.

4.2 Preparation I.

The problem of generally used rubber mold is bad accessibility of fluids to the sample due to its low porosity. The contact between fluid and sample was practically only from up and down side of sample. Therefore, new high porous polyurethane mold was used. Appearance of samples set in polyurethane mold shows Fig. 4.6. Samples had uneven shape with irregular surface. Little CPC spheres coming from porous mold appeared on the surface of samples. Also a small amount of polyurethane mold adhered on the CPC surface. Unfortunately, this way of ending of setting reactions with liquid nitrogen proved to be inappropriate, because samples cracked. The reason of samples cracking could be high internal tension of gasses formed by reaction of liquid nitrogen with water. Ending of setting reaction was carried out with cold ethanol within following experiment.

Fig. 4.6 – The appearance of samples set in polyurethane mold.

4.3 Preparation II.

Appearance of samples after setting in ultrapure water for 3 days shows Fig. 4.7. Samples set in memory foam had uneven shape with irregular surface. Little CPC spheres adhered on the sample surface together with a small amount of memory foam mold. Another disadvantage is disposing memory foam mold that can be used for preparation of only one sample. The memory foam mold was damaged after sample taking out. Sample set in the polypropylene (PP) hose had a regular shape and smooth surface with no visible pores. On the other side, sample set in the rubber mold had a lot of surface pores different sizes. The bigger pores could be caused by preparation procedure. Metal spatula was used to fill the setting molds. The small pores on the sample set in rubber mold surface proof porosity of used setting mold material. Ending of setting reactions was provided with using cold ethanol. The amount of bone cement in vials after taking out samples from ethanol remained. Most residues were in vial with samples set in memory foam. This could affect the structure and properties of the final bone cement. Vials with cement residues shows Fig. 4.8. Samples were hand-sharped to the sizes of 12 mm×6 mm. Appearance of hand-sharped samples are depicted in Fig. 4.9. Visible pores are on the surfaces of samples prepared in plastic hose and memory foam, on the other side on the surface of sample prepared in rubbery mold no visible pores appeared. Sample fractures were investigated by using SEM. Scanning electron micrographs are depicted in Fig. 4.10, 4.11 and 4.12.

The most advanced HAp formation of sample set in memory foam mold was observed due to the best access of setting fluids to the sample surface.

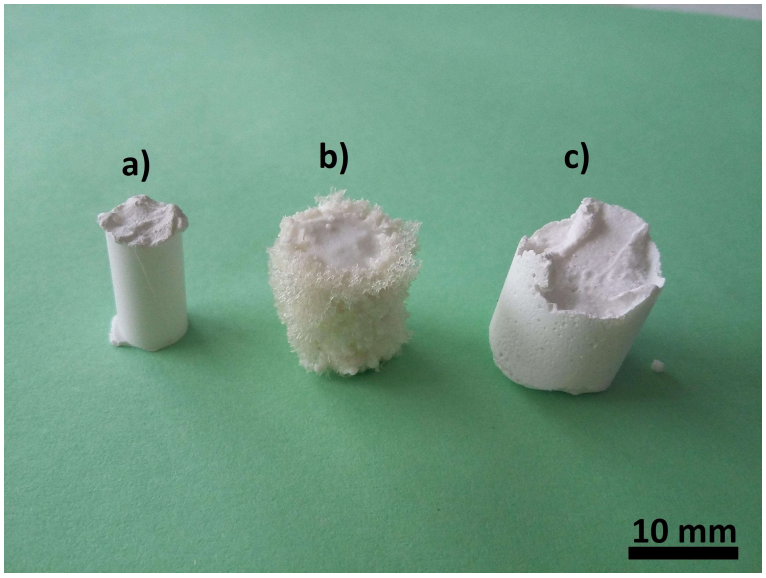

Fig. 4.7 – The appearance of the set samples. Used setting molds: a) PP hose, b) memory foam, c) rubber mold.

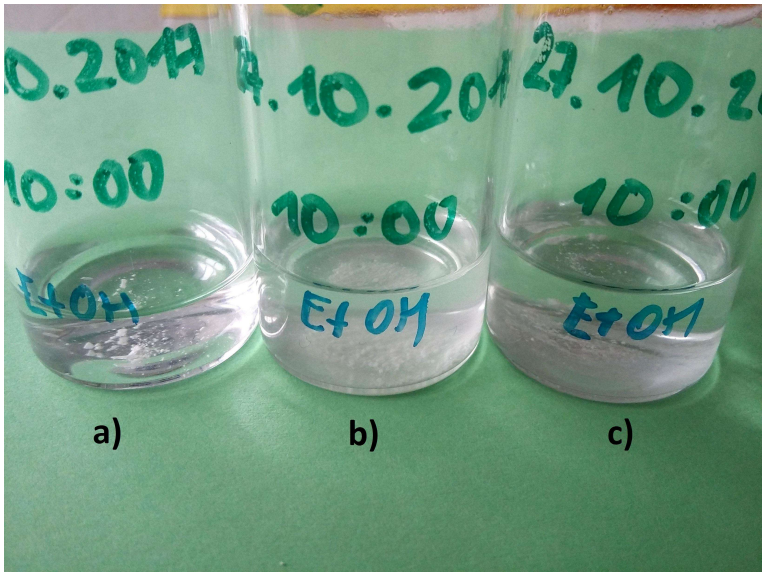

Fig. 4.8 – Vials with bone cement residues. Used setting molds: a) PP hose, b) memory foam, c) rubber mold.

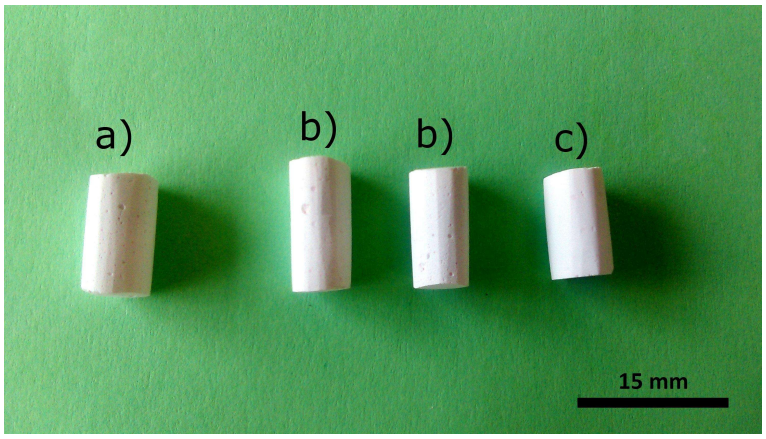

Fig. 4.9 – Appearance of hand-sharped samples. Used materials of molds are: a) PP hose, b) memory foam, c) rubber.

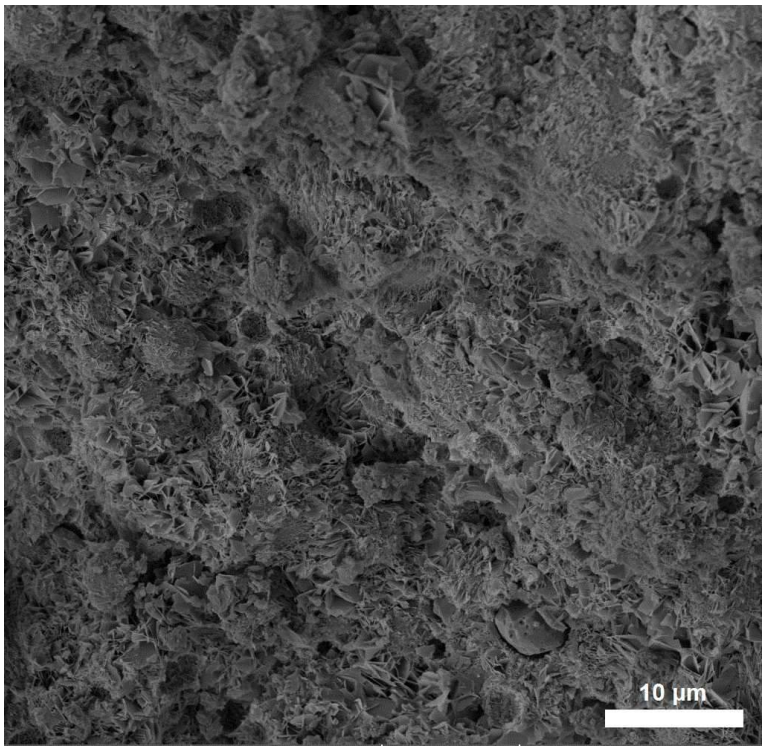

Fig. 4.10 – Scanning electron micrograph of sample set in PP hose.

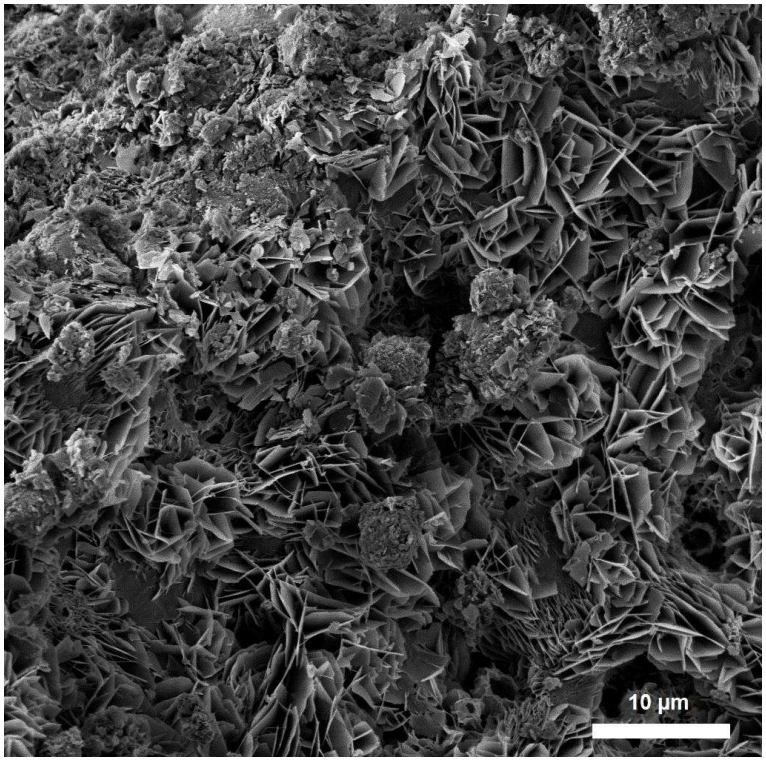

Fig. 4.11 – Scanning electron micrograph of sample set in rubber mold.

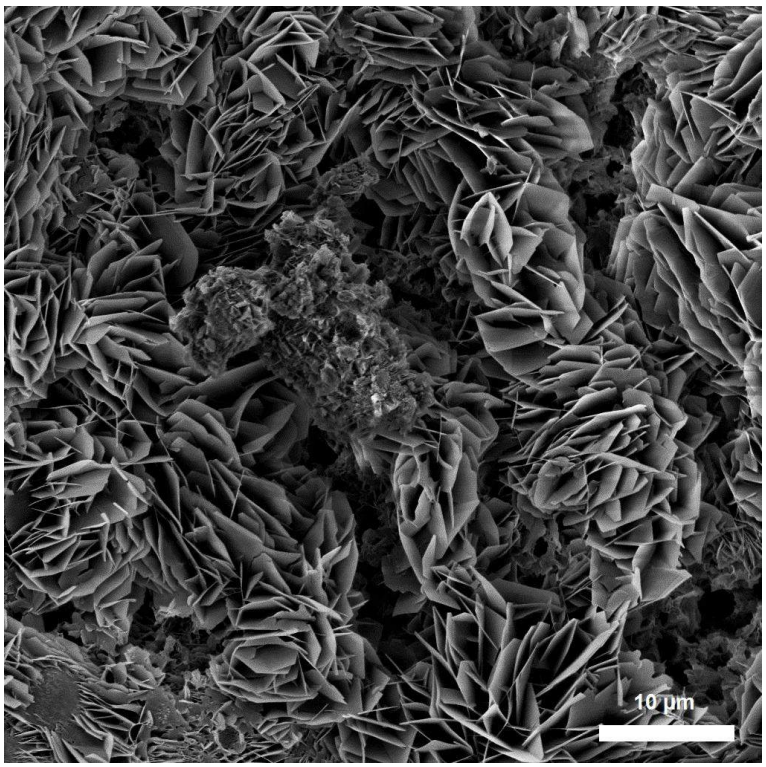

Fig. 4.12 – Scanning electron micrograph of sample set in memory foam mold.

Set samples were tested in mechanical compression tests. Results of measurement shows graph in Fig. 4.13. The most crush-resistant sample was sample set in the plastic hose with the highest value of compression strength equal to 5.43 MPa. Sample set in rubber mold was second most crush-resistant sample with the highest value of compression strength equal to 5.05 MPa. There is a small peak around 0.44 MPa in the crush evolution of sample set in rubber mold. Surface unevenness at the top of sample causes existence of this peak. Samples set in the memory foam were the least resistant with the highest values of compression strength equal to 4.93 MPa.

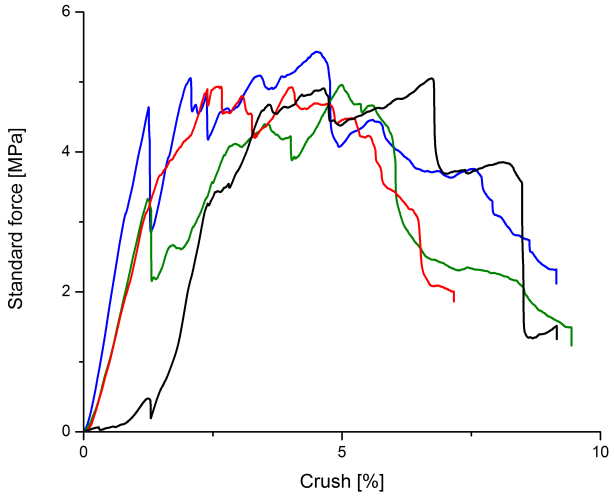

Fig. 4.13 – Results of mechanical compression tests. Blue line represents sample setting in the PP hose; green and red lines represent memory foam mold; black line represents sample setting in the rubber mold.

4.4 Preparation III.

Two samples of bone cement were set in memory foam mold. Then samples were machine milling into cylindrical form with dimensions 12 mm×6 mm. Appearance of samples after mechanical sharpening shows Fig. 4.14.

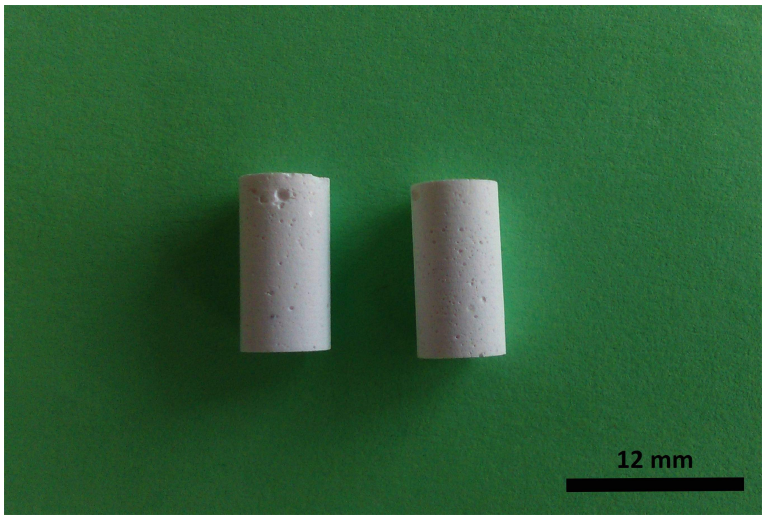

Fig. 4.14 – Appearance of samples after machine milling.

4.5 Preparation IV.

This preparation deals setting of prepared CPC samples in simulated body fluids (SBF) and whole pig blood. Dissolution amount of cement pastes volume was observed immediately after application of setting liquids into the setting mold. Dissolution of cement paste is probably caused by the presence of Ca^{2+} and other ions in used setting environments. Residues were decanted and then dried at 110 °C for 4 hours. Weights of bone cement residues are listed in Tab. 4.1. The largest dissolution of cement paste was determined in samples set in Hank´s solution. Almost the same values of CPC residues were determined in the samples set in Ringer´s solution and physiological solution. The lowest value of residues weight was determined in the samples set in pig blood. A possible reason of the samples set in Hank´s balanced salt solution having highest values of residues weights is modification this solution product by calcium and magnesium ions which can lead to higher dissolution of CPC. *In vitro* dissolution behavior of CaP coatings immersed in Hank´s solution was investigated by Hamdi, M. and Ide-Ektessabi, A. [68]

Setting liquid	Weight of residues (g)
Physiological solution	0.1213
Hank´s solution	0.1311
Ringer´s solution	0.1226
Blood	0.0969

Tab. 4.1 – Weights of CPC residues after 3 days of setting in SBF and pig blood.

pH measurement

Measurement of pH of used setting liquid environments was performed before and after 3 days period at 37 °C of setting. Results of pH measurement are depicted in Tab. 4.2.

Setting liquid	pH before setting	pH after setting
Physiological solution	6.78	6.36
Hank´s solution	7.33	6.21
Ringer´s solution	6.69	6.58
Blood	7.4	8.50

Tab. 4.2 – pH measurements of setting liquids.

Milling

Surface of set samples were modified by machine milling to cylindrical shape. Appearance of sample set in blood for 1 day and after machine milling process is depicted in Fig. 4.15. Detail of its surface with visible macropores shows Fig. 4.16. Sample sizes measured by micrometer are listed in Tab. 4.5 in appendix 1. Sample sizes were in range from 9.410 mm to 12.855 mm in height and from 5.952 mm to 7.054 mm in diameter due to influence by dissolution behavior in the presence of body fluids environments to prepared bone cement samples. Samples designated by $B3_{12h}$ and $P3_{1m}$ were not mechanically tested due to their insufficient length.

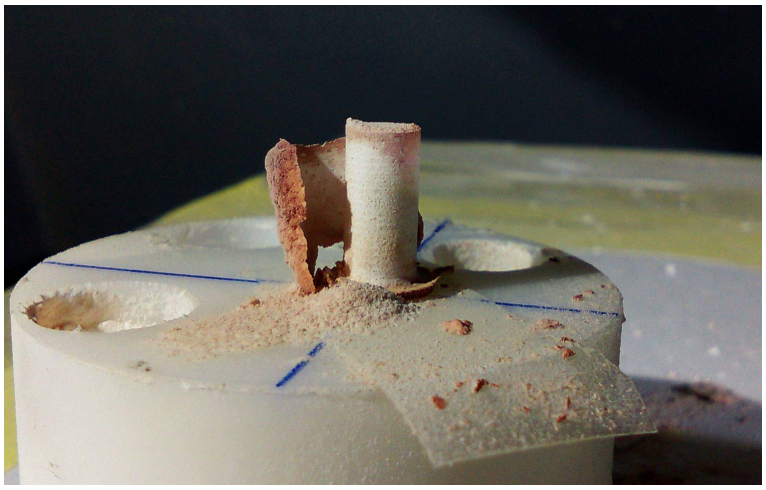

Fig. 4.15 – Appearance of sample set in blood for 1 day and during machine milling process.

Fig. 4.16 – Appearance of sample surface after machine milling process.

Appearance of samples set in blood for 12 h is depicted in Fig. 4.17. Samples surfaces were deformed during removal of the mold due to insufficient hardness. Samples set in SBF for 12 h had solid surfaces and removals of mold were performed without their deformations.

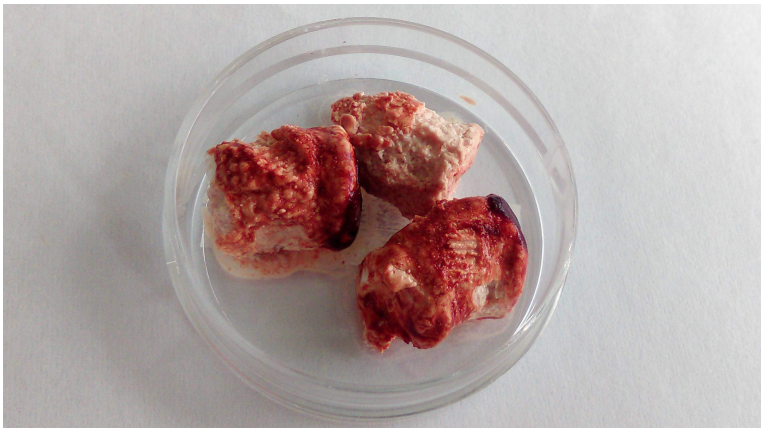

Fig. 4.17 – Appearance of samples set in blood for 12 h after removal of the mold.

Morphology by Scanning Electron Microscopy (SEM)

The surface fractures analysis were made by SEM for samples with different setting times, specifically 1 day, 1 week, 2 weeks and 1 month. The results are illustrated in Fig. 4.18, 4.20, 4.21 and 4.22. An initial stage (1 day of setting) is illustrated in Fig. 4.18 and corresponding to relatively short time of setting reactions. Microstructures of bone cement set for 1 day are represented both unconverted particles of powders and partly covered by a shell of very small CDHA crystals due to their conversion with comparison by SEM of pure α-TCP. High heterogeneity of microstructure of samples set in blood environment containing probably presence of blood cells was observed. Fig. 4.19 shows a fracture surface microstructural detail of a sample 1 day after immersion in blood environment that shows probably microstructure of the place after blood cell location.

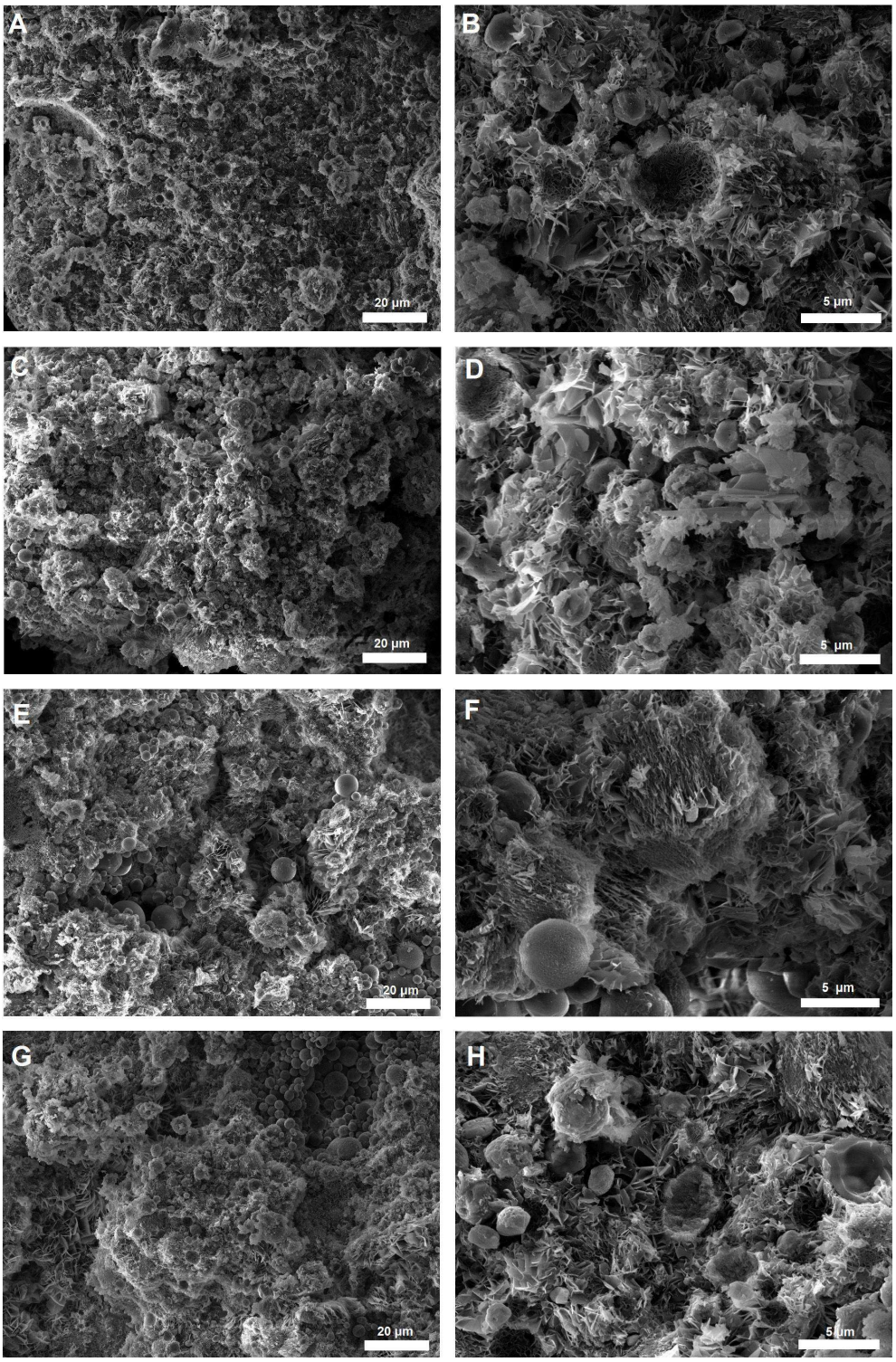

Fig. 4.18 – SEM micrographs of bone cement samples after 1 day of setting. Picture A and B represents the microstructures of a sample set in physiological solution; picture C and D represents the microstructures of a sample set in Hank´s solution; picture E and F represents a microstructures of a sample set in Ringer´s solution; picture G and H represents a microstructures of a sample set in blood (original magnifications: pictures A, C, E and G $\times 2\,000$*, pictures B, D, F and H* $\times 10\,000$*).*

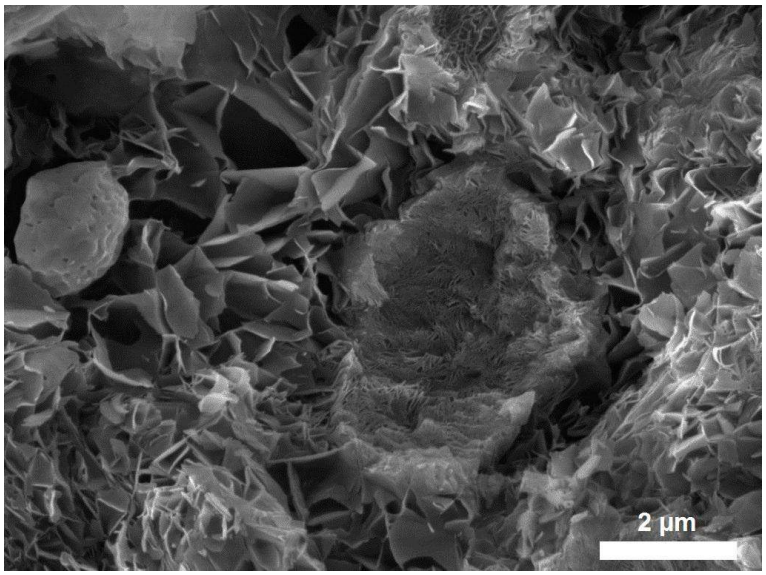

Fig. 4.19 – SEM micrograph of a surface detail of a sample set in blood for 1 day (original magnification: $\times 25\,000$*).*

Micrographs illustrated in Fig. 4.20 shows results of SEM analysis of sample set for 1 week represents intermediate stage, where the formations of HAp crystals structures were observed as well as partly uncorverted and partly covered particles of powders. In the intermediate stage gradual changes morphology, specifically crystal sizes could be observed. In the microstructures of all samples set for 1 week were observed both area of large CDHA crystals and area of partly converted particles of powders (covered by shells of very small crystals). Sample set in pig blood had very heterogeneous surface structure with the presence of very smooth areas in its microstructure. In microstructures of samples set in Hank´s solution, Ringer´s solution and pig blood were observed a large amount of pores in contrast with microstructure of sample set in physiological solution, where are no visible pores. Pore diameter was in range 5-10 μm corresponding with α-TCP particles diameter.

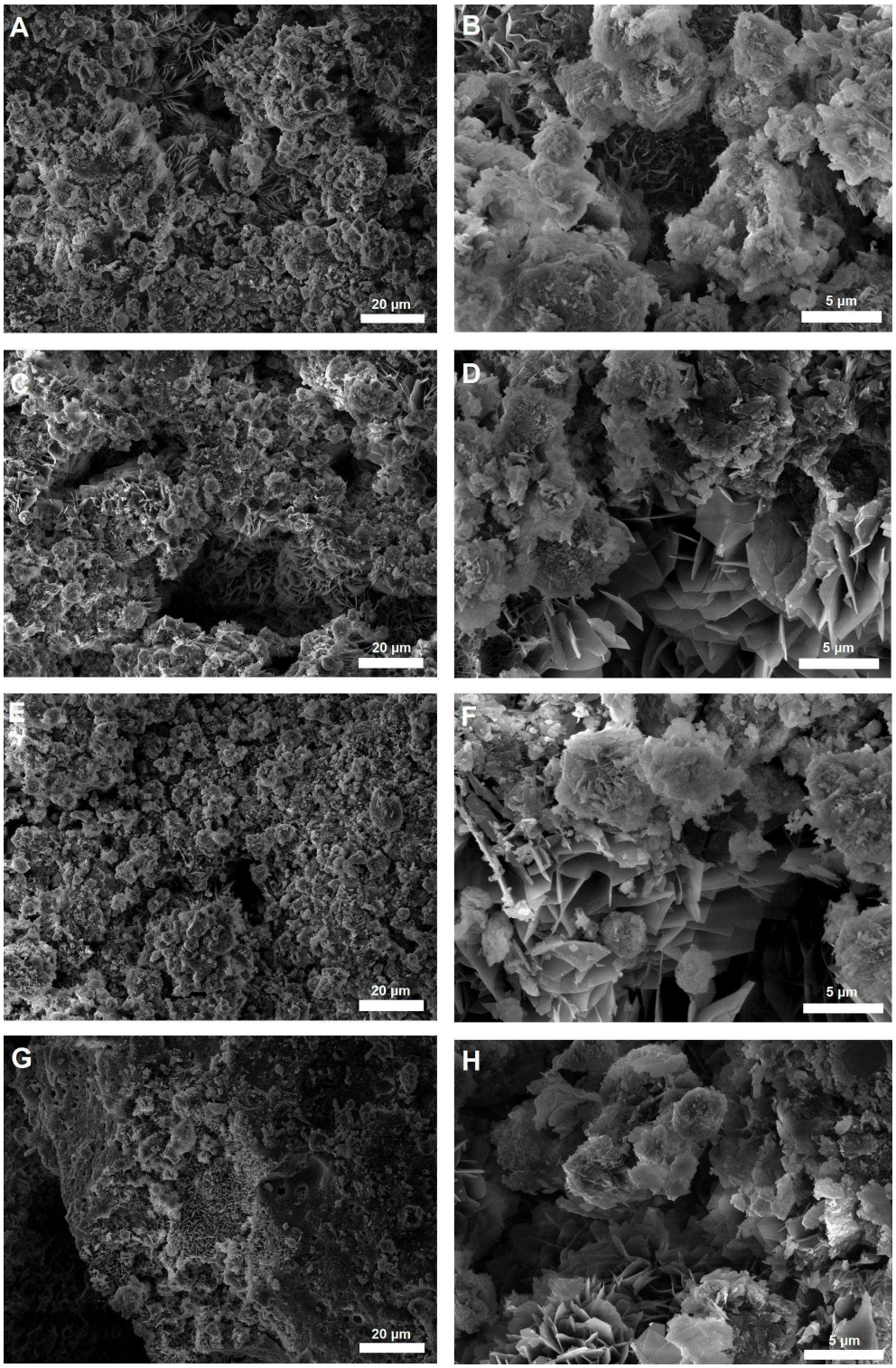

Fig. 4.20 – SEM micrographs of bone cement samples after 1 week of setting. Picture A and B represents the microstructures of a sample set in physiological solution; picture C and D represents the microstructures of a sample set in Hank´s solution; picture E and F represents a microstructures of a sample set in Ringer´s solution; picture G and H represents a microstructures of a sample set in blood (original magnifications: pictures A, C, E and G $\times 2\,000$*, pictures B, D, F and H* $\times 10\,000$*).*

Micrographs illustrated in Fig. 4.21 shows results of SEM analysis of sample set for 2 weeks. Most of powder particles were converted to CDHA large crystals in all sample microstructures. Sample set in blood had very heterogeneous surface structure with the presence of very smooth areas in its microstructure as well as in micrographs observed after 1 week of setting. Sample set in physiological solution resulted low porosity. Otherwise, samples set in Hank´s solution, Ringer´s solution and blood had a significant porous structures. Microstructure of sample set in Ringer´s solution was represented by typical CDHA crystal formation.

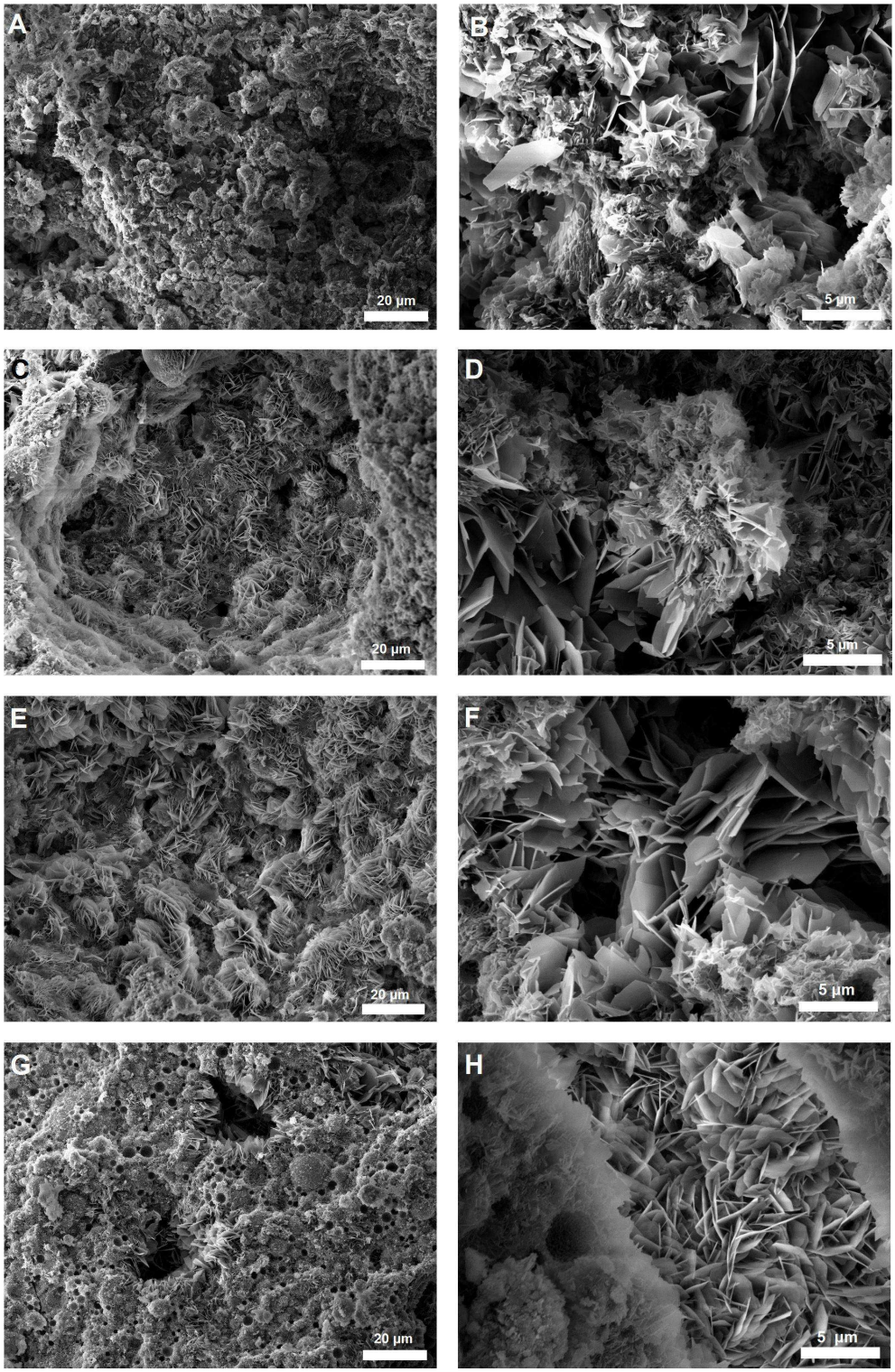

Fig. 4.21 – SEM micrographs of bone cement samples after 2 weeks of setting. Picture A and B represents the microstructures of a sample set in physiological solution; picture C and D represents the microstructures of a sample set in Hank´s solution; picture E and F represents a microstructures of a sample set in Ringer´s solution; picture G and H represents a microstructures of a sample set in blood (original magnifications: pictures A, C, E and G $\times 2\,000$*, pictures B, D, F and H* $\times 10\,000$*).*

Results of sample SEM analysis set for 1 month represents an advanced stage of microstructure evolution are shown in micrographs in Fig. 4.22. The number of CDHA crystals has increased in all observed samples. Total unconverted particles covered small crystals were observed in all set samples. Samples set in physiological solution, Hank´s solution and blood were formed by large CDHA crystals with a lot of pores.

The microstructure of sample set in pig blood contained total unconverted particles without small CDHA crystals on its surface and the smooth areas such as in previous observation. The smooth surface particles could be represented by some of the blood compounds. The microstructure of sample set in Ringer´s solution was different. In this microstructure, two types of crystals could be recognized: large plate-like particles of CDHA and very small crystals on the spheres particle surfaces. In this microstructure, sphere pores with diameter 5-10 μm were not observed.

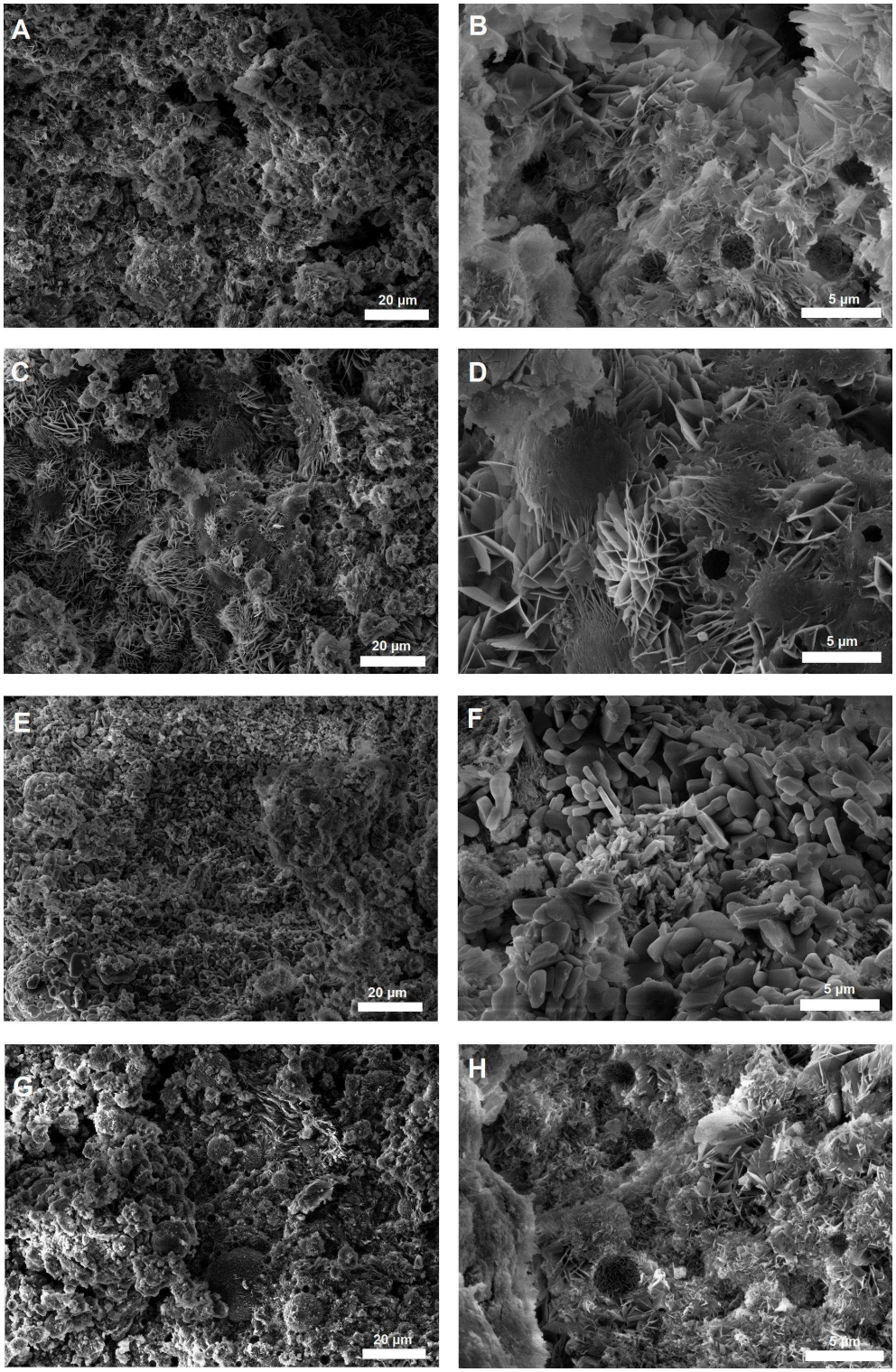

Fig. 4.22 – SEM micrographs of bone cement samples after 1 month of setting. Picture A and B represents the microstructures of a sample set in physiological solution; picture C and D represents the microstructures of a sample set in Hank´s solution; picture E and F represents a microstructures of a sample set in Ringer´s solution; picture G and H represents a microstructures of a sample set in blood (original magnifications: pictures A, C, E and G $\times 2\,000$*, pictures B, D, F and H* $\times 10\,000$*).*

Mechanical properties

Results of mechanical compression tests of samples set for 6 time periods in 4 setting environments are depicted in graphs in Fig. 4.23 and in Fig. 4.24. Maximum standard force represents an average of 3 samples measurements. Measurements were provided until observation a critical crack across the entire sample length.

Samples set in physiological solution for 1 day, 3 days, 1 week, 2 weeks and 1 month exhibited similar mechanical properties with maximum strength about 11 MPa. It follows that physiological solution had effect to accelerate setting and hardening of CPC samples. A lower concentration of phosphates in Hank´s solution equal to 0.77 mmol L^{-1} and zero phosphates concentration in Ringer´s solution with comparison of human whole blood phosphates concentration in the range between 0.8-1.35 mmol L^{-1} caused a delay in the initiation of the setting reaction [71].

Samples set in blood showed a gradual increase of strength in time with the lowest strength after initial 12 hours stage of setting correlating with unset properties observed during setting mold removal. Explanation for this phenomena gives the results of study provided by Combes, C. and Rey C. They discussed effects of blood plasma proteins (e.q. bovine serum albumin (BSA)) with multifunctional roles in the regulation of formation and growth of CDHA. For the low BSA concentrations ([BSA]$<$ 10 g L^{-1}) the protein supported the growth of OCP, whereas for high BSA concentrations ([BSA]$\geq$ 10 g L^{-1}), OCP growth was inhibited [69]. Albumin is a blood plasma protein, which form about 60 % of all plasmatic proteins. The typical concentration of albumin is about 50 g L^{-1} in human blood [70]. Another study provided by Koutsopoulos, S. and Dalas, E. was focused on effect of four natural amino acids with hydrophobic nonpolar side groups (alanine, phenylalanine, prolin and methionine) to the crystallization of HAp. Their results showed that phenylalanine is an effective inhibitor of HAp crystal formation even at low concentration levels. It is important to note that the hydrophobic amino acids tested as possible inhibitors of HAp crystallization were active at concentration levels of the same order with magnitude their physiological concentration values at blood plasma. [72]

Decrease in maximum strength of sample set in Ringer´s solution correlates with a change of its microstructure after 1 month of setting. In this case, a significant factor influencing transformation of crystal structure of samples set in Ringer´s solution could be acidic pH of used setting liquid (see Tab. 4.2). Initial acidic solution pH could influence the structure of CDHA crystals by their subsequent dissolution following by structure transformation. It was measured that solutions pH of Ringer´s solution and blood increased after 3 days of setting, otherwise pH of physiological solution and Hank´s solution decreased. Increase in solution pH may be caused by physiochemical interactions of setting liquids ion molecules with Ca^{2+} follows by inhibiting the transformation of phosphates to CDHA. On the other hand, decrease in solution pH may be caused by release of PO_4^{3-} to the setting liquids.

According to pH measurement results, we can discuss that decreases in mechanical strength of samples set in Hank´s and Ringer´s solutions can be affected both by release of Ca^{2+} and PO_4^{3-} ions from CPC bone cement samples to setting environments. The main factor of samples set in Hank´s and Ringer´s solutions strength decrease after 2 weeks of setting could be presence of sodium chloride, potassium chloride, calcium chloride dihydrate and sodium bicarbonate in both setting solutions chemical compositions. These dissociated salts can form chemical interactions between their chloride anions and Ca^{2+} contained in CPC phosphates, which causes inhibition of CDHA forming. Hank´s

solution contains other chemical compounds, specifically magnesium sulphate, potassium phosphate and sodium phosphate, which on the other hand may support CDHA forming ability corresponding to the final higher strength of these samples. Result showed that decrease in mechanical strength of samples set in Ringer´s solution after 1 month is more significant than mechanical strength of samples set in Hank´s solution can be affected by absence of phosphates in Ringer´s solution as already mentioned.

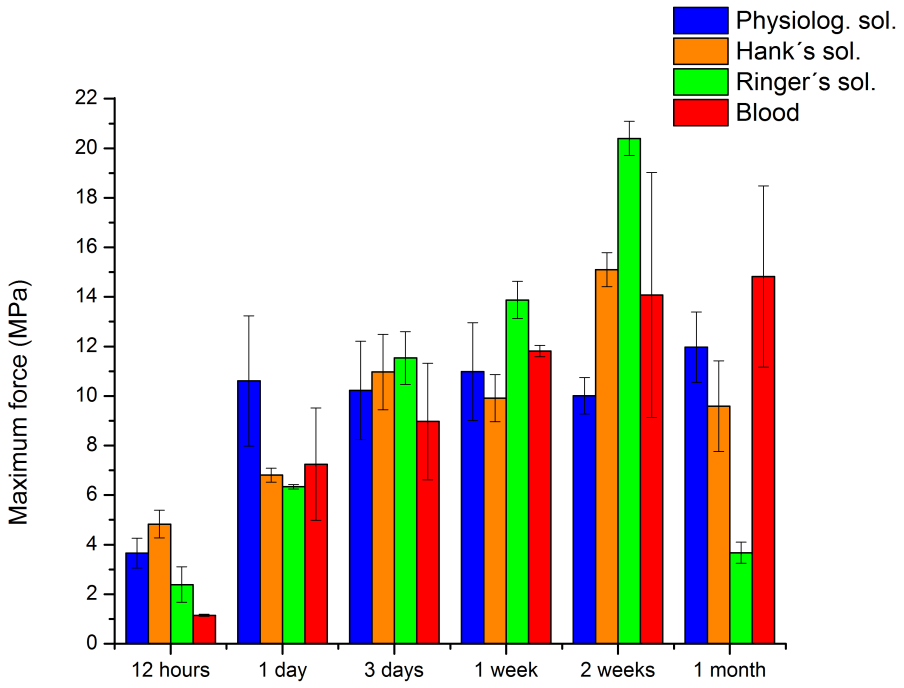

Fig. 4.23 – Results of mechanical compression tests evaluated according to setting times.

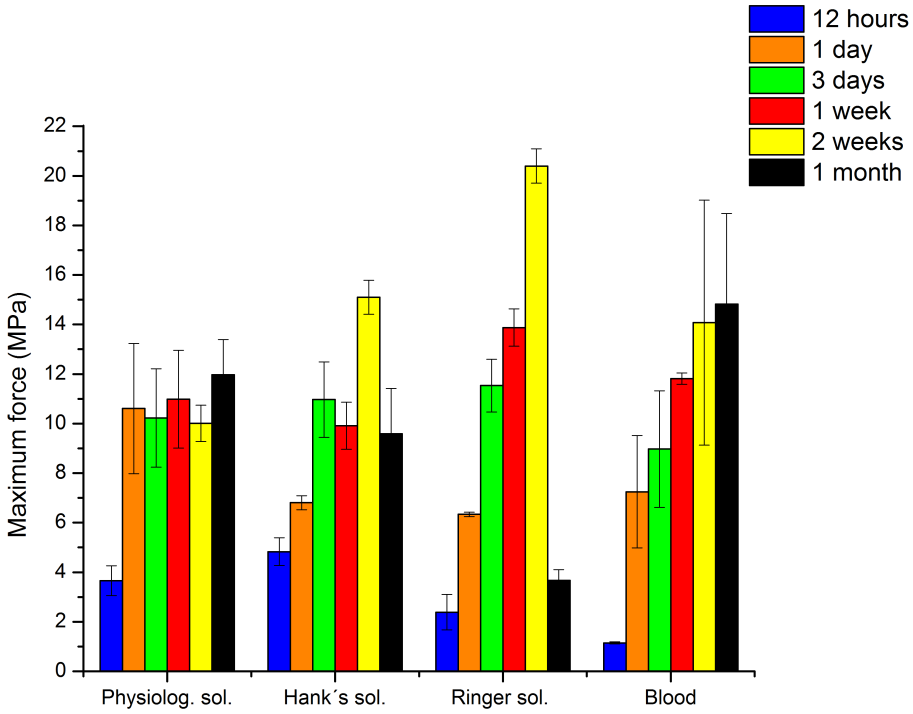

Fig. 4.24 – Results of mechanical compression tests evaluated according to setting environments.

Crush patterns of samples set for 1 day are depicted in Fig. 4.25-4.28. Two samples designated $P1_{1D}$ and $P2_{1D}$ set in physiological solution had the highest values of strength. In general, strength of samples set in physiological solution reached of high values already after 1 day of setting and hereafter has not changed so much with progress of setting time. On the other hand, samples designated $H1_{1D}$, $R2_{1D}$ and $B1_{1D}$ had almost half strength lower than samples $P1_{1D}$ and $P2_{1D}$ and their strength increased gradually in time.

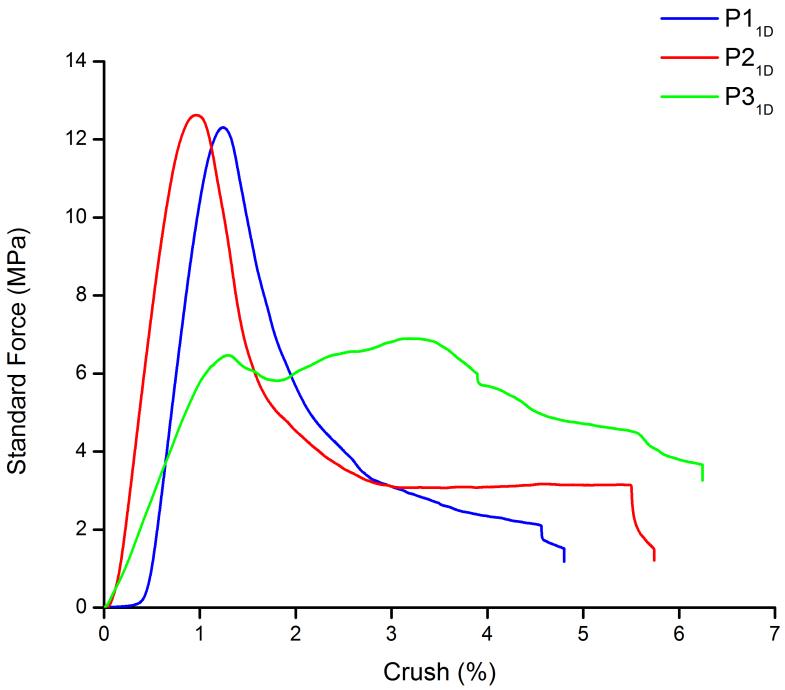

Fig. 4.25 – Results of compression tests of samples set in physiological solution setting environment for 1 day.

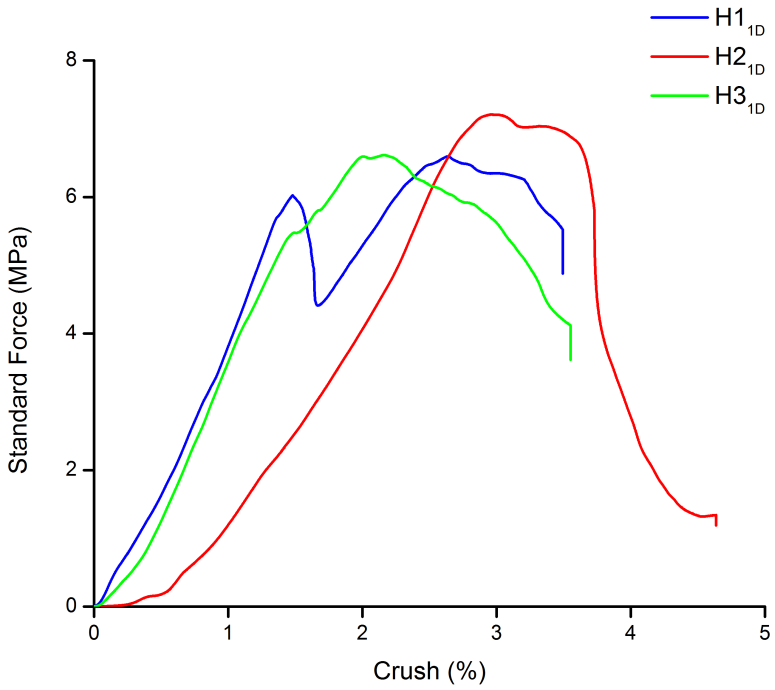

Fig. 4.26 – Results of compression tests of samples set in Hank´s solution setting environment for 1 day.

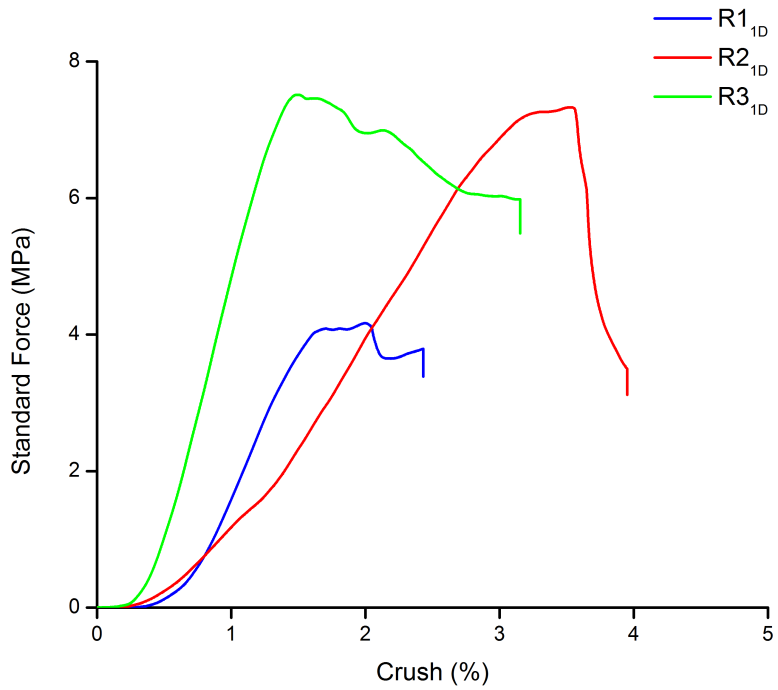

Fig. 4.27 – Results of compression tests of samples set in Ringer´s solution setting environment for 1 day.

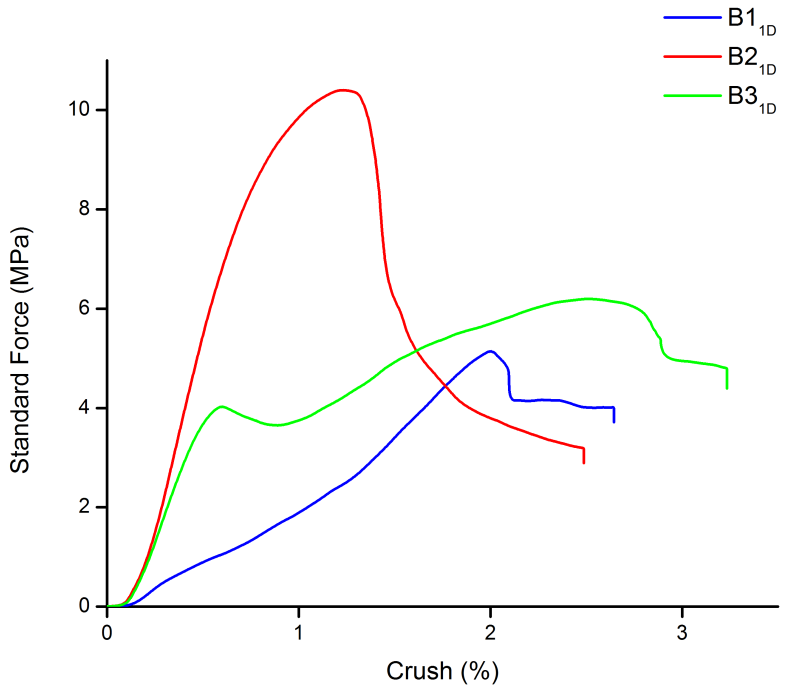

Fig. 4.28 – Results of compression tests of samples set in pig blood setting environment for 1 day.

For the sake of clarity, only one crush pattern representing each setting environment and each setting time was selected for constructions graphs in Fig. 4.29-4.34. The crush patterns for the rest of samples are depicted in Appendix 2.

Samples set in physiological solution and blood for 1 day setting period show similar crush patterns. A significant increase of their strength followed by its fast decreases because of sample crush indicates their mechanical properties, specifically solidity but fragility. Critical breakthrough of these samples occured around 1 % of crush. Otherwise, sample set in Hank´s and Ringer´s solutions showed gradual increase of strength indicates predominately their elastic properties and its critical breakthrough occured aroud 2 % of crush. During the setting period from 1 day to 2 weeks mechanical properties of samples set in Ringer´s solution were changed predominantly to properties representing solid but brittle material, while mechanical properties of samples set in Hank´s solution remained the same. After 2 weeks of setting, results of mechanical properties of samples set in Hank´s solution, Ringer´s solution and physiological solution were significantly changed. Samples set in Hank´s and Ringer´s solutions were became much more solid and fragile with critical breakthrough of these samples occurred around 1 % of crush and on the other hand, sample set in physiological solution and blood were became much more elastic with critical breakthrough which occurred over 2 % of crush.

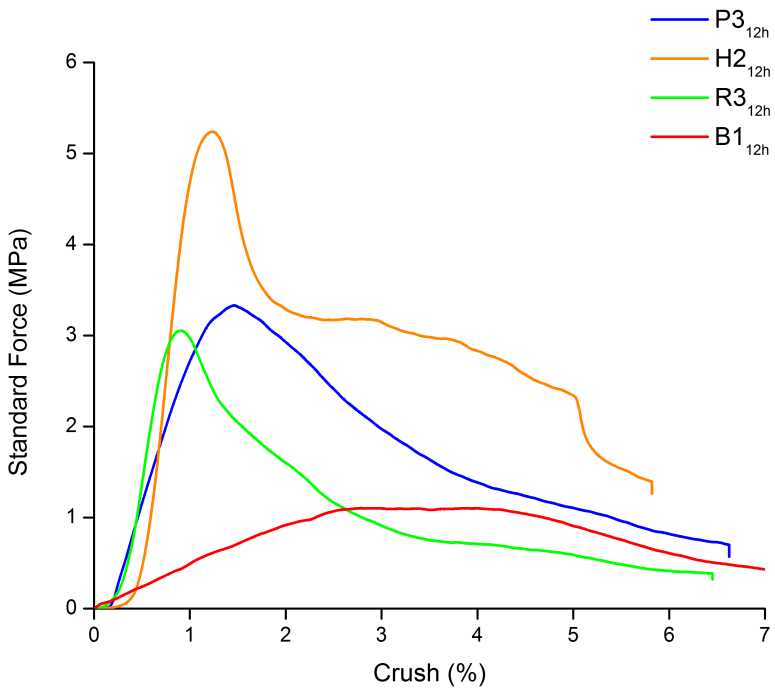

Fig. 4.29 – Results of compression tests of samples set for 12 hours.

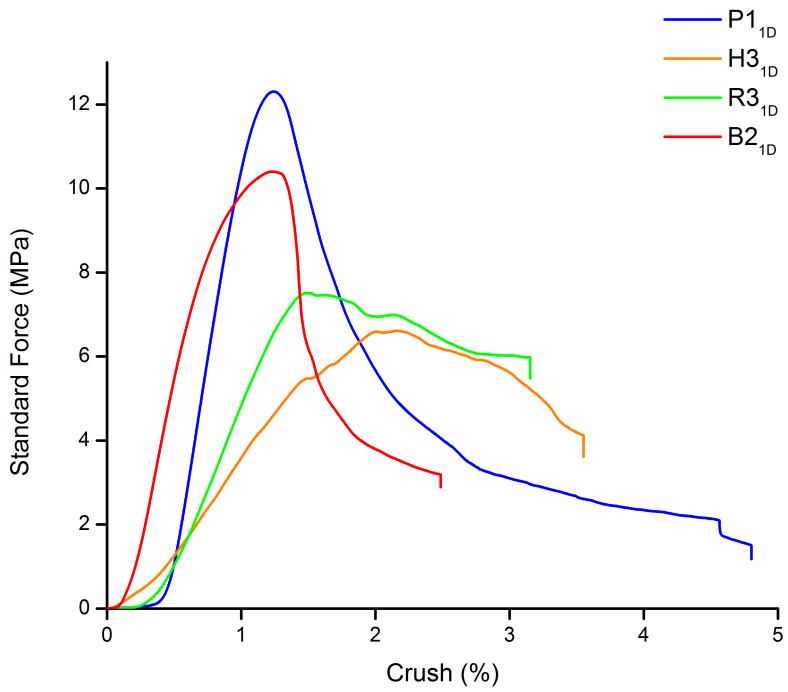

Fig. 4.30 – Results of compression tests of samples set for 1 day.

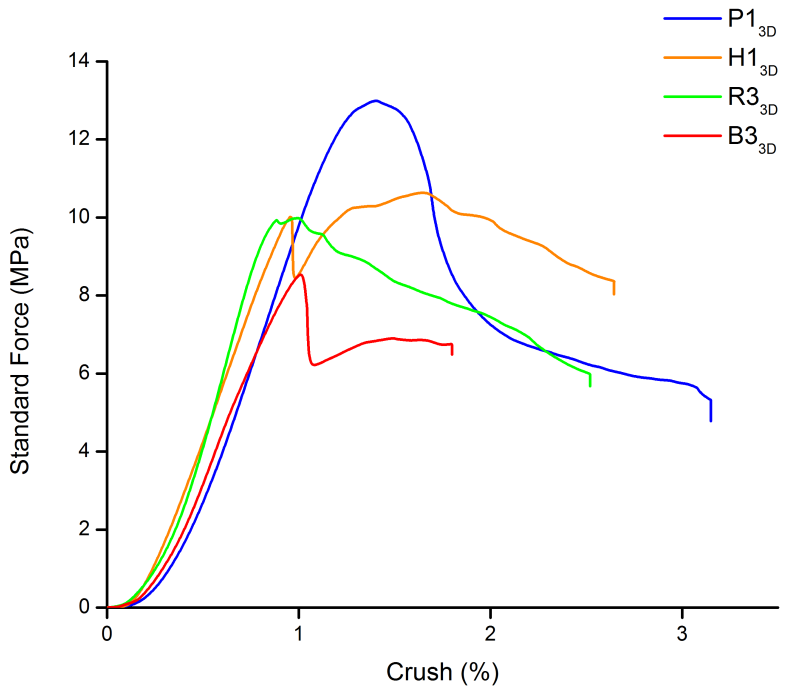

Fig. 4.31 – Results of compression tests of samples set for 3 days.

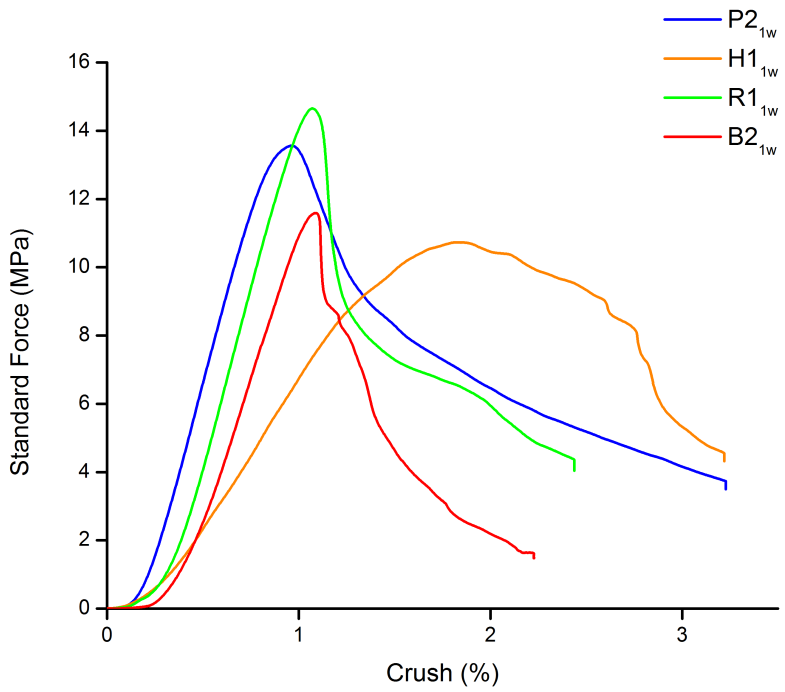

Fig. 4.32 – Results of compression tests of samples set for 1 week.

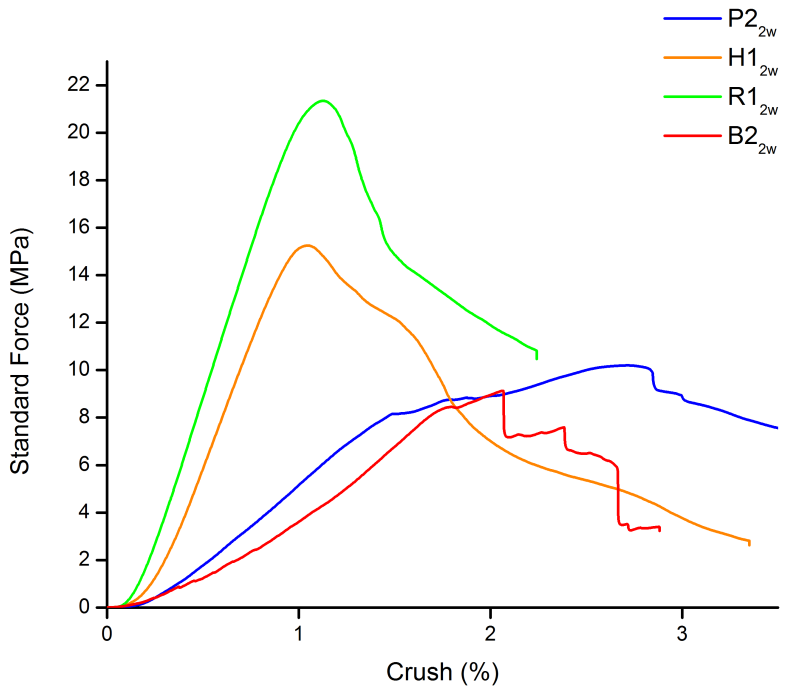

Fig. 4.33 – Results of compression tests of samples set for 2 weeks.

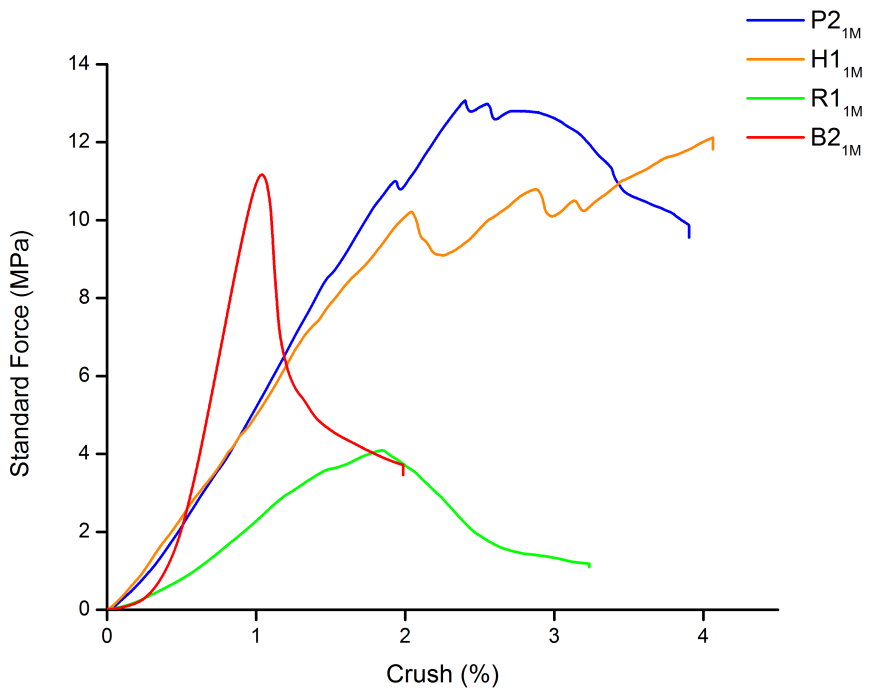

Fig. 4.34 – Results of compression tests of samples set for 1 month.

Crystallization of α-TCP toward to CDHA

To analyze the process of the chemical transformation of α-TCP during the setting of prepared bone cement samples, intensity of selected peaks was investigated. The reaction product of hydrolysis of α-TCP was a CDHA. According to Ginebra, M. P. et al. and Fernández, E. et al., selected peaks for α-TCP and CDHA listed in Tab. 4.3 were investigated. [60, 61]

Phase	2-theta (°)
α-TCP	12.10
	14.02
	22.20
	24.10
	30.74
CDHA	31.76
	32.20

Tab. 4.3 – Characteristic values of 2-theta angle for selected peaks for α-TCP and CDHA.

Diffractograms in Fig. 4.35-4.40 present comparison of XRD patterns of samples set in 4 setting environment for individual setting time. Peaks represent α-TCP decreased during progress of setting. On the other hand, peaks represent CDHA gradually increase during the 3 days period and since then have not changed so much. A small amount of CDHA was detected already after 12 hours of setting. However, it is obvious, that even after 1 month setting period, amount of α-TCP were not transformed to CDHA.

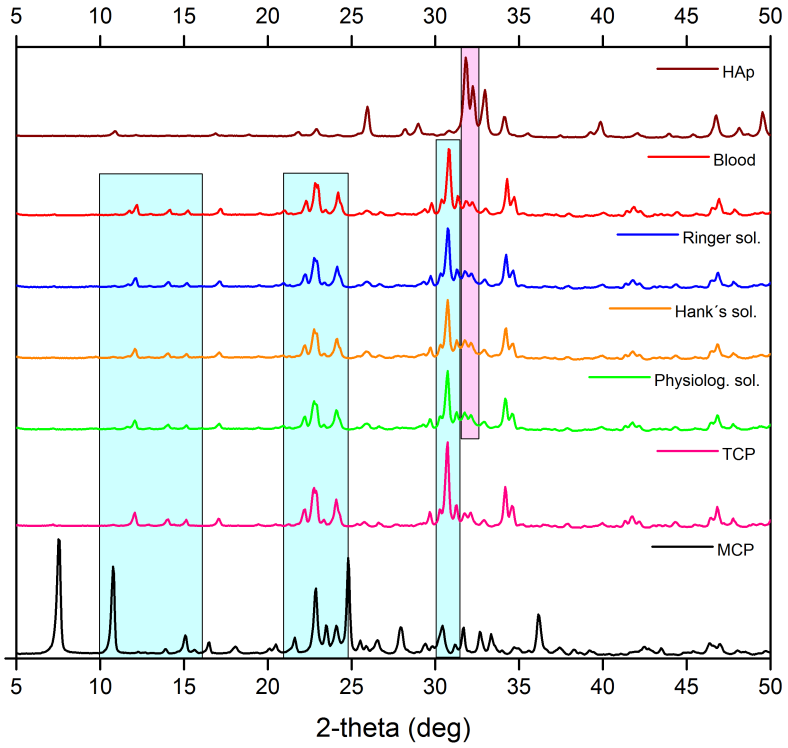

Fig. 4.35 – Diffraction patterns of the bone cement samples set for 12 h.

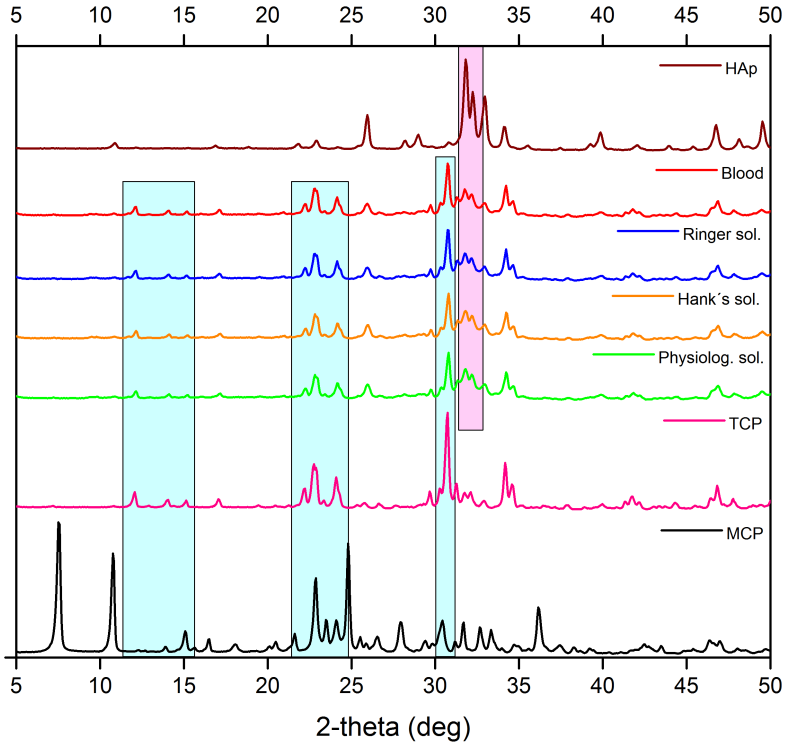

Fig. 4.36 – Diffraction patterns of the bone cement samples set for 1 day.

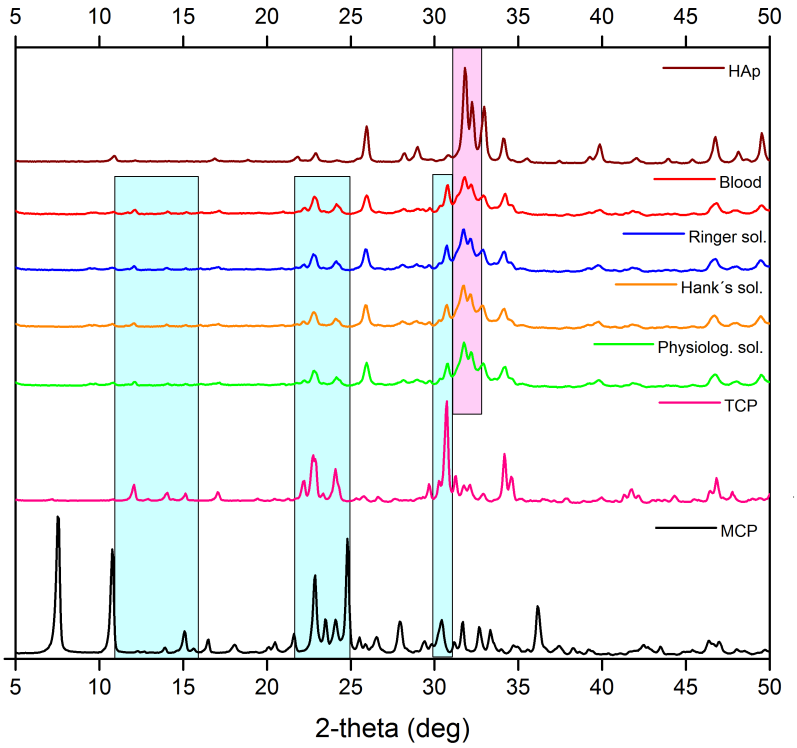

Fig. 4.37 – Diffraction patterns of the bone cement samples set for 3 days.

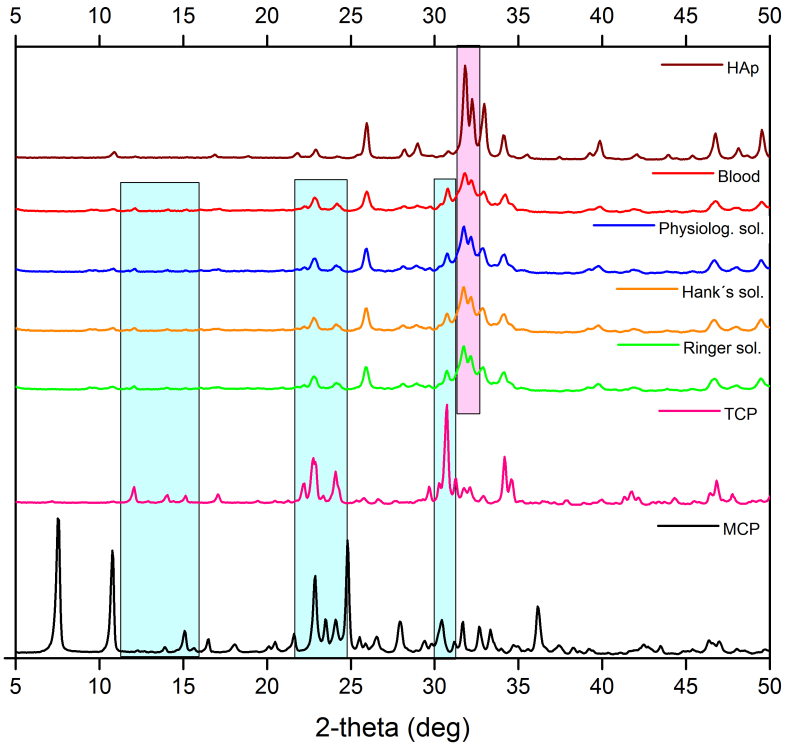

Fig. 4.38 – Diffraction patterns of the bone cement samples set for 1 week.

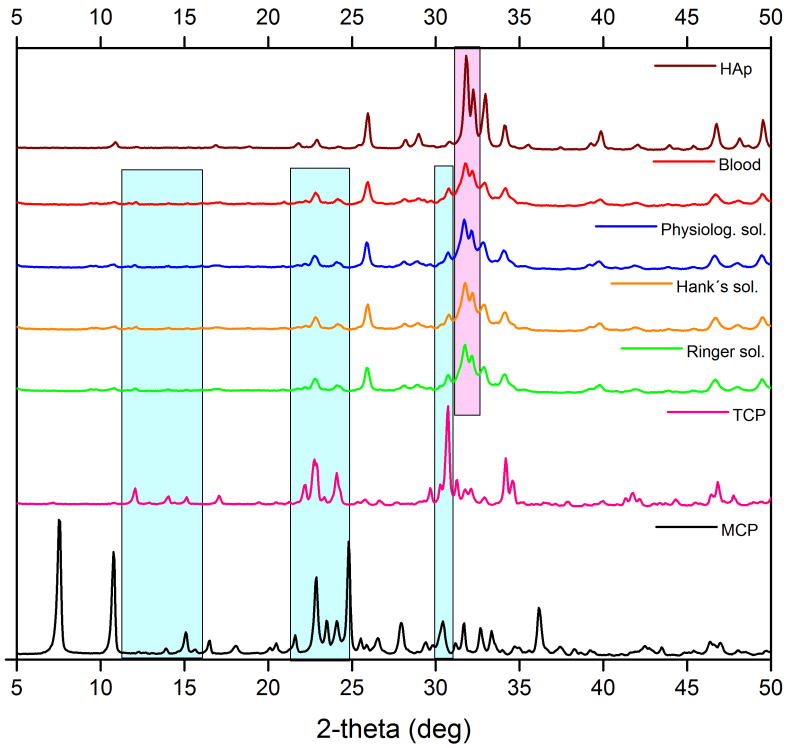

Fig. 4.39 – Diffraction patterns of the bone cement samples set for 2 weeks.

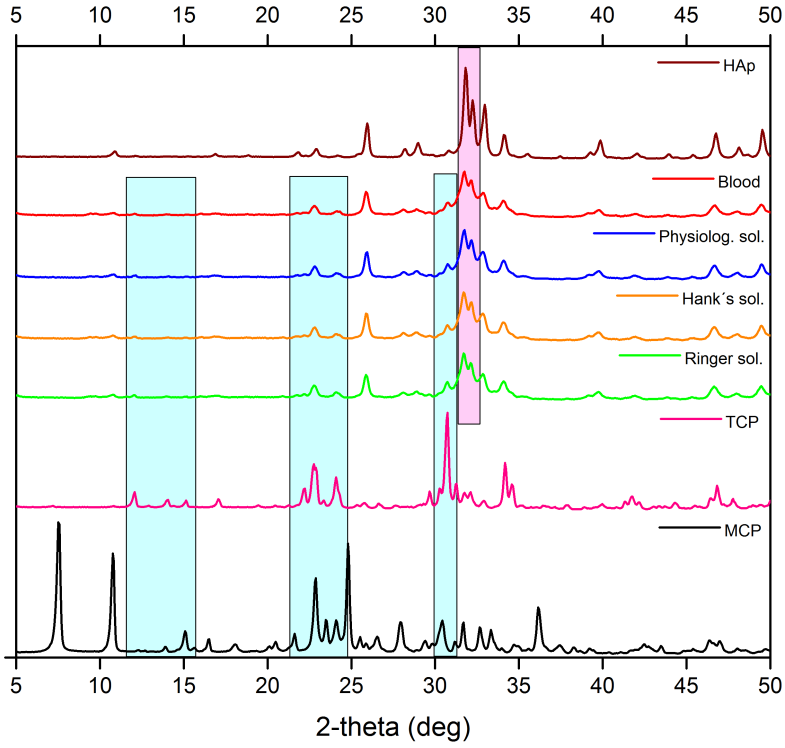

Fig. 4.40 – Diffraction patterns of the bone cement samples set for 1 month.

Diffractograms in Fig. 4.41-4.44 present comparison of XRD patterns of samples set in individual 4 setting environment during 6 setting times. The measured data are from the same measurement as in previous comparison of diffraction patterns. There are not significant differences between these diffraction patterns.

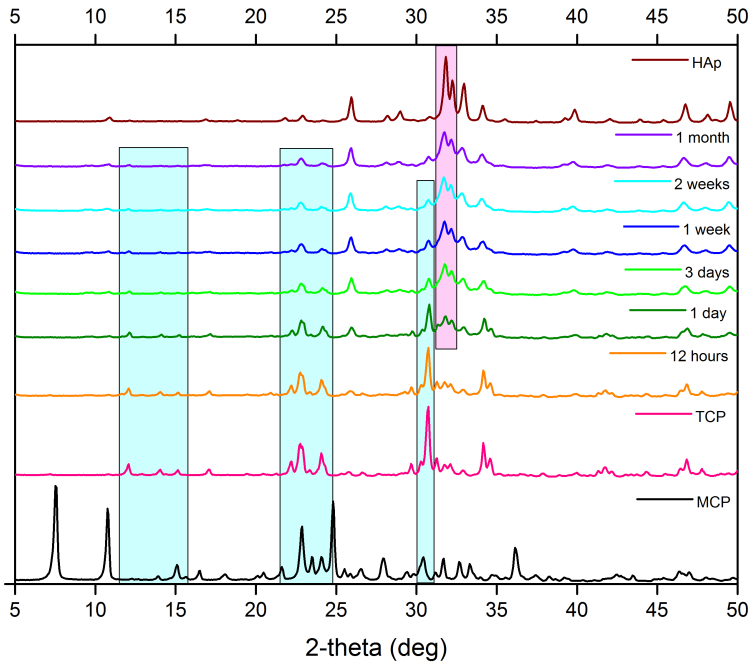

Fig. 4.41 – Diffraction patterns of the bone cement samples set in physiological solution during time.

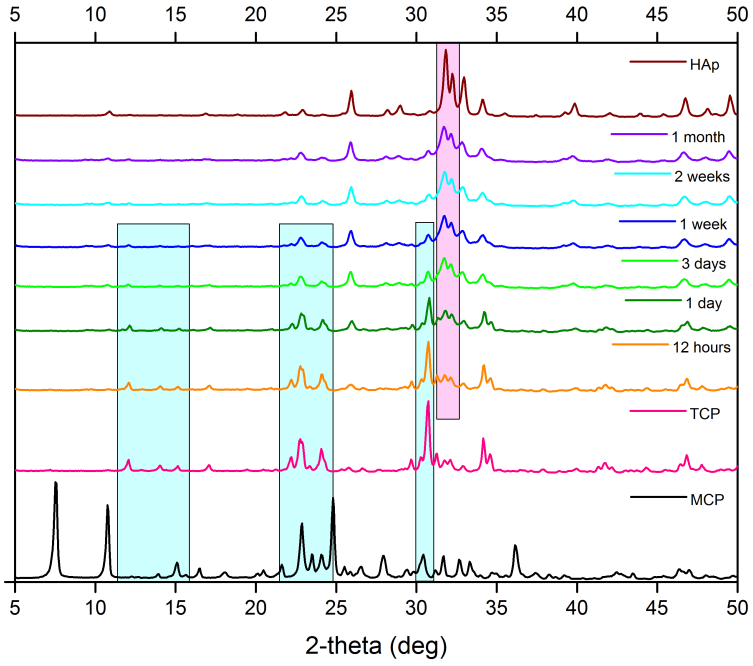

Fig. 4.42 – Diffraction patterns of the bone cement samples set in Hank´s solution during time.

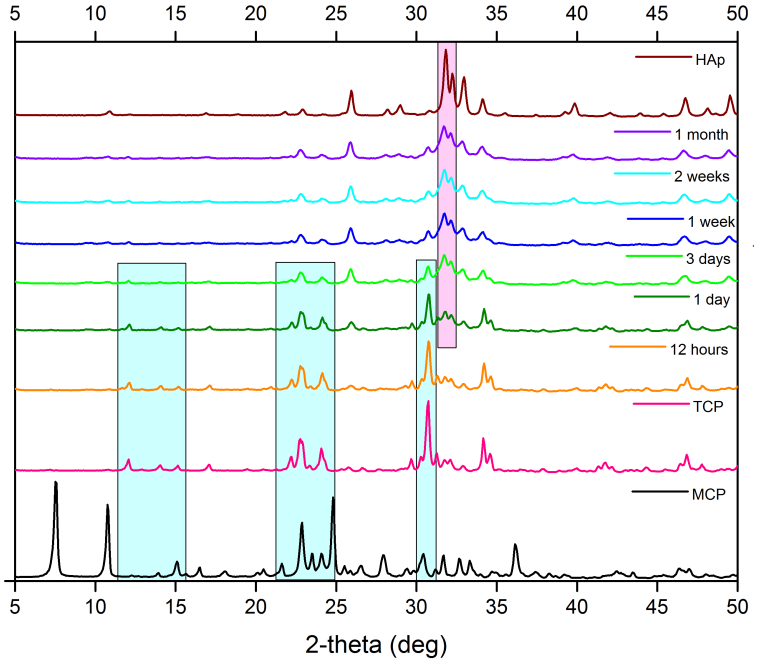

Fig. 4.43 – Diffraction patterns of the bone cement samples set in Ringer´s solution during time.

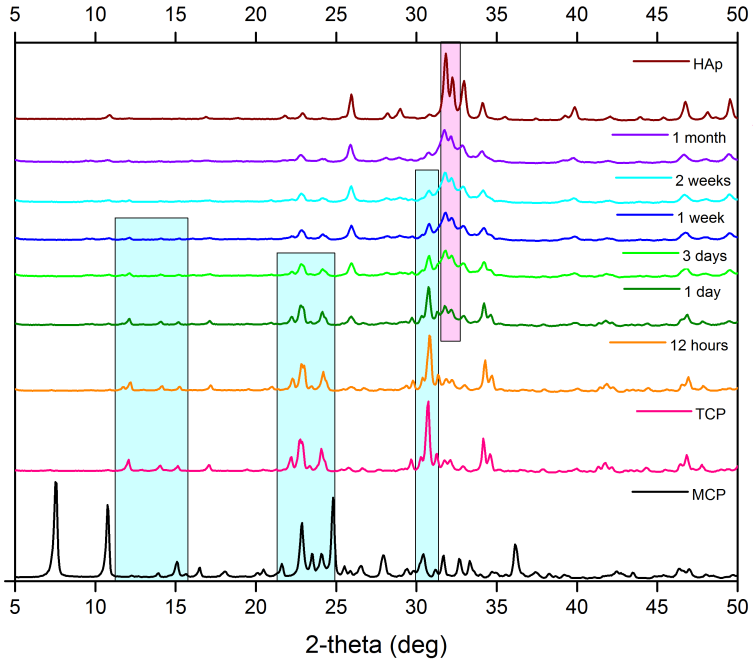

Fig. 4.44 – Diffraction patterns of the bone cement samples set in blood during time.

According to Eq. 4.1 and Tab. 4.3, conversion of α-TCP to CDHA was calculated. [60]

$$w_t = \frac{I_\mathrm{t} M_\mathrm{CDHA}}{M_{\alpha-\mathrm{TCP}} I_0 - T_\mathrm{t}(M_{\alpha-\mathrm{TCP}} - M_\mathrm{CDHA})} \cdot 100 \tag{4.1}$$

where: w_t is an average percentage amount of α-TCP in CPC sample calculated for selected peaks, I_t is a integrated intensity of CPC sample selected peaks, M_CDHA is absorption coefficient of CDHA = 84.97 cm^2 g^{-1}, $M_{\alpha-\mathrm{TCP}}$ is absorption coefficient of α-TCP = 86.43 cm^2 g^{-1}, I_0 is a integrated intensity of α-TCP selected peaks.

Recalculation to percentage amount of CDHA in CPC sample was provided according to Eq. 4.2.

$$w_\mathrm{CDHA} = 100 - w_\mathrm{t} \tag{4.2}$$

The results of conversion calculated according Eq. 4.1 and 4.2 shows the graph in Fig. 4.45. Samples set in physiological solution reached the highest conversion over 50 % after initial 12 hours setting period and over 80 % after final 1 month setting period. In comparison with initial conversion of the samples set in the rest setting environment, conversion of samples set in physiological solution was much more faster because presence of no inhibitor of CDHA transformation in chemical composition of this solution. With correlation of mechanical compression tests we can discuss that setting of CPC samples is most inhibited in blood setting environment with sample conversion only about 40 % after 12 hours. According to calculated conversion of samples set in blood environment is obvious that maximum conversion was reached after 2 weeks of setting while conversion of samples set in physiological solution and Ringer´s solution continued to increase. Interesting phenomenon related to the decrease of conversion about samples set in Hank´s solution after 3 days and 2 weeks of setting were observed. When we compared this fact with XRD patterns, no significant decrease of selected CDHA peak intensity were observed. Described phenomenon may be related with crystal structure transformation of a partial amount of CDHA to another HAp modification consequence of Hank´s solution environment effect on the CaP cement. Further SEM sample analysis set for 3 days and 2 weeks could help clarify this possible dissolution/transformation effect of Hank´s solution on the CaP cement.

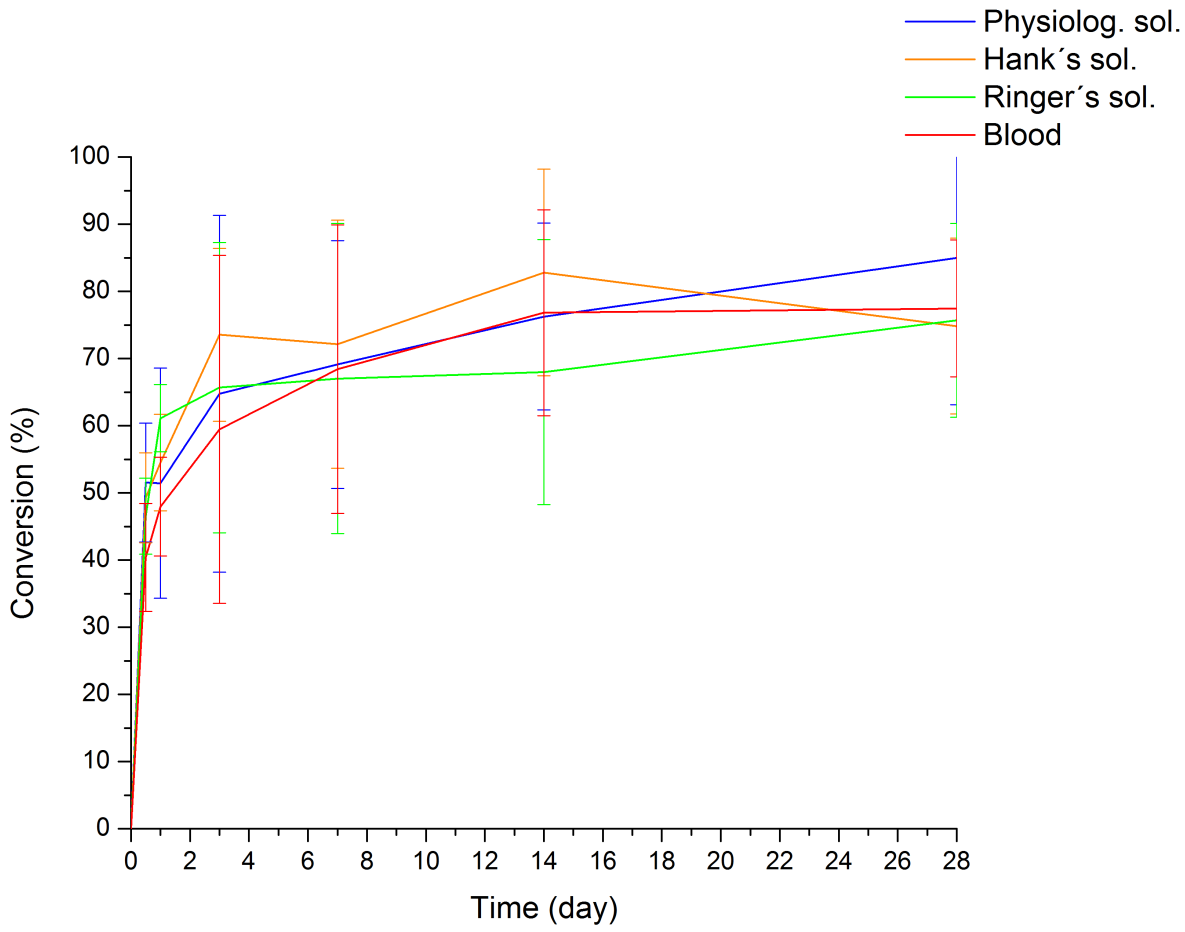

Fig. 4.45 – Conversion of α-TCP to CDHA. Each point represents the mean value of N = 5 peaks ± SD of the mean.

Chemical composition of CPC

In Fig. 4.46 Attenuated Total Reflectance Fourier Transformed Infrared Spectroscopy (ATR-FTIR) spectra of powders, polymer (undissolved) used for sample preparation and 2 sample set in blood (setting times 2 weeks and 1 month) are depicted. For comparison there is depicted spectrum of calcined HAp with FT-IR spectrum almost identical as a FT-IR spectrum of CDHA. FT-IR spectra of the CPC samples are very similar, both with presence of low intense peak at 1824 cm^{-1} for sample set in blood for 2 weeks and at 1818 cm^{-1} for sample set in blood for 1 month proving the presence of triblock copolymer. Functional groups identification was provided according to mentioned literature sources. [65–67]. Fig. 4.47 represents magnified spectrum of selected wavenumbers range.

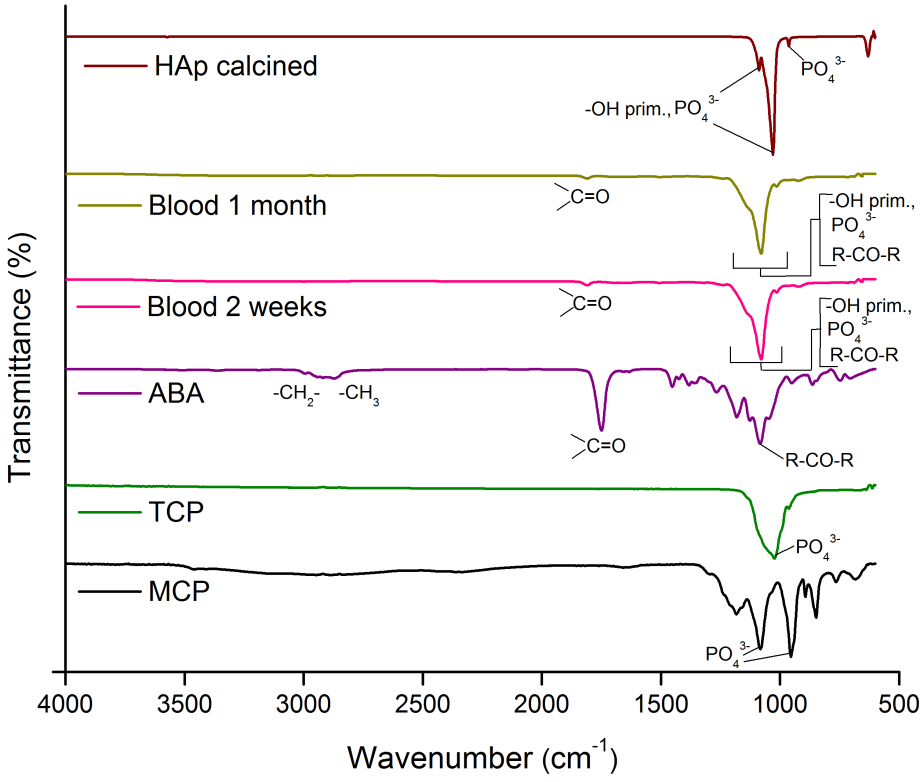

Fig. 4.46 – ATR-FTIR spectra of bone cement chemical components, calcined HAp and 2 set samples.

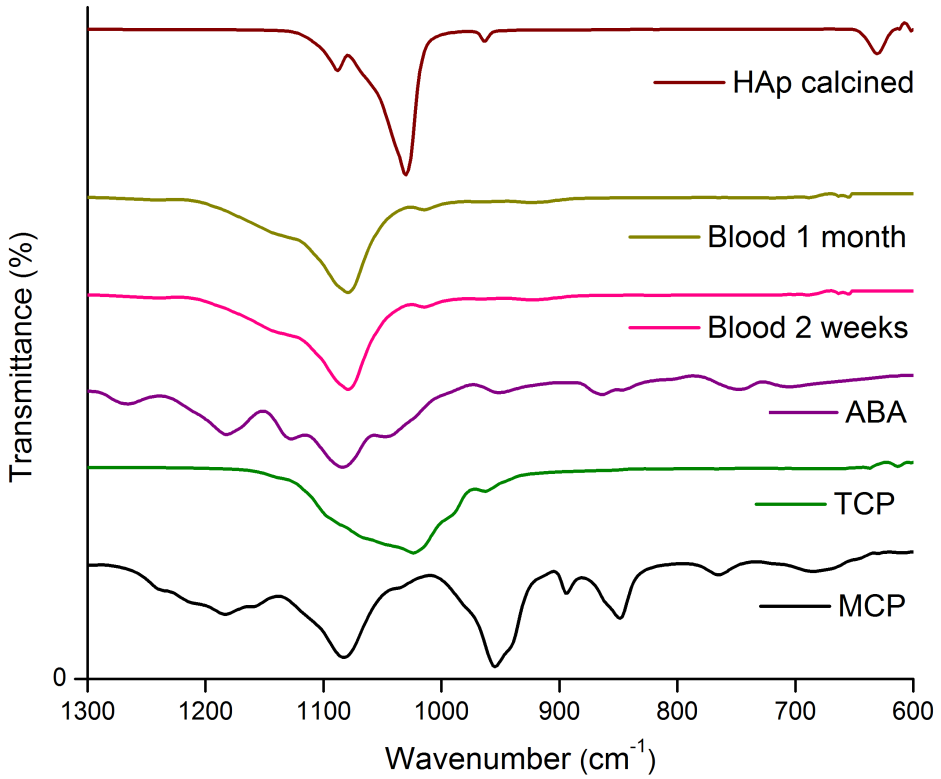

Fig. 4.47 – Magnified ATR-FTIR spectra of bone cement chemical components, calcined HAp and 2 set samples.

X-ray computed microtomography (μ-CT)

The main purpose of X-ray μ-CT measurement was determined porosity of samples set both in Ringer´s solution and blood for 1 month setting period. The reason of μ-CT measurement was evaluation of porosity and its possible effect to compressive strength. Sample set in blood showed an increase of mechanical strength and on the other hand, sample set in Ringer´s solution showed a significant decrease of mechanical strength. Percentage porosity was calculated according to Eq. 4.3.

$$P = \frac{\Sigma V_{\mathrm{v}}}{V_{\mathrm{M}}} \cdot 100 \tag{4.3}$$

where: V_{v} is voids volume, V_{M} is a material volume.

Results showed, that porosity of sample set in Ringer´s solution is equal 7.4 %.
In Fig. 4.48, μ-CT histogram of sample set in Ringer´s solution is depicted, represented a quantity of voids contained in material volume. The small pores with volume range between 0.00-0.02 mm^3 are the most frequent. In general, pores with volume under 0.1 mm^3 are the most frequent.

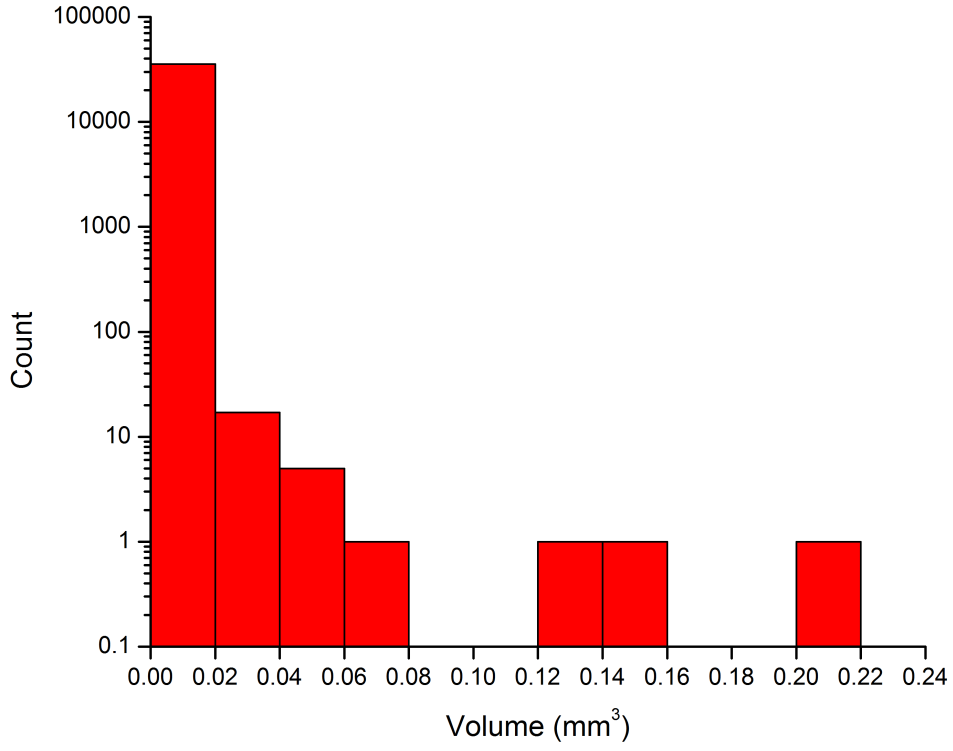

Fig. 4.48 – μ-CT histogram of CPC sample set in Ringer´s solution for 1 month.

Fig. 4.49 shows μ-CT projection of CPC sample set in Ringer´s solution with pore volume distribution and Fig. 4.50 shows 3D μ-CT projections of this CPC sample.

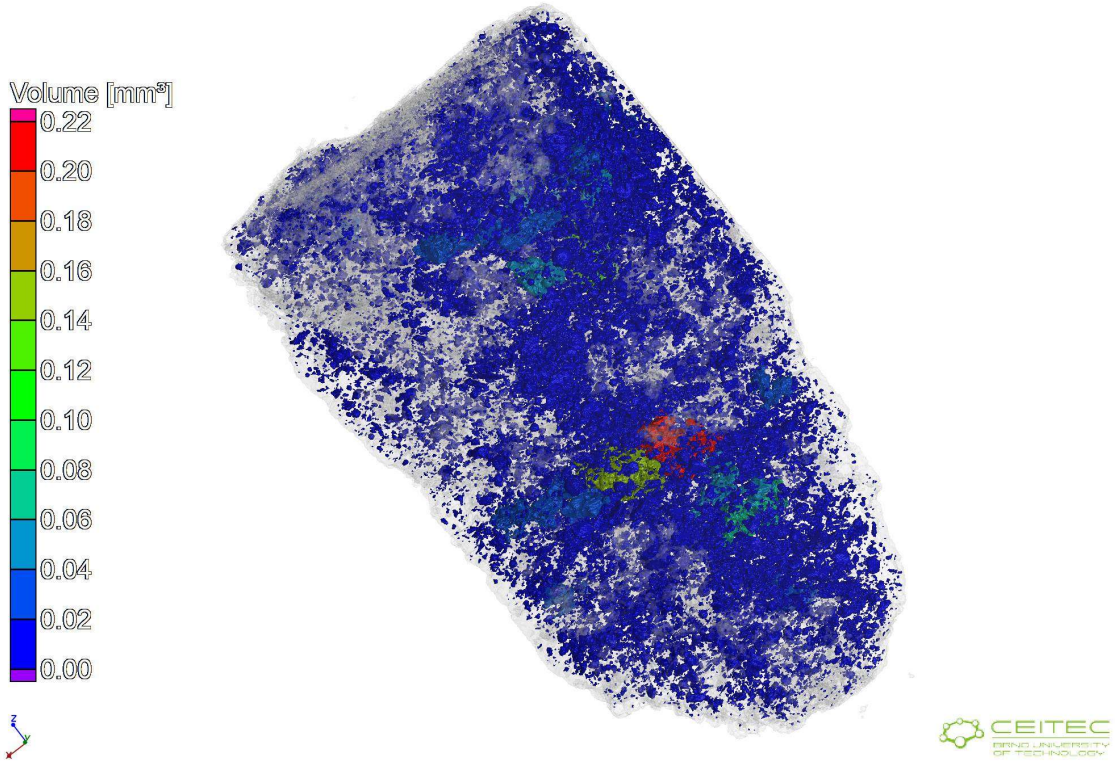

Fig. 4.49 – μ-CT projection of CPC sample set in Ringer´s solution for 1 month.

Fig. 4.50 – 3D μ-CT projection of CPC sample set in Ringer´s solution for 1 month.

Porosity of sample set in blood was calculated to 9.5 %. In Fig. 4.51, the histogram of sample set in blood is depicted, represented a quantity of voids contained in material volume. The small pores with volume range between 0.00-0.02 mm^3 were the most frequent. In general, the most frequent pore volume in material are with volume value under 0.1 mm^3. In comparison with sample set in Ringer´s solution, sample set in blood had a greater diversity of pores volume.

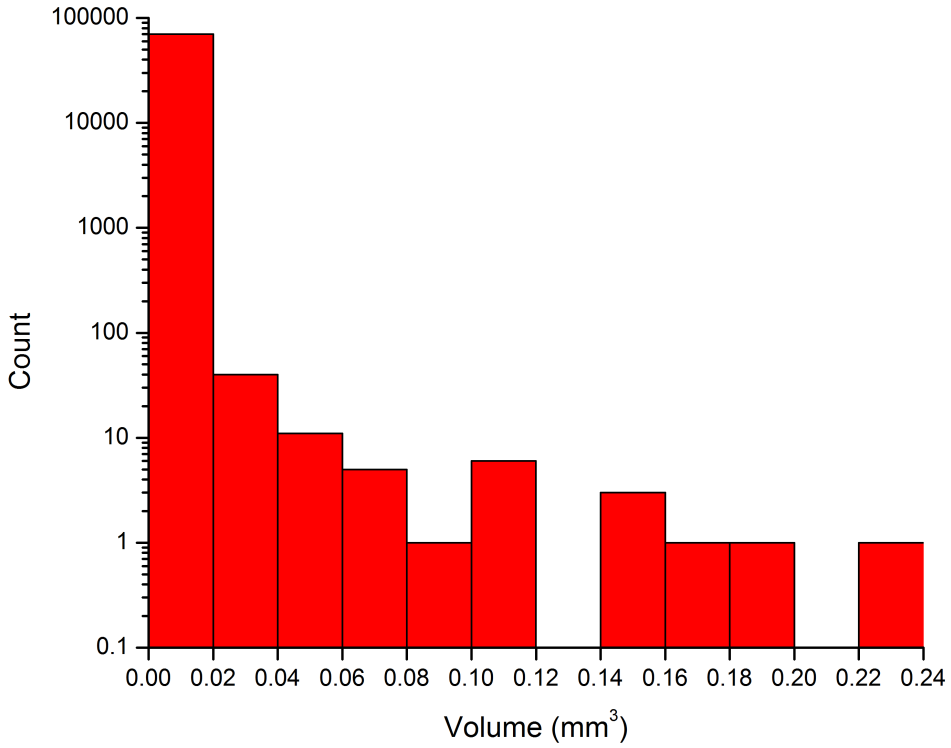

Fig. 4.51 – μ-CT histogram of CPC sample set in blood for 1 month.

Fig. 4.52 shows μ-CT projection of CPC sample set in blood with pore volume distribution and Fig. 4.53 shows 3D μ-CT projections of this CPC sample.

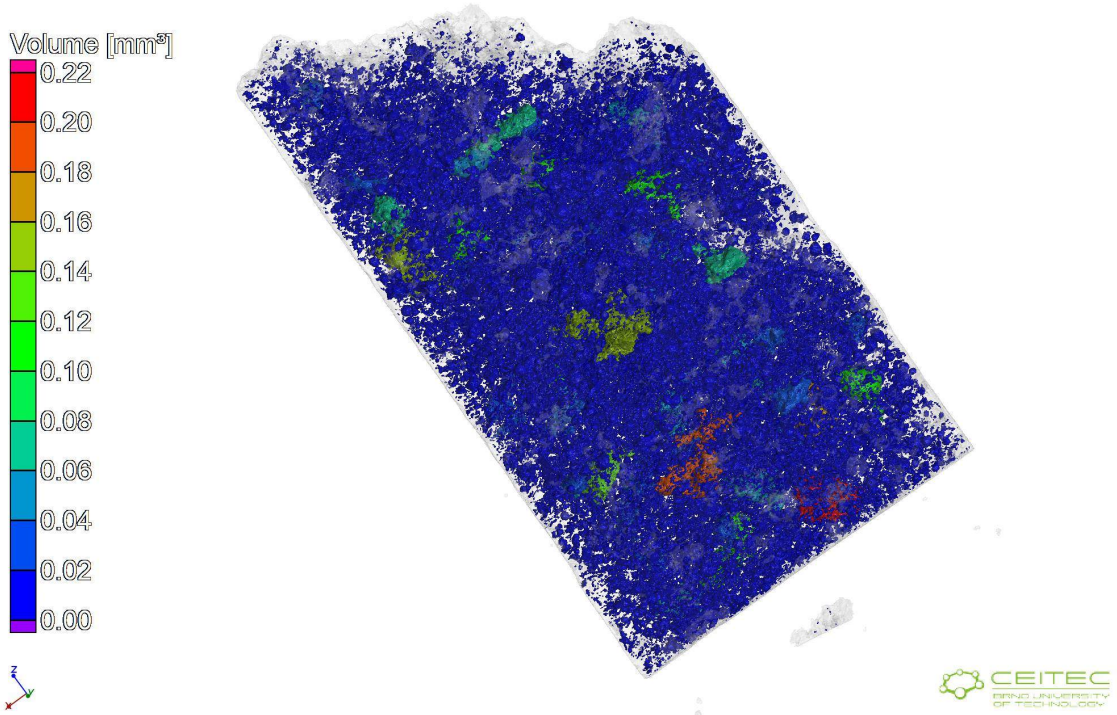

Fig. 4.52 – μ-CT projection of CPC sample set in blood for 1 month.

Fig. 4.53 – 3D μ-CT projection of CPC sample set in blood for 1 month.

According to mechanical compression tests results, higher porosity of sample set in Ringer´s solution than porosity of sample set in blood was expected, but this assumption did not confirmed.

CONCLUSION

The main aim of presented work was to study body fluids effects on setting, structure and mechanical properties of CaP bone cement. Sample preparation experiments followed by their setting in ultrapure water were provided because of determination of preparation technique. Results from preparation optimization showed that the most advanced CDHA formation of sample set in memory foam mold was observed due to the best access of setting liquids to their surface.

Sample surfaces were treated by machine milling due to reaching accurate sample sizes. Unfortunately, dissolution of amount sample volume due to effects of ionic SBF was observed immediately after their applications resulted in insufficient sizes of some samples.

A fracture surface SEM analysis were provided, resulted to increase of CDHA forming correlated with progressive setting time all samples. Besides fully transformed particles to CDHA crystals, unconverted powder particles were observed within microstructures of all sample types even after 1 month of setting confirmed inhibiting effect of SBF on setting CaP cement. Sample porosity according to SEM micrographs were evaluated, resulted in presence of sphere pores with diameter between 5-10 μm corresponding with α-TCP particles diameter for samples set in Hank´s solution, Ringer´s solution and pig blood after 1 week of setting. Representation of these pores in structures of CPC set in Hank´s solution and pig blood even increased after a 1 month. On the other hand, microstructures of samples set in physiological solution after 1 week and 1 month contained no pores, which may correlated with their insignificant compressive strength decrease during the rest of setting period followed after 1 day of setting.

Microstructure of sample set in Ringer´s solution after a month were reorganizated into different type represented by a plate-like less porous CDHA crystals, which correlates with significant decrease of their compressive strength after 1 month of setting. Reorganization of CDHA crytal structure of sample set in Ringer´s solution could be caused by PLGA-PEG-PLGA copolymer degradation accompanied by acidic products release, specifically lactid acid and glycolic acid. Acidic environments could dissolve CDHA structure resulted to reorganization of crystal structure. According to these results, higher porosity of sample set in Ringer´s solution than porosity of sample set in blood for 1 month was expected, but this assumption did not confirmed. Results of μ-CT measurement showed even lower porosity of sample set in Ringer´s solution (7.4 %) in comparison with sample set in blood (9.5 %), which proved that porosity was not a major factor influencing mechanical compressive strength. Besides plate-like crystals a small CDHA shells crystals were observed as in a rest of observed sample microstructures. Effects of chemical composition of Ringer´s solution to delay the initiation of setting reaction were discussed. As a main factor influencing delay of initiation setting reaction and consenquently hardening of CaP bone cement set in Ringer´s solution a zero concentration of phosphates was evaluated.

In the case of blood setting environment effect, delay of initiation of setting reactions caused by a blood plasma proteins presence (e.q. albumin) and hydrophobic non-polar amino acids presence resulting to inhibition of CDHA crystal formation were observed as well. Otherwise, samples set in blood had highest compression strength after 1 month of setting even with presence of a lot of micropores. This result could be affected by highest concentration level of phosphates in blood as used liquid setting environment.

The main purpose of FT-IR measurements was comparison of samples set in blood environments for 2 setting times (2 week and 1 month) from chemical compositions followed

by degradation PLGA-PEG-PLGA level evaluation. Results showed no difference between their FT-IR spectra proved their identical chemical compositions. Amount of PLGA-PEG-PLGA copolymer was measured by FT-IR analysis even after 1 month of setting, because the degradation of copolymer could be affected by used SBF setting environments.

XRD diffraction patterns confirmed α-TCP gradual conversion to CDHA without any differences between individual evaluation of used setting environments, but according to conversion graph, CDHA increase during whole setting period, except samples set in Hank´s solution. Decrease of CDHA quantity after 3 days and 2 weeks of samples set in Hank´s solution corresponded with decrease of their mechanical strength, which could be affected by a changing microstructure due to ion effects, respectively primary caused by presence of magnesium sulfate and phosphates in Hank´s solution setting environment. The highest conversion after 12 hours setting period of samples set in physiological solution was observed, which reflected their highest compression strength and non-porous microstructure as mentioned. The result may be affected by presence of no CDHA crystal formation inhibitors. Samples set in blood environment had α-TCP conversion value only about 40 % after 12 hours represented the lowest value of all calculated conversions. Conversions of sample set in blood, physiological and Ringer´s solutions increased even after 2 weeks of setting.

Results showed, that native blood liquid setting environment has significant effect on the structure and properties of CPC, specifically on the porosity, setting rate and mechanical properties. Results of this study are essential to predicting properties of this CPC material *in vivo*.

BIBLIOGRAPHY

1. American Dental Association, Guide to Dental Materials and Devices, 4th ed., Chicago. 1968/1969, 40-55. ASIN: B01CSL0I6O.

2. BROWN, W.E., Chow, L.C., A new calcium phosphate water-setting cement, Cements Research Progress, Westerville, (1986), 352-379.

3. GRUNINGER, S. E., C. Siew, L. C. Chow, A. O´Young, N. K. Ts´ao, WE. Brown. Evaluation of the biocompatibility of a new calcium phosphate setting cement. J Dent Res. 1984, 63, 63-200.

4. BLACK, J. Biological performance of materials: fundamentals of biocompatibility. 4th ed. Boca Raton: CRC Taylor and Francis, 2006. ISBN 0-8493-3959-6.

5. KOLMAS, Joanna, Agnieszka KAFLAK, Aneta ZIMA and Anna ŚLÓSARCZYK. Alpha-tricalcium phosphate synthesized by two different routes: Structural and spectroscopic characterization. Ceramics International. 2015, 41(4), 5727-5733. DOI: 10.1016/j.ceramint.2014.12.159. ISSN 02728842.

6. DOS SANTOS, L.A, R.G CARRODÉGUAS, S.O ROGERO, O.Z HIGA, A.O BOSCHI and A.C.F DE ARRUDA. α-Tricalcium phosphate cement: "in vitro" cytotoxicity. Biomaterials. 2002, 23(9), 2035-2042. DOI: 10.1016/S0142-9612(01)00333-7. ISSN 01429612.

7. CARRODEGUAS, R.G. and S. DE AZA. α-Tricalcium phosphate: Synthesis, properties and biomedical applications. Acta Biomaterialia. 2011, 7(10), 3536-3546. DOI: 10.1016/j.actbio.2011.06.019. ISSN 17427061.

8. YUBAO, Li, Zhang XINGDONG and K. DE GROOT. Hydrolysis and phase transition of alpha-tricalcium phosphate. Biomaterials. 1997, 18(10), 737-741. DOI: 10.1016/S0142-9612(96)00203-7. ISSN 01429612.

9. Liu J, Zhao L, Ni L, et al. The effect of synthetic α-tricalcium phosphate on osteogenic differentiation of rat bone mesenchymal stem cells. American Journal of Translational Research. 2015;7(9):1588-1601.

10. KREIDLER, Eric R. and Floyd A. HUMMEL. Phase relations in the system - ($SrO - P_2O_5$ and the influence of water vapor on the formation of ($Sr_4P_2O_9$. Inorganic Chemistry. 1967, 6(5), 884-891. DOI: 10.1021/ic50051a007. ISSN 0020-1669.

11. MATHEW, M., L. W. SCHROEDER, B. DICKENS and W. E. BROWN. The crystal structure of α-($Ca_3(PO_4)_2$. Acta Crystallographica Section B Structural Crystallography and Crystal Chemistry. 33(5), 1325-1333 DOI: 10.1107/S0567740877006037. ISSN 05677408.

12. DICKENS, B., BROWN, W. E., Acta Crystallographica, B28, 1972, 3056-3065

13. KOLMAS, Joanna, Agnieszka KAFLAK, Aneta ZIMA and Anna ŚLÓSARCZYK. Alpha-tricalcium phosphate synthesized by two different routes: Structural and spectroscopic characterization. Ceramics International. 2015, 41(4), 5727-5733. DOI: 10.1016/j.ceramint.2014.12.159. ISSN 02728842.

14. HUGHES, E., T. YANNI, P. JAMSHIDI and L. M. GROVER. Inorganic cements for biomedical application: calcium phosphate, calcium sulphate and calcium silicate. Advances in Applied Ceramics [online]. 2014, 114(2), 65-76. DOI: 10.1179/1743676114Y.0000000219. ISSN 1743-6753.

15. MONTUFAR, E.B., Y. MAAZOUZ and M.P. GINEBRA. Relevance of the setting reaction to the injectability of tricalcium phosphate pastes. Acta Biomaterialia. 2013, 9(4), 6188-6198. DOI: 10.1016/j.actbio.2012.11.028. ISSN 17427061.

16. BOHNER, M. Calcium orthophosphates in medicine: from ceramics to calcium phosphate cements. Injury. 2000, 31, D37-D47. DOI: 10.1016/S0020-1383(00)80022-4. ISSN 00201383.

17. REIS, Rui L. a Julio. SAN ROMÁN. Biodegradable systems in tissue engineering and regenerative medicine. Boca Raton: CRC Press, c2005. ISBN 9780849319365.

18. UCHINO, Tomohiro, Kohei YAMAGUCHI, Ichiro SUZUKI, Masanobu KAMITAKAHARA, Makoto OTSUKA and Chikara OHTSUKI. Hydroxyapatite formation on porous ceramics of alpha-tricalcium phosphate in a simulated body fluid. Journal of Materials Science: Materials in Medicine. 2010, 21(6), 1921-1926. DOI: 10.1007/s10856-010-4042-4. ISSN 0957-4530.

19. BOHNER, M., U. GBURECK and J.E. BARRALET. Technological issues for the development of more efficient calcium phosphate bone cements: A critical assessment. Biomaterials. 2005, 26(33), 6423-6429. DOI: 10.1016/j.biomaterials.2005.03.049. ISSN 01429612.

20. MATSUNAGA, Katsuyuki, Tomonori KUBOTA, Kazuaki TOYOURA and Atsutomo NAKAMURA. First-principles calculations of divalent substitution of Ca^2+ in tricalcium phosphates. Acta Biomaterialia. 2015, 23, 329-337. DOI: 10.1016/j.actbio.2015.05.014. ISSN 17427061.

21. GBURECK, Uwe, Jake E. BARRALET, Kerstin SPATZ, Liam M. GROVER a Roger THULL. Ionic modification of calcium phosphate cement viscosity. Part I: hypodermic injection and strength improvement of apatite cement. Biomaterials. 2004, 25(11), 2187-2195. DOI: 10.1016/j.biomaterials.2003.08.066. ISSN 01429612.

22. SARDA, S., E. FERNÁNDEZ, M. NILSSON, M. BALCELLS and J. A. PLANELL. Kinetic study of citric acid influence on calcium phosphate bone cements as water-reducing agent. Journal of Biomedical Materials Research. 2002, 61(4), 653-659 DOI: 10.1002/jbm.10264. ISSN 00219304.

23. BENDER, SA, JP SCHMITZ and JL ONG. Effect of Biofluid Environment on the Dissolution and Flexural Strength of Calcium Phosphate Bone Cements. Implant Dentistry. 2001, 10(2), 143-148. DOI: 10.1097/00008505-200104000-00012. ISSN 1056-6163.

24. O'NEILL, R., H.O. MCCARTHY, E.B. MONTUFAR, M.-P. GINEBRA, D.I. WILSON, A. LENNON a N. DUNNE. Critical review: Injectability of calcium phosphate pastes and cements. Acta Biomaterialia. 2017, 50, 1-19. DOI: 10.1016/j.actbio.2016.11.019. ISSN 17427061.

25. MAYR-WOHLFART, U., Fiedler, J., Günther, K.-P., Puhl, W. and Kessler, S. (2001), Proliferation and differentiation rates of a human osteoblast-like cell line (SaOS-2) in contact with different bone substitute materials. J. Biomed. Mater. Res., 57: 132–139. DOI: 10.1002/1097-4636(200110)57:1<132::AID-JBM1152>3.0.CO;2-K

26. EHARA, A., Ogata, K., Imazato, S., Ebisu, S., Nakano, T., Umakoshi, Y., Effects of α-TCP and TetCP on MC3T3-E1 proliferation, differentiation and mineralization. Biomaterials. 2003, 24, 831-836. DOI: 10.1016/S0142-9612(02)00411-8.

27. HERTEN, M., D. ROTHAMEL, F. SCHWARZ, K. FRIESEN, G. KOEGLER and J. BECKER. Surface- and nonsurface-dependent in vitro effects of bone substitutes on cell viability. Clinical Oral Investigations. 2009, 13(2), 149-155. DOI: 10.1007/s00784-008-0214-8. ISSN 1432-6981.

28. TAMAI, M., Ryusuke NAKAOKA and Toshie TSUCHIYA. Cytotoxicity of Various Calcium Phosphate Ceramics. Key Engineering Materials. 2006, 309-311, 263-266. DOI: 10.4028/www.scientific.net/KEM.309-311.263. ISSN 1662-9795.

29. KOJIC, Z., Stojanovic, D., Popadic, S., Jokanovic, M., Jokanovic, D., The irritative property of alpha-tricalcium phosphate to the rabbit skin. General physiology and biophysics. 2009, 28 Spec. No: 168-73.

30. WILTFANG, J., H. A. MERTEN, K. A. SCHLEGEL, S. SCHULTZE-MOSGAU, F. R. KLOSS, S. RUPPRECHT and P. KESSLER. Degradation characteristics of α and β tri-calcium-phosphate (TCP) in minipigs. Journal of Biomedical Materials Research. 2002, 63(2), 115-121. DOI: 10.1002/jbm.10084. ISSN 0021-9304.

31. KIHARA, Hidemichi, Makoto SHIOTA, Yasuo YAMASHITA and Shohei KASUGAI. Biodegradation process of α-TCP particles and new bone formation in a rabbit cranial defect model. Journal of Biomedical Materials Research Part B: Applied Biomaterials. 2006, 79B(2), 284-291. DOI: 10.1002/jbm.b.30540. ISSN 1552-4973.

32. MUSHA, Yoshiro, Tomohiro UMEDA, Sayuri YOSHIZAWA, Toshio SHIGEMITSU, Kazuhiro MIZUTANI and Kiyoshi ITATANI. Effects of blood on bone cement made of calcium phosphate: Problems and advantages. Journal of Biomedical Materials Research Part B: Applied Biomaterials. 2010, 92B(1), 95-101. DOI: 10.1002/jbm.b.31493. ISSN 15524973.

33. TURNER, Thomas M., Robert M. URBAN, Kern SINGH, Deborah J. HALL, Susan M. RENNER, Tae-Hong LIM, Michael J. TOMLINSON a Howard S. AN. Vertebroplasty comparing injectable calcium phosphate cement compared with polymethylmethacrylate in a unique canine vertebral body large defect model. The Spine Journal. 2008, 8(3), 482-487. DOI: 10.1016/j.spinee.2006.12.007. ISSN 15299430.

34. YOO, Jeong Hyun, Kang Sik LEE a Soo Ho LEE. The Analysis of Osteoconducting Ability of Alpha-Tricalcium Phosphate-Based Bone Filler Powder. Key Engineering Materials. 2006, 309-311, 259-262. DOI: 10.4028/www.scientific.net/KEM.309-311.259. ISSN 1662-9795.

35. YAMADA, Masahiro, Makoto SHIOTA, Yasuo YAMASHITA a Shohei KASUGAI. Histological and histomorphometrical comparative study of the degradation and osteoconductive characteristics of α- and β-tricalcium phosphate in block grafts. Journal

of Biomedical Materials Research Part B: Applied Biomaterials. 2007, 82B(1), 139-148. DOI: 10.1002/jbm.b.30715. ISSN 15524973.

36. NYAN, Myat, Daisuke SATO, Hidemichi KIHARA, Tetsu MACHIDA, Keiichi OHYA a Shohei KASUGAI. Effects of the combination with α-tricalcium phosphate and simvastatin on bone regeneration. Clinical Oral Implants Research. 2009, 20(3), 280-287. DOI: 10.1111/j.1600-0501.2008.01639.x. ISSN 09057161.

37. COLPO, Julio C., Caroline PIGATTO, Nayrim BRIZUELA, Javier ARAGÓN a Luís A. L. DOS SANTOS. Antibiotic and anesthetic drug release from double-setting α-TCP cements. Journal of Materials Science. 2018, 53(10), 7112-7124. DOI: 10.1007/s10853-018-2071-4. ISSN 0022-2461.

38. FADEEVA, I. V., Ya. Yu. FILIPPOV, A. S. FOMIN, N. V. PETRAKOVA, A. V. KNOTKO, A. P. RYZHOV, V. I. PUTLYAEV and S. M. BARINOV. Microstructure and properties of α-tricalcium phosphate-based bone cement. Inorganic Materials. 2017, 53(3), 292-299. DOI: 10.1134/S0020168517030049. ISSN 0020-1685.

39. KUTIKOV, Artem B. a Jie SONG. An amphiphilic degradable polymer/hydroxyapatite composite with enhanced handling characteristics promotes osteogenic gene expression in bone marrow stromal cells. Acta Biomaterialia. 2013, 9(9), 8354-8364 DOI: 10.1016/j.actbio.2013.06.013. ISSN 17427061.

40. VASCONCELLOS, Letícia Araújo a Luís Alberto DOS SANTOS. Calcium phosphate cement scaffolds with PLGA fibers. Materials Science and Engineering. 2013, 33(3), 1032-1040. DOI: 10.1016/j.msec.2012.10.019. ISSN 09284931.

41. BARBIERI, Davide, Huipin YUAN, Xiaoman LUO, Silvia FARÈ, Dirk W. GRIJPMA a Joost D. DE BRUIJN. Influence of polymer molecular weight in osteoinductive composites for bone tissue regeneration. Acta Biomaterialia. 2013, 9(12), 9401-9413 .DOI: 10.1016/j.actbio.2013.07.026. ISSN 17427061.

42. KAMERER, DB., HIRSCH, BE., SNYDERMAN, CH., CONSTANTINO, P., FRIEDMAN, CD. Hydroxyapatite cement: a new method for achieving watertight closure in transtemporal surgery. Am J Otol. 1994 Jan;15(1):47-9.

43. BOHNER, M. New hydraulic cements based on α-tricalcium phosphate–calcium sulfate dihydrate mixtures. Biomaterials. 2004, 25(4), 741-749. DOI: 10.1016/S0142-9612(03)00573-8. ISSN 01429612.

44. BI, Long, Wenjun CHENG, Hongbin FAN and Guoxian PEI. Reconstruction of goat tibial defects using an injectable tricalcium phosphate/chitosan in combination with autologous platelet-rich plasma. Biomaterials. 2010, 31(12), 3201-3211. DOI: 10.1016/j.biomaterials.2010.01.038. ISSN 01429612.

45. SIEK, Dominika, Anna ŚLÓSARCZYK, Agata PRZEKORA, Anna BELCARZ, Aneta ZIMA, Grażyna GINALSKA a Joanna CZECHOWSKA. Evaluation of antibacterial activity and cytocompatibility of α-TCP based bone cements with silver-doped hydroxyapatite and $CaCo_3$. Ceramics International. 2017, 43(16), 13997-14007. DOI: 10.1016/j.ceramint.2017.07.131. ISSN 02728842.

46. NETTI, Paulo A. Biomedical foams for tissue engineering applications. Amsterdam: Elsevier/WP, Woodhead Publishing is an imprint of Elsevier, 2014. Woodhead Publishing series in biomaterials, no. 76. ISBN 9780857096968.

47. DOUGLAS, Timothy E. L., Josefien SCHIETSE, Aneta ZIMA, et al. Novel self-gelling injectable hydrogel/alpha-tricalcium phosphate composites for bone regeneration: Physiochemical and microcomputer tomographical characterization. Journal of Biomedical Materials Research Part A. 2018, 106(3), 822-828. DOI: 10.1002/jbm.a.36277. ISSN 15493296.

48. GBURECK, U. Mechanical activation and cement formation of β-tricalcium phosphate. Biomaterials. 2003, 24(23), 4123-4131. DOI: 10.1016/S0142-9612(03)00283-7. ISSN 01429612.

49. UNOSSON, J., ENGQVIST, H. Development of a Resorbable Calcium Phosphate Cement with Load Bearing Capacity. Bioceramics Development and Applications. 2016, 04(01), DOI: 10.4172/2090-5025.1000074. ISSN 20905025.

50. FERNA´NDEZ, E., F. J. GIL, M. P. GINEBRA, F. C. M. DRIESSENS, J. A. PLANELL and S. M. BEST. Calcium phosphate bone cements for clinical applications. Part II: Precipitate formation during setting reactions. Journal of Materials Science: Materials in Medicine. 10(3), 177-183. DOI: 10.1023/A:1008989525461. ISSN 09574530.

51. GRUMEZESCU, Alexandru Mihai. Nanobiomaterials in hard tissue engineering: applications of nanobiomaterials. Boston: Elsevier/WA, William Andrew is an imprint of Elsevier, 2016. Applications of nanobiomaterials, v. 4.

52. GINEBRA, Maria-Pau, Cristina CANAL, Montserrat ESPANOL, David PASTORINO a Edgar B. MONTUFAR. Calcium phosphate cements as drug delivery materials. Advanced Drug Delivery Reviews. 2012, 64(12), 1090-1110. DOI: 10.1016/j.addr.2012.01.008. ISSN 0169409X.

53. APELT, D., F. THEISS, A.O. EL-WARRAK, et al. In vivo behavior of three different injectable hydraulic calcium phosphate cements. Biomaterials. 2004, 25(7-8), 1439-1451. DOI: 10.1016/j.biomaterials.2003.08.073. ISSN 01429612.

54. OOMS, E.M, J.G.C WOLKE, M.T VAN DE HEUVEL, B JESCHKE a J.A JANSEN. Histological evaluation of the bone response to calcium phosphate cement implanted in cortical bone. Biomaterials. 2003, 24(6), 989-1000. DOI: 10.1016/S0142-9612(02)00438-6. ISSN 01429612.

55. KNAACK, D., M.E. GOAD, M. AIOLOVA, C. REY, A. TOFIGHI, P. CHAKRAVARTHY, D.D. LEE. Resorbable calcium phosphate bone substitute. Journal of biomedical materials research. 1998, 43(4), 399-409. PMID: 9855198.

56. MIÑO-FARIÑA, Natalia, Fernando MUÑOZ-GUZÓN, Mónica LÓPEZ-PEÑA, Maria-Pau GINEBRA, Sergio DEL VALLE-FRESNO, Dolors AYALA a Antonio GONZÁLEZ-CANTALAPIEDRA. Quantitative analysis of the resorption and osteoconduction of a macroporous calcium phosphate bone cement for the repair of a critical size defect in the femoral condyle. The Veterinary Journal. 2009, 179(2), 264-272. DOI: 10.1016/j.tvjl.2007.09.011. ISSN 10900233.

57. KUTIKOV, Artem B. a Jie SONG. An amphiphilic degradable polymer/hydroxyapatite composite with enhanced handling characteristics promotes osteogenic gene expression in bone marrow stromal cells. Acta Biomaterialia. 2013, 9(9), 8354-8364. DOI: 10.1016/j.actbio.2013.06.013. ISSN 17427061.

58. MICHLOVSKÁ, L., Lucy VOJTOVÁ, Ludmila MRAVCOVÁ, Soňa HERMANOVÁ, Jiří KUČERÍK, Josef Jančář. Funktionalization Conditions of PLGA-PEG-PLGA Copolymer with Itaconic Anhydride. Macromolecular Symposia. 2012, 295, 119-124. DOI: 10.1002/masy.200900071.

59. HAVALDAR, Raviraj, SC PILLI a BB PUTTI. Insights into the effects of tensile and compressive loadings on human femur bone. Advanced Biomedical Research. 2014, 3(1), 101. DOI: 10.4103/2277-9175.129375. ISSN 2277-9175.

60. GINEBRA, M.P., E. FERNÁNDEZ, E.A.P. DE MAEYER, R.M.H. VERBEECK, M.G. BOLTONG, J. GINEBRA, F.C.M. DRIESSENS a J.A. PLANELL. Setting Reaction and Hardening of an Apatitic Calcium Phosphate Cement. Journal of Dental Research. 2016, 76(4), 905-912. DOI: 10.1177/00220345970760041201. ISSN 0022-0345.

61. FERNÁNDEZ, E., M. P. GINEBRA, M. G. BOLTON, F. C. M. DRIESSENS, J. GINEBRA, E. A. P. De MAEYER, R. M. H. VERBEECK, J. A. PLANELL. Kinetic study of the setting reaction of a calcium phosphate bone cement. Journal of biomedical materials research. 1996, 32(3), 367-74. DOI: 10.1002/(SICI)1097-4636(199611)32:3<367::AID-JBM9>3.0.CO;2-Q.

62. CHEN, Shyuan-Yow, Shih-Fu OU, Nai-Cia TENG, Chun-Ming KUNG, Hsien-Lung TSAI, Kuo-Tien CHU a Keng-Liang OU. Phase transformation on bone cement: Monocalcium phosphate monohydrate into calcium-deficient hydroxyapatite during setting. Ceramics International. 2013, 39(3), 2451-2455. DOI: 10.1016/j.ceramint.2012.08.097. ISSN 02728842.

63. SAFC Biosciences, Product Information - Hanks´ Balanced Salt Solution, 2006. Available from: *https : //www.sigmaaldrich.com/content/dam/sigma − aldrich/docs/Sigma/Product_Information_Sheet/p*55037*.pdf*

64. Sigma-Aldrich, Product Information - 96724 Ringers solution 1/4 strength tablets. Available from: *https : //www.sigmaaldrich.com/content/dam/sigma − aldrich/docs/Sigma − Aldrich/Datasheet/*1/96724*dat.pdf*

65. BERZINA-CIMDINA, Liga a Natalija BORODAJENKO. Research of Calcium Phosphates Using Fourier Transform Infrared Spectroscopy. THEOPHANIDES, Theophile, ed. Infrared Spectroscopy - Materials Science, Engineering and Technology. InTech, 2012, 2012-04-25. DOI: 10.5772/36942. ISBN 978-953-51-0537-4.

66. MICHLOVSKÁ, L.: Functionalization of biodegradable polymers by itaconic anhydride. Brno: Brno University of Technology, Faculty of Chemistry, 2009. 59 p. Supervisor Ing. Lucy Vojtová, Ph.D.

67. HUANG, Chen a Peng CAO. Tuning Ca: P ratio by NaOH from monocalcium phosphate monohydrate (MCPM). Materials Chemistry and Physics. 2016, 181, 159-166. DOI: 10.1016/j.matchemphys.2016.06.045. ISSN 02540584.

68. HAMDI, M. a A. IDE-EKTESSABI. Dissolution behavior of simultaneous vapor deposited calcium phosphate coatings in vitro. Materials Science and Engineering: C. 2007, 27(4), 670-674. DOI: 10.1016/j.msec.2006.06.008. ISSN 09284931.

69. COMBES, C. a C. REY. Adsorption of proteins and calcium phosphate materials bioactivity. Biomaterials. 2002, 23(13), 2817-2823. DOI: 10.1016/S0142-9612(02)00073-X. ISSN 01429612.

70. CARTER, D.C., HO, J.X., Anfinsen, C.B., Edsall, J.T., Richards, F.M., Eisenberg, D.S., Schumaker, V.N. Advances in protein chemistry - Lipoproteins, apolipoproteins, and lipases. San Diego: Academic Press, 1994, 193. ISBN 9780080582184.

71. MELLIER, Charlotte, François-Xavier LEFÈVRE, Franck FAYON, et al. A straightforward approach to enhance the textural, mechanical and biological properties of injectable calcium phosphate apatitic cements (CPCs): CPC/blood composites, a comprehensive study. Acta Biomaterialia. 2017, 62, 328-339. DOI: 10.1016/j.actbio.2017.08.040. ISSN 17427061.

72. KOUTSOPOULOS, S. a E. DALAS. Inhibition of Hydroxyapatite Formation in Aqueous Solutions by Amino Acids with Hydrophobic Side Groups. Langmuir. 2000, 16(16), 6739-6744. DOI: 10.1021/la000057z. ISSN 0743-7463.

APPENDICES

Appendix 1.: Sample size measurement

Setting environment	Sample designation	Lenght (mm)	Diameter (mm)
Physiological solution	$P1_{12h}$	10.921	5.998
	$P2_{12h}$	12.078	5.982
	$P3_{12h}$	10.951	5.981
Hank´s solution	$H1_{12h}$	12.079	5.994
	$H2_{12h}$	12.080	6.012
	$H3_{12h}$	11.027	5.971
Ringer´s solution	$R1_{12h}$	10.327	6.011
	$R2_{12h}$	9.444	5.997
	$R3_{12h}$	12.080	5.993
Blood	$B1_{12h}$	9.866	5.983
	$B2_{12h}$	9.951	6.010

Tab. 4.4 – Sample sizes after 12 hours of setting and machine milling.

Setting environment	Sample designation	Lenght (mm)	Diameter (mm)
Physiological solution	$P1_{1d}$	12.018	5.965
	$P2_{1d}$	12.022	5.958
	$P3_{1d}$	11.677	5.989
Hank´s solution	$H1_{1d}$	12.855	5.971
	$H2_{1d}$	11.469	5.962
	$H3_{1d}$	12.811	5.952
Ringer´s solution	$R1_{1d}$	11.380	7.054
	$R2_{1d}$	12.171	5.971
	$R3_{1d}$	11.568	5.976
Blood	$B1_{1d}$	11.859	5.971
	$B2_{1d}$	12.016	5.974
	$B3_{1d}$	12.026	5.960

Tab. 4.5 – Sample sizes after 1 day of setting and machine milling.

Setting environment	Sample designation	Lenght (mm)	Diameter (mm)
Physiological solution	$P1_{3d}$	12.066	6.028
	$P2_{3d}$	12.078	5.981
	$P3_{3d}$	12.068	6.008
Hank´s solution	$H1_{3d}$	12.098	5.977
	$H2_{3d}$	12.116	5.959
	$H3_{3d}$	12.087	6.012
Ringer´s solution	$R1_{3d}$	12.092	5.981
	$R2_{3d}$	12.084	5.982
	$R3_{3d}$	11.089	5.961
Blood	$B1_{3d}$	12.088	5.979
	$B2_{3d}$	12.093	6.026
	$B3_{3d}$	12.098	5.980

Tab. 4.6 – Sample sizes after 3 days of setting and machine milling.

Setting environment	Sample designation	Lenght (mm)	Diameter (mm)
Physiological solution	$P1_{1w}$	12.075	6.007
	$P2_{1w}$	12.075	6.001
	$P3_{1w}$	12.091	5.988
Hank´s solution	$H1_{1w}$	11.408	6.063
	$H2_{1w}$	11.189	6.007
	$H3_{1w}$	11.209	5.989
Ringer´s solution	$R1_{1w}$	12.095	5.986
	$R2_{1w}$	12.104	6.022
	$R3_{1w}$	12.088	5.991
Blood	$B1_{1w}$	12.105	6.059
	$B2_{1w}$	12.083	6.046
	$B3_{1w}$	12.108	6.012

Tab. 4.7 – Sample sizes after 1 week of setting and machine milling.

Setting environment	Sample designation	Lenght (mm)	Diameter (mm)
Physiological solution	$P1_{2w}$	11.105	5.974
	$P2_{2w}$	10.496	6.008
	$P3_{2w}$	11.026	5.998
Hank´s solution	$H1_{2w}$	12.099	5.988
	$H2_{2w}$	12.080	5.979
	$H3_{2w}$	12.134	5.983
Ringer´s solution	$P1_{2w}$	12.081	5.952
	$R2_{2w}$	12.085	5.984
	$R3_{2w}$	12.085	6.002
Blood	$B1_{2w}$	12.066	6.001
	$B2_{2w}$	9.493	6.046
	$B3_{2w}$	11.616	6.007

Tab. 4.8 – Sample sizes after 2 weeks of setting and machine milling.

Setting environment	Sample designation	Lenght (mm)	Diameter (mm)
Physiological solution	$P1_{1m}$	10.005	5.990
	$P2_{1m}$	9.410	6.007
Hank´s solution	$H1_{1m}$	12.070	5.994
	$H2_{1m}$	11.999	6.026
	$H3_{1m}$	11.002	6.015
Ringer´s solution	$R1_{1m}$	10.837	6.014
	$R2_{1m}$	10.261	5.985
	$R3_{1m}$	9.638	6.007
Blood	$B1_{1m}$	12.073	6.005
	$B2_{1m}$	12.061	5.996
	$B3_{1m}$	9.497	6.037

Tab. 4.9 – Sample sizes after 1 month of setting and machine milling.

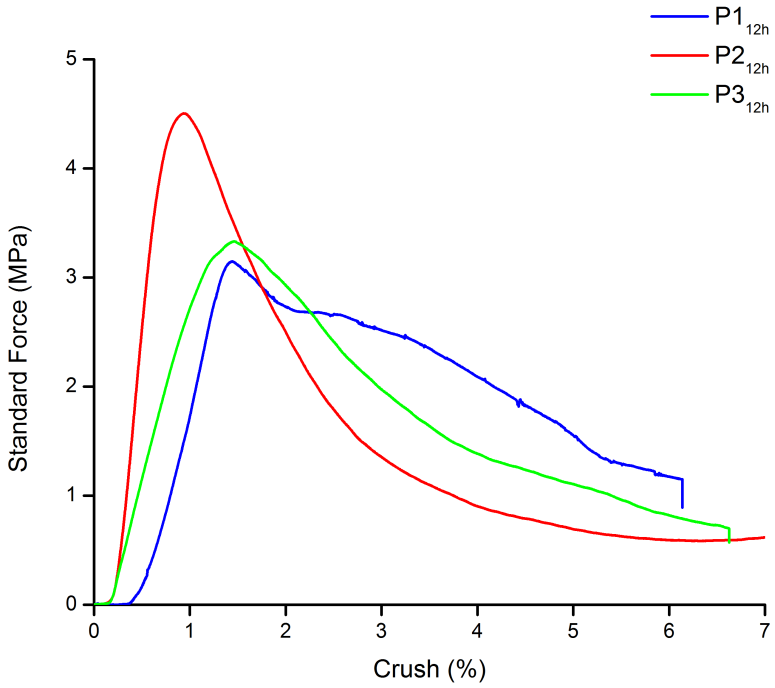

Fig. 4.54 – Results of compression tests of samples set in physiological solution setting environment for 12 hours.

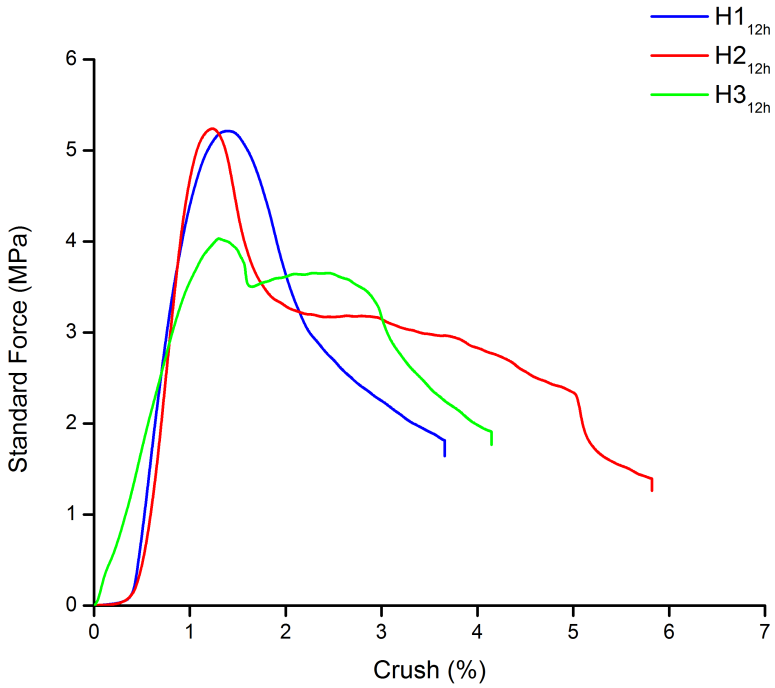

Fig. 4.55 – Results of compression tests of samples set in Hank´s solution setting environment for 12 hours.

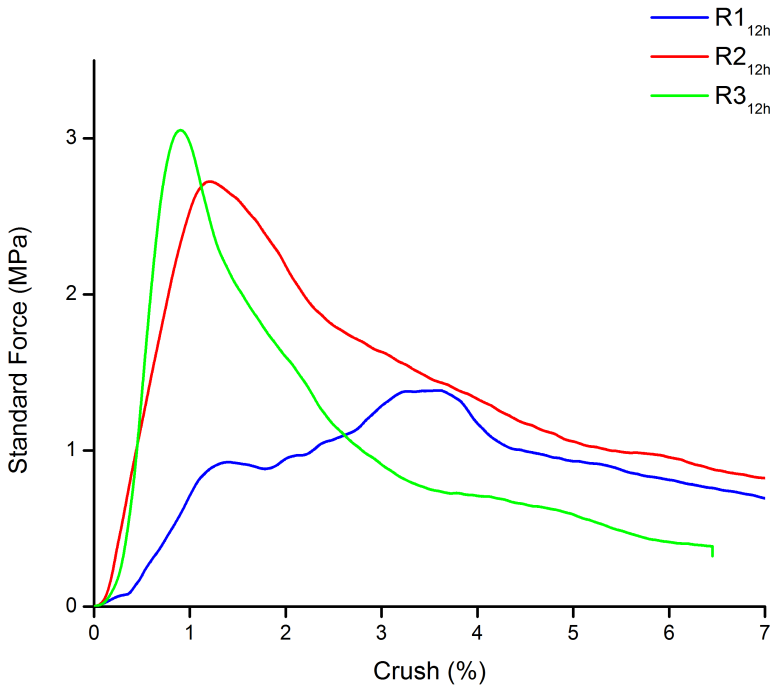

Fig. 4.56 – Results of compression tests of samples set in Ringer´s solution setting environment for 12 hours.

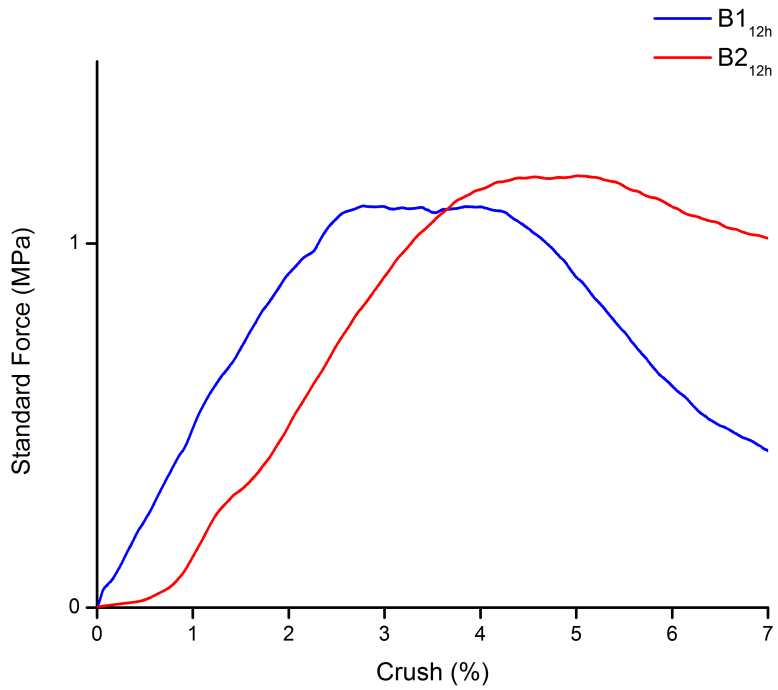

Fig. 4.57 – Results of compression tests of samples set in blood setting environment for 12 hours.

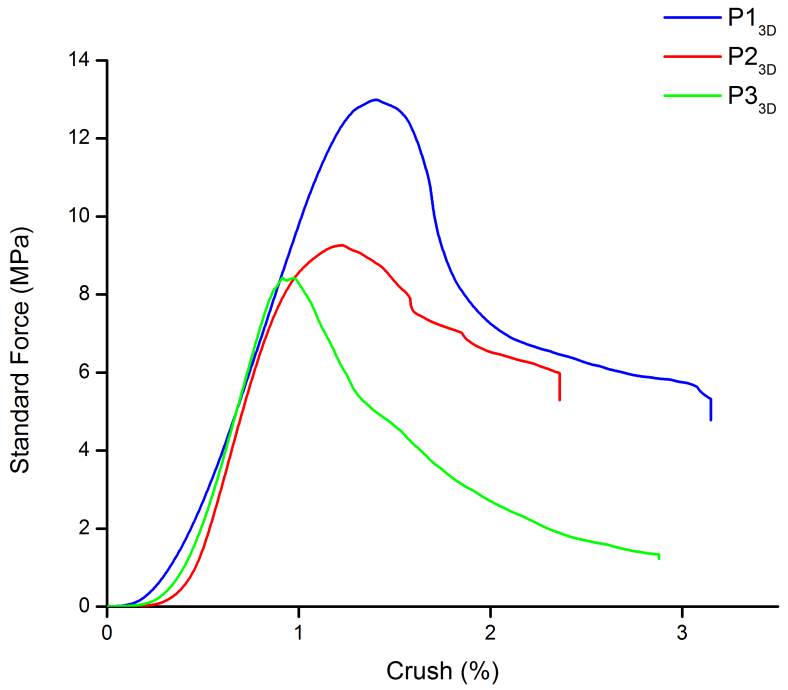

Fig. 4.58 – Results of compression tests of samples set in physiological solution setting environment for 3 days.

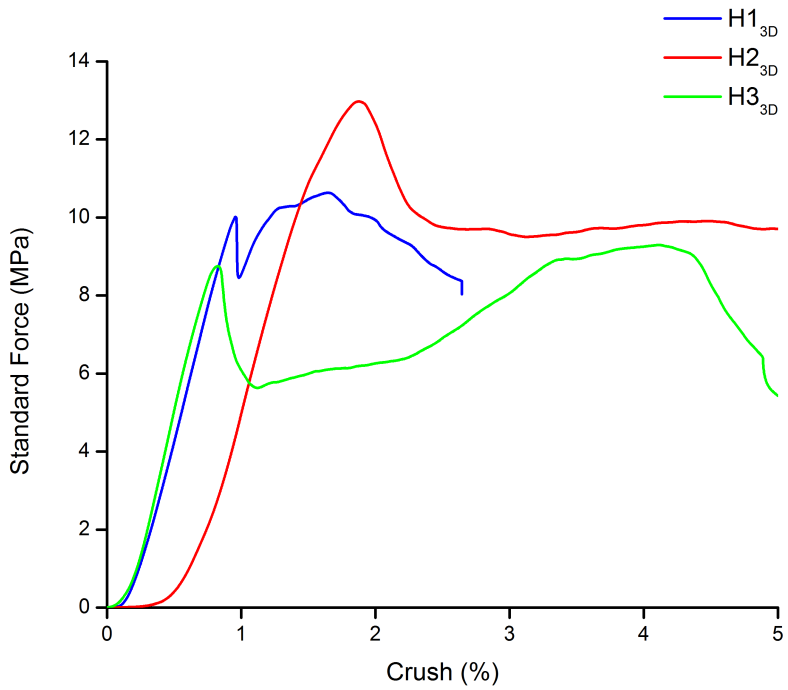

Fig. 4.59 – Results of compression tests of samples setin Hank´s solution setting environment for 3 days .

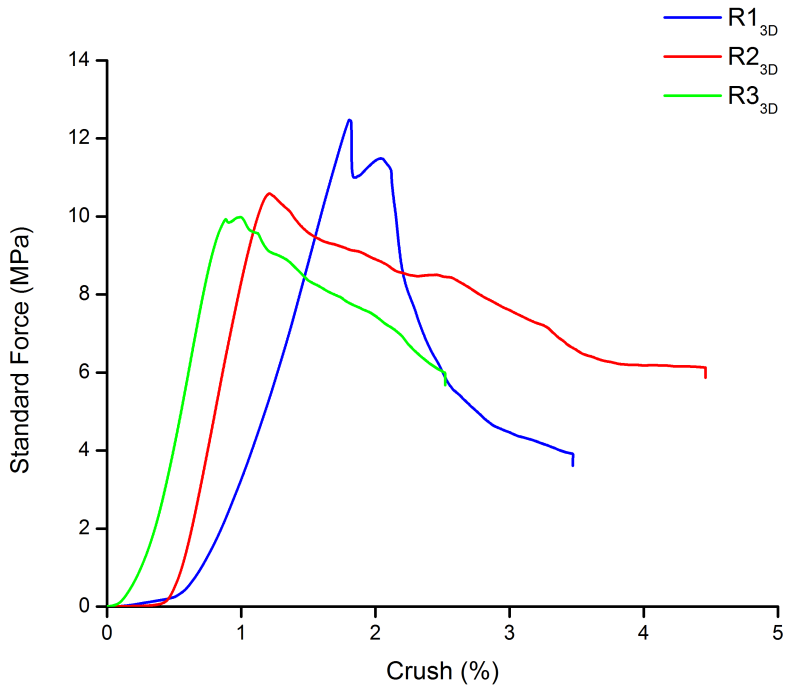

Fig. 4.60 – Results of compression tests of samples set in Ringer´s solution setting environment for 3 days.

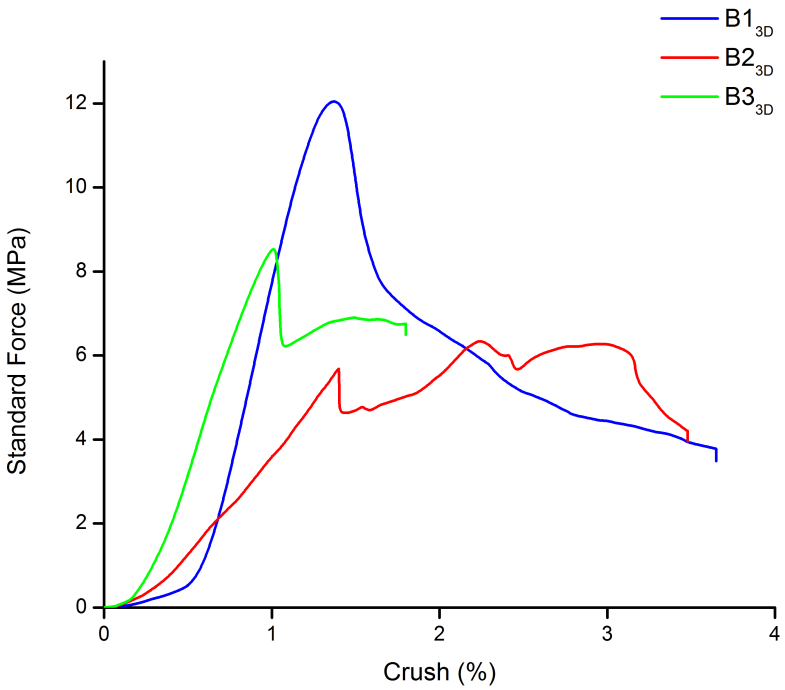

Fig. 4.61 – Results of compression tests of samples set in blood setting environment for 3 days.

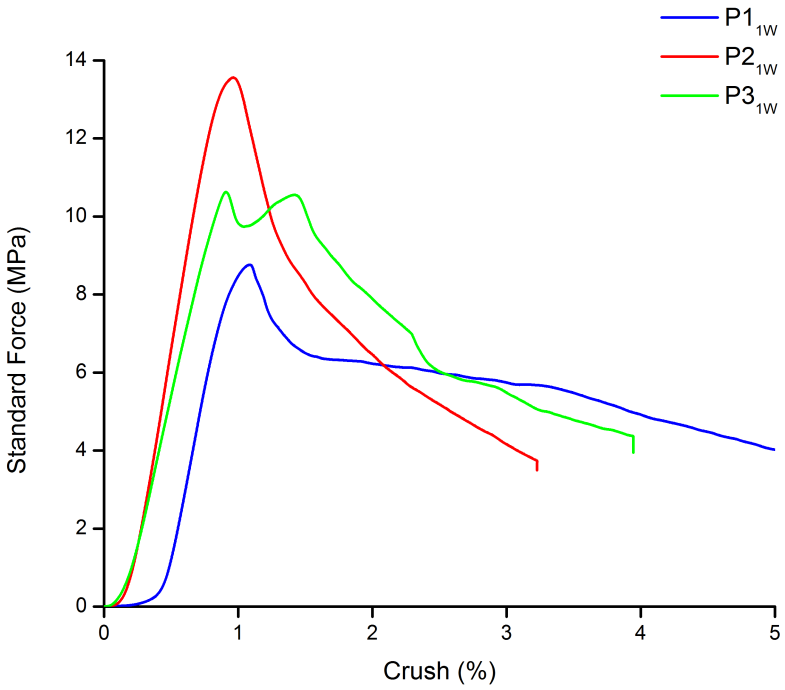

Fig. 4.62 – Results of compression tests of samples set in physiological solution setting environment for 1 week.

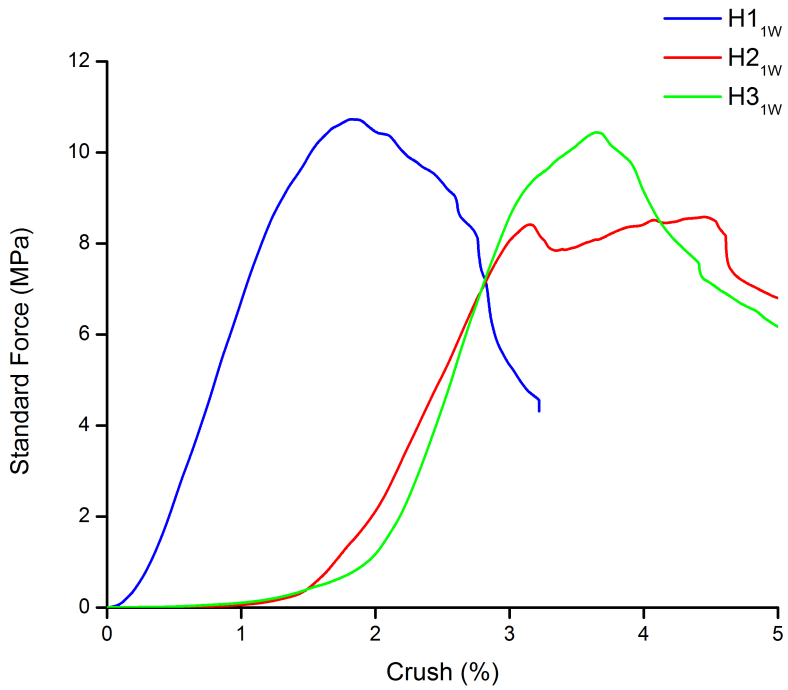

Fig. 4.63 – Results of compression tests of samples set in Hank´s solution setting environment for 1 week.

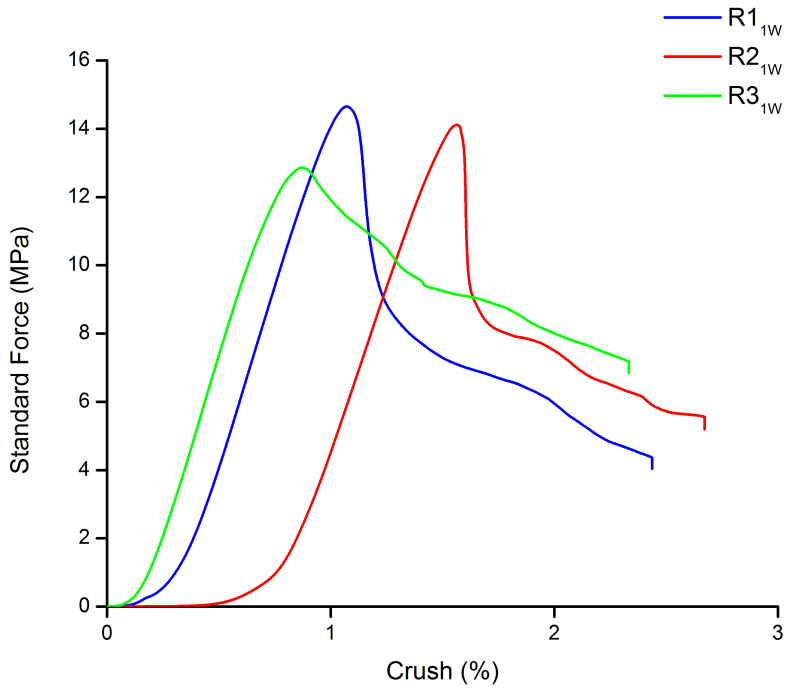

Fig. 4.64 – Results of compression tests of samples se in Ringer´s solution setting environmentt for 1 week.

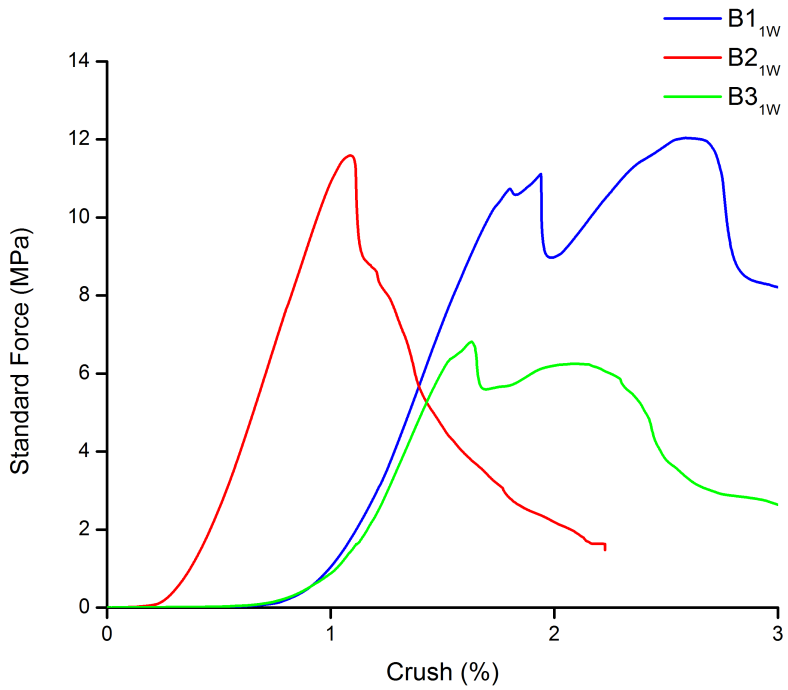

Fig. 4.65 – Results of compression tests of samples set in blood setting environment for 1 week.

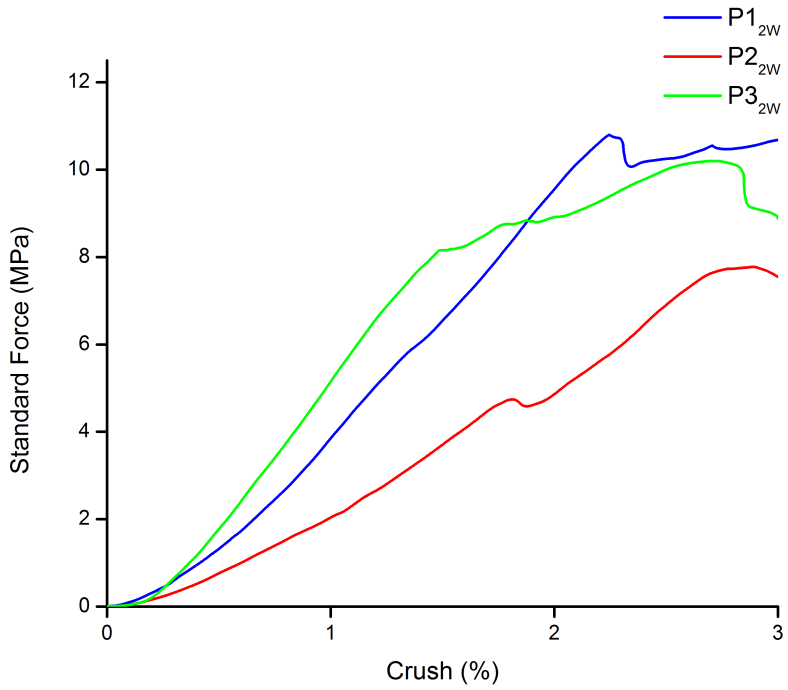

Fig. 4.66 – Results of compression tests of samples se in physiological solution setting environmentt for 2 weeks.

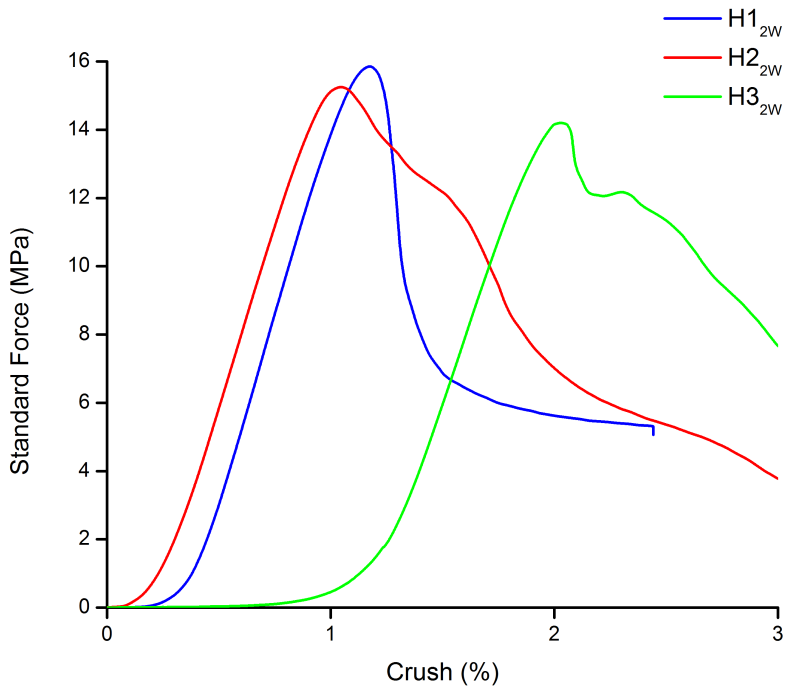

Fig. 4.67 – Results of compression tests of samples set in Hank´s solution setting environment for 2 weeks.

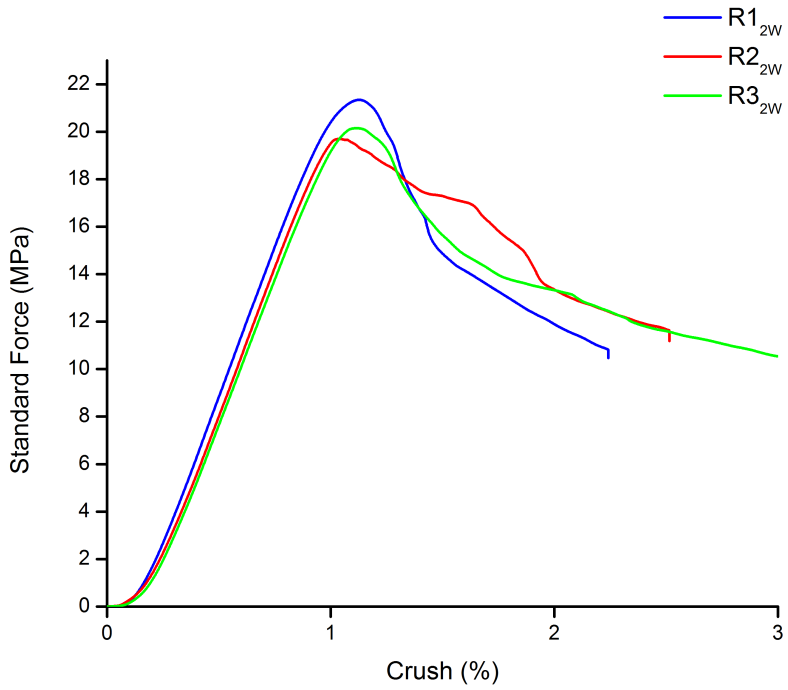

Fig. 4.68 – Results of compression tests of samples set in Ringer´s solution setting environment for 2 weeks.

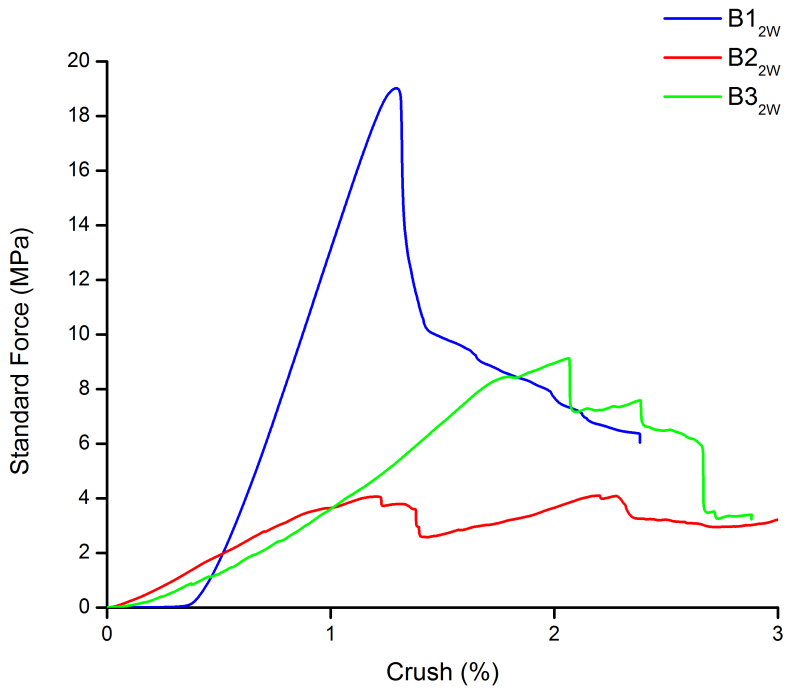

Fig. 4.69 – Results of compression tests of samples set in blood setting environment for 2 weeks.

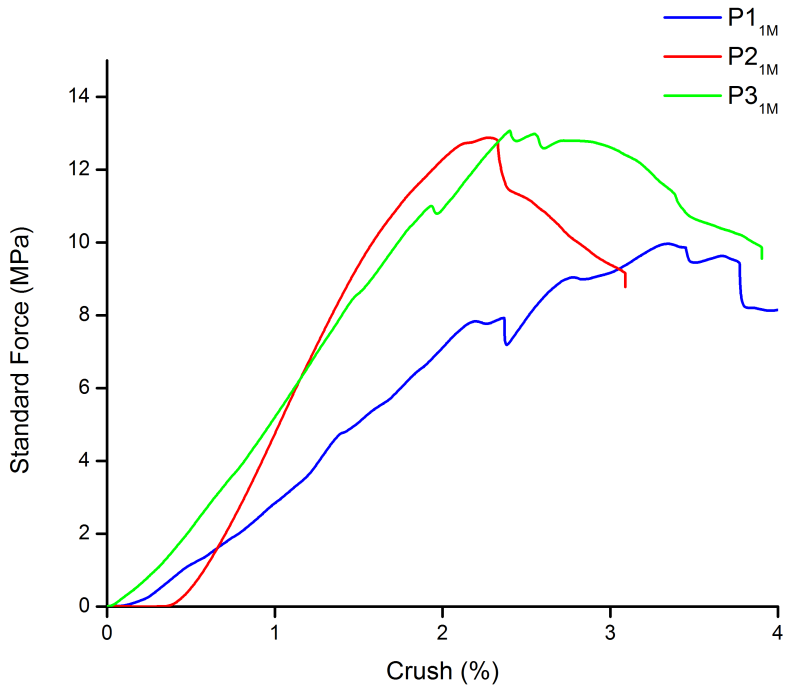

Fig. 4.70 – Results of compression tests of samples set in physiological solution setting environment for 1 month.

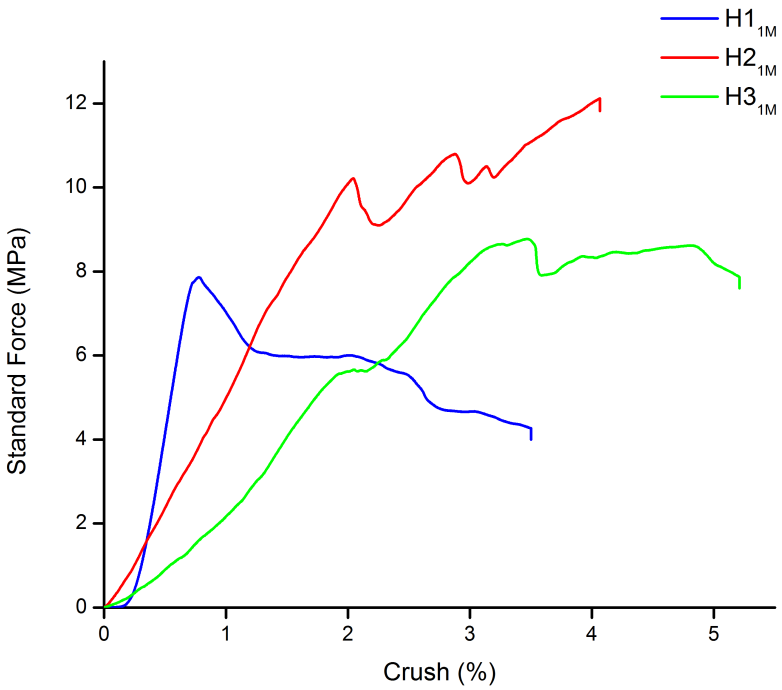

Fig. 4.71 – Results of compression tests of samples set in Hank´s solution setting environment for 1 month.

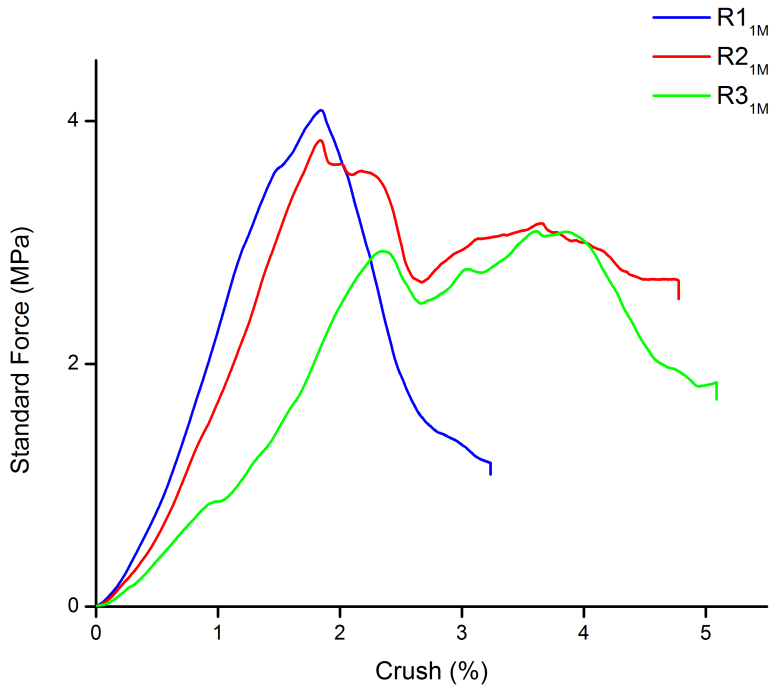

Fig. 4.72 – Results of compression tests of samples set in Ringer´s solution setting environment for 1 month.

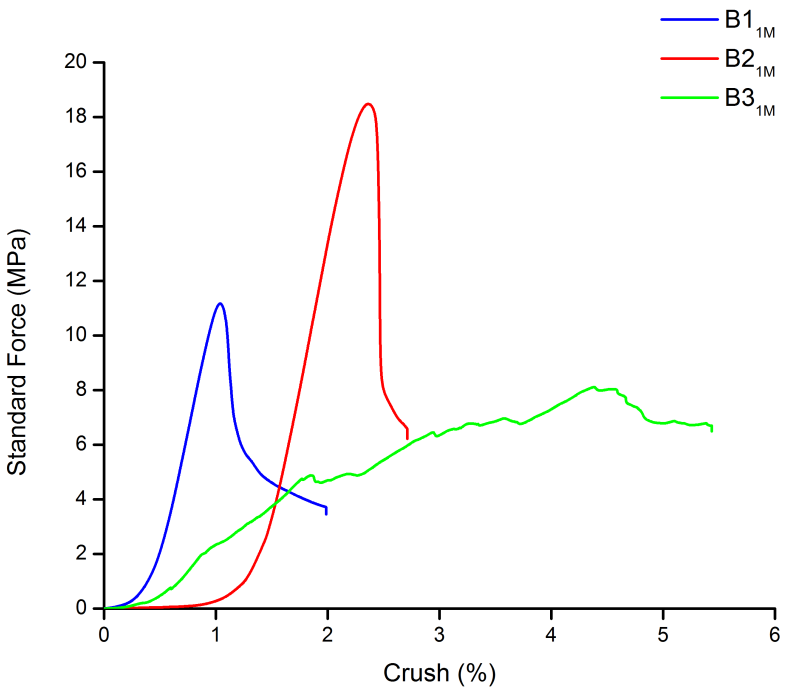

Fig. 4.73 – Results of compression tests of samples set in blood setting environment for 1 month.

LIST OF FIGURES

LIST OF TABLES

LIST OF SHORTCUTS

AMC	amorphous calcium phosphate
α-TCP	α-tricalcium phosphate
α-TCP DS	double-setting α-tricalcium phosphate
ATR	Attenuated Total Reflectance
BCP	biphasic calcium phosphate
BMP	bone morphogenic protein
BPR	Biopex®
BSA	bovine serum albumin
β-TCP	β-tricalcium phosphate
CaP	calcium phosphate
CDHA	calcium-deficient hydroxyapatite
CPC	calcium phosphate cement
CSD	calcium-sulfate dehydrate
CT	computed microtomography
DCP	dicalcium phosphate
DCPA	dicalcium phosphate anhydrous
DCPD	dicalcium phosphate dihydrate
FTIR	Fourier Transformed Infrared Spectroscopy
GA	glycolic acid
GPC	gel permeation chromatography
GG	gellan gum
HAp	hydroxyapatite
HW	high voltage
LA	lactic acid
L/P	liquid to powder ratio
MCP	monocalcium phosphate
MCPM	monocalcium phosphate monohydrate
OCP	octacalcium phosphate
PEG	poly(ethylene glycol)
PHA	precipitated hydroxyapatite
PLA	poly(lactic acid)
PLGA	poly(lactic-co-glycolic acid)
PMMA	poly(methyl methacrylate)
PP	polypropylene
SBF	simulated body fluid
SE	secondary electron
SEM	Scanning Electron Microscopy
SD	standard deviation
TTCP	tetracalcium phosphate
VEGF	vascular endothelial growth factor
XRD	X-ray diffraction

LIST OF SYMBOLS

D_{th}	theoretical density
I_0	integrated intensity of α-TCP selected peaks
I_{t}	integrated intensity of CPC sample selected peaks
$M_{\alpha-\mathrm{TCP}}$	absorption coefficient of α-TCP
M_{CDHA}	absorption coefficient of CDHA
M_n	number average molecular weight
M_w	average molecular weight
V	cell volume
V_{M}	material volume
V_0	volume per formula unit
V_{v}	voids volume
w_t	average percentage amount of α-TCP
Z	number of formula units per cell